

SPRINGER BRIEFS IN EARTH SCIENCES

Matías Reolid

José Miguel Molina

Luis Miguel Nieto

Francisco Javier Rodríguez-Tovar

The Toarcian Oceanic Anoxic Event in the South Iberian Palaeomargin



Springer

SpringerBriefs in Earth Sciences

More information about this series at <http://www.springer.com/series/8897>

Matías Reolid · José Miguel Molina
Luis Miguel Nieto
Francisco Javier Rodríguez-Tovar

The Toarcian Oceanic Anoxic Event in the South Iberian Palaeomargin

 Springer

Matías Reolid
Departamento de Geología and CEACTION
Universidad de Jaén
Jaén
Spain

Luis Miguel Nieto
Departamento de Geología and CEACTION
Universidad de Jaén
Jaén
Spain

José Miguel Molina
Departamento de Geología and CEACTION
Universidad de Jaén
Jaén
Spain

Francisco Javier Rodríguez-Tovar
Departamento de Estratigrafía y
Paleontología
Universidad de Granada
Granada
Spain

ISSN 2191-5369

SpringerBriefs in Earth Sciences

ISBN 978-3-319-67210-6

DOI 10.1007/978-3-319-67211-3

ISSN 2191-5377 (electronic)

ISBN 978-3-319-67211-3 (eBook)

Library of Congress Control Number: 2017951056

© The Author(s) 2018

This work is subject to copyright. All rights are reserved by the Publisher, whether the whole or part of the material is concerned, specifically the rights of translation, reprinting, reuse of illustrations, recitation, broadcasting, reproduction on microfilms or in any other physical way, and transmission or information storage and retrieval, electronic adaptation, computer software, or by similar or dissimilar methodology now known or hereafter developed.

The use of general descriptive names, registered names, trademarks, service marks, etc. in this publication does not imply, even in the absence of a specific statement, that such names are exempt from the relevant protective laws and regulations and therefore free for general use.

The publisher, the authors and the editors are safe to assume that the advice and information in this book are believed to be true and accurate at the date of publication. Neither the publisher nor the authors or the editors give a warranty, express or implied, with respect to the material contained herein or for any errors or omissions that may have been made. The publisher remains neutral with regard to jurisdictional claims in published maps and institutional affiliations.

Printed on acid-free paper

This Springer imprint is published by Springer Nature

The registered company is Springer International Publishing AG

The registered company address is: Gewerbestrasse 11, 6330 Cham, Switzerland

Acknowledgements

This research was funded through Project CGL2015-66835-P (Secretaría de Estado de I+D+I, Spain), Research Groups RNM-200 and RNM-178 (Junta de Andalucía), and the Unidad Científica de Excelencia (UCE-2016-05). Financial support by the Departamento de Geología and the CEACTierra (Universidad de Jaén) allowed preparation of this book. This work is a contribution of the IGCP 655 *Toarcian Oceanic Anoxic Event: Impact on marine carbon cycle and ecosystems* (IUGS-UNESCO). Dr. Jesús Reolid (Universität Hamburg) helped in the fieldwork. Prof. Pascual Rivas and J. Carlos Braga (Universidad de Granada) helped in the identification of ammonoids. Prof. Emanuela Mattioli (Université Lyon-1) identified the calcareous nannofossils. Dr. José Francisco Baeza Carratalá (Universidad de Alicante) classified the brachiopods from La Cerradura section. Finally, Dr. Soulimane Choukri (Université Abou Bekr Belkaid Tlemcen) collaborated and revised the classification of ostracods. We are grateful to the comments of an anonymous reviewer as well as the work of the Editor of Springer, Alexis Vizcaino, for his help and managing of the publication process.

Contents

1	Introduction	1
	References.	2
2	The Betic External Zones	5
2.1	The External Zones and the South Iberian Palaeomargin	5
2.1.1	Tectonic Units and Palaeogeographic Domains.	6
2.1.2	Higher Range Sedimentary Cycles	8
2.1.3	Geodynamic Evolution of the South Iberian Palaeomargin	11
2.2	Sedimentary and Palaeogeographic Evolution of the Lower Jurassic	14
2.2.1	The Gavilán Formation	14
2.2.2	The Zegri Formation	15
	References.	19
3	External Subbetic Outcrops	23
3.1	Fuente Vidriera Section	23
3.1.1	Mineralogy	24
3.1.2	Trace Fossils	26
3.1.3	Foraminiferal and Ostracod Assemblages	29
3.1.4	Stable Isotopes	32
3.1.5	Geochemical Proxies.	34
3.1.6	Interpretation.	37
3.2	Cueva del Agua Section.	44
3.2.1	Facies and Microfacies	44
3.2.2	Microfossil Assemblages.	49
3.2.3	Geochemistry	52
3.2.4	Interpretation.	53

- 3.3 La Cerradura Section 58
 - 3.3.1 Macroinvertebrates 59
 - 3.3.2 Trace Fossils 62
 - 3.3.3 Calcareous Nannofossils 62
 - 3.3.4 Geochemistry 66
 - 3.3.5 Interpretation 68
- References. 74
- 4 Median Subbetic Outcrops 85**
 - 4.1 Iznalloz Section 85
 - 4.1.1 Ammonite Biostratigraphy 85
 - 4.1.2 Lithofacies and Microfacies 88
 - 4.1.3 Microfossil Assemblages. 92
 - 4.1.4 Trace Fossils 95
 - 4.1.5 Interpretation 97
 - 4.2 Arroyo Mingarrón Section 103
 - 4.2.1 Lithofacies and Microfacies 106
 - 4.2.2 Calcareous Nannofossil 108
 - 4.2.3 Geochemistry 110
 - 4.2.4 Interpretation 112
 - References. 115
- 5 General Conclusions 121**

Chapter 1

Introduction

The Early Toarcian Oceanic Anoxic Event (T-OAE) was one of the most important environmental changes of the Mesozoic, resulting in a mass extinction event of benthic and pelagic groups in marine ecosystems (Hallam 1996; Wignall et al. 2005). Typically, the T-OAE is characterised by the record of organic-rich sediments associated with a negative excursion in $\delta^{13}\text{C}$ (Jenkyns and Clayton 1997; Cohen et al. 2004; Hesselbo et al. 2007; Suan et al. 2008; Hermoso et al. 2009; Bodin et al. 2010; Gómez and Arias 2010; Littler et al. 2010; Izumi et al. 2012; Ait-Itto et al. 2017; among others).

There is no consensus about the genesis of the T-OAE. Proposals include the massive enrichment of isotopically light carbon and its transfer between the different reservoirs, now interpreted in light of diverse phenomena such as a massive dissociation of methane hydrates in marine sediments (e.g., Hesselbo et al. 2000, 2007), or the production of thermogenic methane during the concomitant intrusive eruption in the Karoo-Ferrar province (e.g., McElwain et al. 2005). Several environmental changes may have been involved in the mass extinction event, including generalised anoxia, the enhancement of greenhouse conditions and a warming trend, and/or the incidence of sea-level changes (e.g., Hallam 1986, 1987; Elmi 1996; Hylton and Hart 2000; McArthur et al. 2000; Bailey et al. 2003; Ruban and Tyszka 2005; Wignall et al. 2005; Gómez and Goy 2011; Suan et al. 2011). Although considered as a global phenomenon, the expression of the T-OAE varies worldwide as revealed, for example, by the diachronous record, the associated facies, and the distinctive incidence on benthic and nektonic environments between the Tethyan and Boreal provinces (Wignall et al. 2005).

The South Iberian Palaeomargin during the Pliensbachian and Toarcian was a complex context, where the deposits are actually represented by the Subbetic outcrops (Betic Cordillera, southern Spain). The Toarcian deposits of the Subbetic represent a hemipelagic marine setting close to the Hispanic Corridor, a passage between the Western Tethys and the Proto-Atlantic seaway (Aberhan 2001; Bailey et al. 2003; Rodríguez-Tovar and Reolid 2013), at an approximate palaeolatitude of 30° N, near the Iberian Meseta (Osete et al. 2011). The fragmentation of the

palaeomargin during the Late Pliensbachian and the configuration in different tilted blocks with variable subsidence determined differences in thickness and facies during the Toarcian. In this context, the record of the T-OAE is not homogeneous in the palaeomargin and is very different to the typical black shales of the central and North Europe sections. Nevertheless, data from the Subbetic allow understanding the evolution of this part of the Western Tethys, being essential for the advance of the knowledge of the complexity of the global T-OAE. In this book we report the state of the art for the T-OAE in the Subbetic from the analysis of well studied reference sections of the Subbetic taking into account the biotic and abiotic signals.

References

- Aberhan M (2001) Bivalve palaeobiogeography and the Hispanic Corridor: time of opening and effectiveness of a proto-Atlantic seaway. *Palaeogeogr Palaeoclimatol Palaeoecol* 165:375–394
- Ait-Itto F-Z, Price GD, Ait Addi A, Chafiki D, Mannani I (2017) Bulk-carbonate and belemnite carbon-isotope records across the Pliensbachian-Toarcian boundary on the northern margin of Gondwana (Issouka, Middle Atlas, Morocco). *Palaeogeogr Palaeoclimatol Palaeoecol* 466:128–136
- Bailey TR, Rosenthal Y, McArthur JM, van de Schootbrugge B, Thirlwall MF (2003) Paleooceanographic changes of the Late Pliensbachian-Early Toarcian interval: a possible link to the genesis of an anoxic event. *Earth Planet Sci Lett* 212:307–320
- Bodin S, Mattioli E, Frölich S, Marshall JD, Boutib L, Lahsini S, Redfern J (2010) Toarcian carbon isotope shifts and nutrient changes from the Northern margin of Gondwana (High Atlas, Morocco, Jurassic): palaeoenvironmental implications. *Palaeogeogr Palaeoclimatol Palaeoecol* 297:377–390
- Cohen AS, Coe AL, Harding SM, Scwark L (2004) Osmium isotope evidence for the regulation of atmospheric CO₂ by continental weathering. *Geology* 32:157–160
- Elmi S (1996) Stratigraphic correlations of the main Jurassic events in the Western Mediterranean Tethys (western Algeria and eastern Morocco). *Geores Forum* 1–2:343–357
- Gómez JJ, Arias C (2010) Rapid warming and ostracods mass extinction at the Lower Toarcian (Jurassic) of central Spain. *Mar Micropaleontol* 74:119–135
- Gómez JJ, Goy A (2011) Warming-driven mass extinction in the Early Toarcian (Early Jurassic) of northern and central Spain. Correlation with other time-equivalent European sections. *Palaeogeogr Palaeoclimatol Palaeoecol* 306:176–195
- Hallam A (1986) The Pliensbachian and Tithonian extinction events. *Nature* 319:765–768
- Hallam A (1987) Radiations and extinctions in relation to environmental change in the marine Lower Jurassic of northwest Europe. *Paleobiology* 13:152–168
- Hallam A (1996) Major bio-events in the Triassic and Jurassic. In: Walliser OH (ed) *Global events and event stratigraphy*. Springer, Berlin, pp 265–283
- Hermoso M, Minoletti F, Le Callonnec L, Jenkyns HC, Hesselbo SP, Rickaby REM, Renard M, de Rafaeli M, Emmanuel L (2009) Global and local forcing of Early Toarcian seawater chemistry: a comparative study of different paleoceanographic settings (Paris and Lusitanian basins). *Paleoceanography* 24:PA4208
- Hesselbo SP, Gröcke DR, Jenkyns HC, Bjerrum CJ, Farrimond P, Morgans-Bell HS, Green OR (2000) Massive dissociation of gas hydrate during a Jurassic oceanic anoxic event. *Nature* 406:392–395
- Hesselbo SP, Jenkyns HC, Duarte LV, Oliveira LCV (2007) Carbon-isotope record of the Early Jurassic (Toarcian) Oceanic Anoxic Event from fossil wood and marine carbonate (Lusitanian Basin, Portugal). *Earth Planet Sci Lett* 253:455–470

- Hylton MD, Hart MB (2000) Benthic foraminiferal response to Pliensbachian-Toarcian (Lower Jurassic) sea-level change and oceanic anoxia in NW Europe. *Geores Forum* 6:455–462
- Izumi K, Miyaji T, Tanabe K (2012) Early Toarcian (Early Jurassic) oceanic anoxic event recorded in the shelf deposits in the northwestern Panthalassa: evidence from the Nishinakayama Formation in the Toyora area, west Japan. *Palaeogeogr Palaeoclimatol Palaeoecol* 315–316:100–108
- Jenkyns HC, Clayton CK (1997) Lower Jurassic epicontinental carbonates and mudstones from England and Wales: chemostratigraphic signals and the early Toarcian anoxic event. *Sedimentology* 44:687–706
- Littler K, Hesselbo SP, Jenkyns HC (2010) A carbon-isotope perturbation at the Pliensbachian-Toarcian boundary: evidence from the Lias Group, NE England. *Geol Mag* 147:181–192
- McArthur JM, Donovan DT, Thirlwall MF, Fouke BW, Matthey D (2000) Strontium isotope profile of the Early Toarcian (Jurassic) oceanic anoxic event, the duration of ammonite biozones, and belemnite palaeotemperatures. *Earth Planet Sci Lett* 179:269–285
- McElwain JC, Wade-Murphy J, Hesselbo SP (2005) Changes in carbon dioxide during an anoxic event linked to intrusion of Gondwana coals. *Nature* 435:479–482
- Osete ML, Gómez JJ, Pavón-Carrasco FJ, Villalain JJ, Palencia-Ortas A, Ruiz-Martínez VC, Heller F (2011) The evolution of Iberia during the Jurassic from palaeomagnetic data. *Tectonophysics* 502:105–120
- Rodríguez-Tovar FJ, Reolid M (2013) Environmental conditions during the Toarcian Oceanic Anoxic Event (T-OAE) in the westernmost Tethys: influence of the regional context on a global phenomenon. *Bull Geosci* 88:697–712
- Ruban DA, Tyszka J (2005) Diversity dynamics and mass extinctions of the Early-Middle Jurassic foraminifers: a record from the Northwestern Caucasus. *Palaeogeogr Palaeoclimatol Palaeoecol* 222:329–343
- Suan G, Pittet B, Bour I, Mattioli E, Duarte LV, Mailliot S (2008) Duration of the Early Toarcian carbon isotope excursion deduced from spectral analysis: consequence for its possible causes. *Earth Planet Sci Lett* 267:666–679
- Suan G, Nikitenko BL, Rogov MA, Baudin F, Spangenberg JE, Knyazev VG, Glinskikh LA, Goryacheva AA, Adatte T, Riding JB, Föllmi KB, Pittet B, Mattioli E, Lécuyer C (2011) Polar record of Early Jurassic massive carbon injection. *Earth Planet Sci Lett* 312:102–113
- Wignall PB, Newton RJ, Little CTS (2005) The timing of paleoenvironmental change and cause-and-effect relationships during the Early Jurassic mass extinction in Europe. *Am J Sci* 305:1014–1032

Chapter 2

The Betic External Zones

The Betic Cordillera is the major geological domain situated to the S and SE of the Iberian Peninsula. It is bounded by the Iberian Massif and the Iberian Mountain Range to the N and by the Atlantic Ocean and Mediterranean Sea to the SW, S, and SE (Fig. 2.1). It belongs, along with other mountain ranges of North Africa, to the western segment of the Perimediterranean Alpine Orogen. In the Betic Cordillera, three main geological domains of greater rank are differentiated: the Betic External Zones, the Betic Internal Zones and the Campo de Gibraltar Complex. The general knowledge of the geology of the Betic Cordillera has been shown with in previous works (Sanz de Galdeano 1997; Gibbons and Moreno 2002; Vera 2004) and its exhaustive analysis is not the objective of this publication. However, we will present here a synthesis of the External Zones focused in the Subbetic domain.

2.1 The External Zones and the South Iberian Palaeomargin

The outcropping sedimentary rocks of the Betic External Zones were deposited in the South Iberian Palaeomargin (Western Tethys) during the Mesozoic and most of the Cenozoic, and were mainly deformed during the Miocene, between the Burdigalian and the Late Miocene. García-Hernández et al. (1980) proposed a first model of the palaeogeographic evolution of this margin during the Mesozoic, and established a tectonic and palaeogeographic subdivision in geological units that, with some nuances, is still used nowadays (Vera 2004).

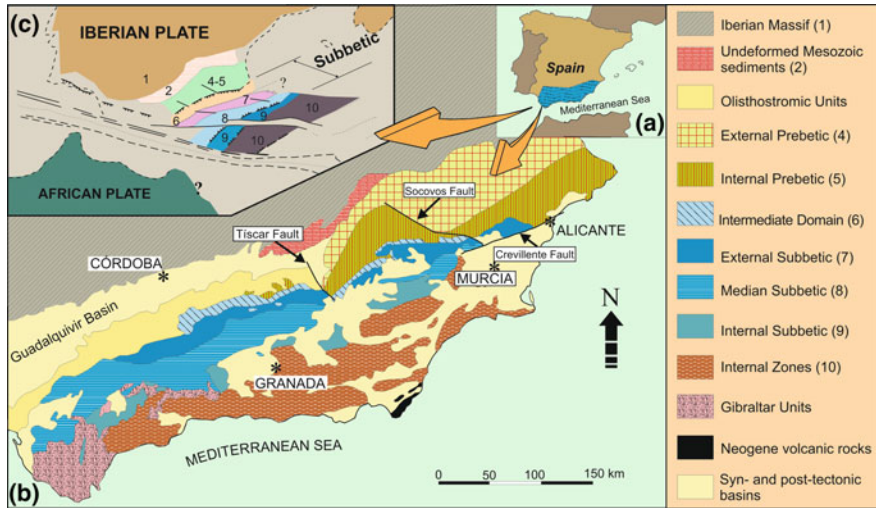


Fig. 2.1 Geological map of the Betic Cordillera

2.1.1 Tectonic Units and Palaeogeographic Domains

In the Betic External Zones units of diverse range have been defined by tectonic and stratigraphic criteria. These units comprise deposits accumulated in the South Iberian Palaeomargin, in palaeogeographic domains individualised throughout the successive stages of its Mesozoic history. The higher rank division of the Betic External Zones is into Prebetic and Subbetic. These terms designate areas clearly differentiated by its regional geographic position as well as by its structural, stratigraphic or palaeogeographic characteristics. This terminology has been used with equivalent meaning since its original definition (Blumenthal 1927; Fallot 1945, 1948; Fontboté 1970). From a tectonic point of view, the Prebetic, located to the north, consists of parautochthonous or moderately allochthonous sedimentary rocks, whereas the Subbetic allochthony is beyond doubt and the rocks generally more deformed than those of the Prebetic. The Subbetic is relatively well-organised from a structural point of view, but the deformation is locally such intense that large sections of it, predominantly made up of Triassic terrains, have lost their internal coherence and have been transformed into disorganised masses called Subbetic Chaotic Complexes. Part of these chaotic masses was gravitationally slipped and included in the mid-Miocene sediments of the southern edge of the Guadalquivir Basin, forming the Guadalquivir Olisthostromic Complex, or Subbetic Olisthostromic Complex (Pérez-López and Sanz de Galdeano 1994) or Evaporite-bearing Accretionay Complex (Pérez-Valera et al. 2017).

The subdivision in Prebetic and Subbetic is even more necessary from a stratigraphic and palaeogeographic point of view. The Prebetic successions mainly contain shallow marine facies, with important continental episodes, even with

intervals of erosion, depending on the sectors. In contrast, in the Subbetic the pelagic facies are dominant from the Upper Pliensbachian (Domerian), when the main phase of intracontinental rifting began and the large shallow marine carbonate platforms disappeared (Vera 2001). This interpretation is evidenced in the palaeogeographic and palinspastic reconstructions for the Jurassic and Cretaceous of Azema et al. (1979) and García-Hernández et al. (1980, 1989).

The Subbetic, the southernmost major unit of the External Zones (Fig. 2.1), is composed of sedimentary rocks from the Triassic to the Middle Miocene and to a minor extent by volcanic and subvolcanic rocks. Within the Subbetic there are different thrusting sheet units structurally organised. The distribution of these units is broadly consistent with the established palaeogeographic subdomains, mainly for the Jurassic. The boundaries between palaeogeographic subdomains, however, do not always coincide with tectonic boundaries (thrust faults). The palaeogeographic nomenclature of the Subbetic was introduced by García-Dueñas (1967) and is constituted by three large subdomains WSW-ENE elongated: External Subbetic, Median Subbetic and Internal Subbetic. This triple division was completed with two modifications (Vera 2004). The first was the assignment to the Subbetic of the Intermediate Domain (Ruiz-Ortiz 1980, 1981). The Intermediate Domain, located to the N of the External Subbetic, was separated from both Prebetic and Subbetic in previous classifications (Azema et al. 1979; Vera 1986), but was ultimately included in the Subbetic because of its similarities in facies and tectonic style, in contrast with the much different Prebetic, to which the Intermediate Domain overthrusts extensively. The second modification is the distinction of the Western Subbetic as a particular subdomain called Penibetic (Martín-Algarra 1987; Martín-Algarra and Vera 1982, 1989, 1994; Vera 2001), for its stratigraphic, palaeogeographic, and tectonic peculiarities.

In conclusion, in the Subbetic, and especially in the central sector of the cordillera, four sets of tectonic units, of structural guideline WSW-ENE are distinguished. They come from four pre-existing palaeogeographic subdomains (Fig. 2.2). The northernmost unit (Intermediate Domain) was the most subsident and in displays the maximum sediment thickness of the Jurassic and Cretaceous in the whole basin. In the second unit (External Subbetic), located immediately to the S and SE of the previous one, the subsidence was minimal during the Middle and Late Jurassic, which determined the development of condensed facies. The third unit, more southerly (Median Subbetic), was again more subsident and characterised by a predominance of marly facies in the Middle-Upper Jurassic and Cretaceous with intercalations of submarine volcanic rocks in its central part, especially abundant in the Jurassic. Finally towards the S appears the last palaeogeographic subdomain (Internal Subbetic-Penibetic) that during the Middle-Late Jurassic constituted a pelagic swell with slight subsidence (Internal Subbetic in the oriental and central sectors of the mountain range), and that in the western sector has own entity (Penibetic) for its peculiar Jurassic facies and for the frequent stratigraphic hiatuses occurred in the Lower Cretaceous.

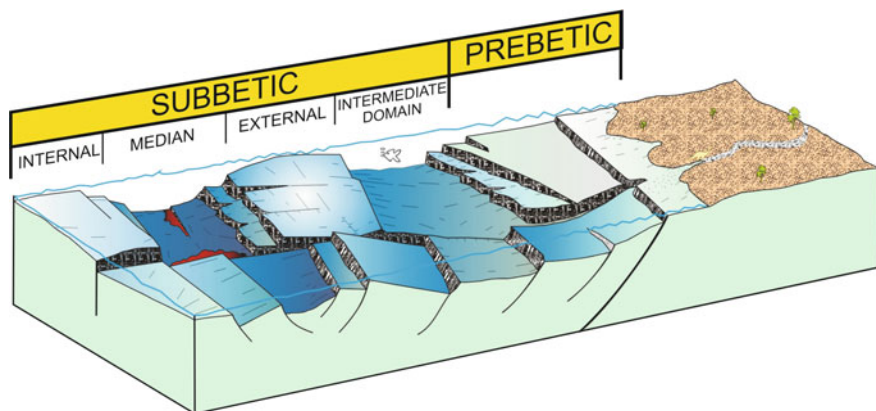


Fig. 2.2 Configuration of the sea floor topography of the South Iberian Palaeomargin during the Jurassic

2.1.2 Higher Range Sedimentary Cycles

Sedimentary cycles of great order have been differentiated in the stratigraphic record of the South Iberian Palaeomargin (Vera 2004; Fig. 2.3). The criteria that can be used for the differentiation of these large cycles are diverse, but the ones that will be distinguished below are based on the recognition of stratigraphic discontinuities in wide sectors of the basin, which are an expression of tectonic, climatic, oceanographic and/or eustatic events that affected the South Iberian Palaeomargin as a whole. The defined cycles have very different durations, from more than 45 My (Cycle I) to about 8 My (Cycle VII), all within the range of second order cycles of the most usual classifications. Within these larger cycles, lower-range cycles are differentiated based on the recognition of other stratigraphic discontinuities and various stratigraphic features, associated to events of similar significance but with less intensity or more local character than those of the larger cycles.

Seven major sedimentary cycles (Cycles I to VII) were differentiated between the beginning of the Triassic and the Upper Miocene (Fig. 2.3). An additional cycle (Cycle VIII) includes sedimentary rocks that have usually been considered as postorogenic (Upper Tortonian to Holocene), that fill the postorogenic sedimentary basins. These basins are not part of the Betic External Zones in the strictest sense of the term. It should be noted that the age of the boundaries between cycles is not always exactly the same in all sectors of the basin, since the phenomena that caused them were often heterochronous.

Cycle I comprises the Triassic and early Jurassic rocks (Fig. 2.3). The earliest are those of Buntsandstein facies which appear in the Tabular Cover and Prebetic, very rarely in the Subbetic. The Muschelkalk facies appear broadly in the Betic External Zones, although the most extensive Triassic outcrops correspond to the Keuper facies. The Jurassic rocks included in this cycle are those of

◀**Fig. 2.3** Chronostratigraphic chart for the Subbetic (modified of Vera 2004). 1 Keuper Facies. 2 *Microcodium* calcarenites (Majalcorón Fm). 3 Dolostones. 4 Shallow carbonate platform limestones and oolitic limestones. 5 Shallow carbonate platform limestones and calcarenites. 6 Pelagic limestones/marls alternance with ammonites. 7 Cherty limestones (Veleta Fm). 8 Radiolarite facies. 9 Pelagic limestones/marls alternance with calcareous tempestites (Milanos Fm). 11 Condensed pelagic limestones, mainly ammonitico rosso facies. 12 Pelagic oolitic limestones and ammonitico rosso facies (Torcal Fm). 13 Black lutites and marls, with radiolarites and calcareous turbidites (Carbonero Fm and Fardes Fm). 14 Marls and marly-limestones with terrigenous turbidites (Cerrajón Fm). 15 White marls and marly-limestones with planktic foraminifera (Capas Blancas Fm). 16 Pink marly-limestones with planktic foraminifera and coccolites (Capas Rojas Fm and Quípar-Jorquera Fm). 17 White marls and marly-limestones with calcareous turbidite beds. 18 Calcilimolites (Represa Fm). 19 Hiatus. 20 Submarine volcanic rocks. 21 Mainly unconformities. 22 Turbidites, mainly calcareous. 23 Evaporite-bearing accretionary complex. AR Ammonitico Rosso Superior Fm. B Baños Fm. C Camarena Fm. Ca Carretero Fm. Car Carbonero Fm. CB Capas Blancas Fm. Ce Cerrajón Fm. CR Capas Rojas Fm. E Endrinal Fm. F Fardes Fm. G Gavilán Fm. J Jabalcuz Fm. Mi Milanos Fm. MJ Majalcorón Fm. QJ Quípar-Jorquera Fm. R Represa Fm. RJ Radiolarítica Jarropa Fm. T Torcal Fm. To Toril Fm. V Veleta Fm. Vi Los Villares Fm. Z Zegrí Fm

Hettangian-Carixian age. In the Subbetic they are represented by carbonates deposited in shallow marine platforms (Gavilán Fm), within which have been differentiated two cycles of minor order (García-Hernández et al. 1989; Andreo et al. 1991). The events associated with the discontinuity at the top of Gavilán Fm (limit between cycles I and II) were initiated during the Late Carixian (Early Pliensbachian), since its fossilisation occurred between the terminal Carixian and the basal Domerian, according to the sectors. The Domerian (Upper Pliensbachian) is clearly included in Cycle II and consists of pelagic sediments.

The upper boundary of Cycle II is located near the Bathonian-Callovian transition. In the subbetic pelagic swells (External and Internal Subbetics) this boundary coincides with a very clear stratigraphic discontinuity (Fig. 2.3), a paraconformity whose surface is covered by crusts of iron and manganese oxides (hardground), locally with stromatolithic and microbial structures (Martín-Algarra and Sánchez-Navas 2000; Reolid and Molina 2010; Nieto et al. 2012). When the discontinuities in different sections are analyzed in detail, it is observed that this is a complex discontinuity, composed of three minor discontinuities very close in time (O'Dogherty et al. 2000) developed during the Late Bathonian.

The Cycle III begins after the Upper Bathonian discontinuity, but the Callovian sediments are absent in large sectors of the External Betic Zones (Fig. 2.3). In the pelagic swells of the External and Internal Subbetic its upper limit (top of the Upper Ammonitic Rosso Fm) is located from the Middle Berriasian (Nieto 1997) to the end of the Berriasian (Molina 1987) depending on the sector. In the Intermediate Domain this upper boundary coincides with the limit between the Toril Fm and the Los Villares Fm dated as Upper Berriasian and, therefore, with the first input of sand size terrigenous into the pelagic basin throughout mesozoic history, although this input was initially very moderate.

The Cycle IV has the lower limit in the intra-Berriasian discontinuity described above and ends near the boundary between the Lower Cretaceous and the Upper

Cretaceous (Fig. 2.3). In the Intermediate Domain the upper limit of the cycle coincides with the end of the turbiditic sedimentation of the Cerrajón Fm, that has been dated as the transit between Middle Albian and Upper Albian (de Gea et al. 2001), whereas in other sectors of the Subbetic coincides with the end of a sedimentary hiatus (Fig. 2.3) of wide space-time extension.

The Cycle V begins with the above mentioned intra-Albian discontinuity and reaches the boundary between the Cretaceous and Paleocene (Fig. 2.3). In the Subbetic the sedimentary characteristics are quite uniform and in the majority of this palaeogeographic domain the Quípar-Jorquera Fm (Vera et al. 1982) and Capas Rojas Fm (Vera et al. 1982; Vera and Molina 1999) were deposited, both consisting of pelagic marine sediments (not necessarily deep). The presence in some sectors of the Median and Internal Subbetic of *Microcodium* calcarenites (Majalcorón Fm; Molina et al. 2003, 2006) whose bottom almost coincides with the boundary between the Cretaceous and Paleocene supports the argument of setting the upper limit of this cycle coinciding with this chronostratigraphic boundary.

The Cycle VI starts at the end of the previous cycle, while the upper boundary is located within the Burdigalian (Fig. 2.3). In the central sector of the Subbetic, a stage of “Burdigalian Paroxysm” (Hermes 1985), coincident with the boundary between the Lower and Upper Burdigalian (Soria 1994a, 1998), marks the end of the sedimentation of the Almidar Fm among whose sediments are intercalated acid pyroclastic rocks (Soria 1994b). In the Subbetic, this cycle mostly consists of pelagic marls with turbidite intercalations, although in some localised sectors limestones and calcarenites were deposited on shallow platforms (Molina and Nieto 2003).

The Cycle VII has as its lower limit the intra-Burdigalian discontinuity mentioned above and as upper limit the intra-Tortonian discontinuity detected in different sectors of the Subbetic (Estévez et al. 1982). It comprises rocks that have been considered “synorogenic” (Vera 2000) and are mostly white marls with abundant foraminifera, coccoliths and diatoms.

The Cycle VIII has as its lower limit the intra-Tortonian discontinuity, while the upper one is the end of the sedimentary fill in each postorogenic basin, which originates from a continental elevation and the consequent nesting of fluvial networks and massive erosion of subhorizontal materials of this cycle in the different postorogenic basins.

2.1.3 *Geodynamic Evolution of the South Iberian Paleomargin*

The following evolutionary episodes are differentiated according to Vera (2004) (see Fig. 2.4):

- A. *Initial episode of intracontinental rifting (Cycle I)*. Corresponds to the initial phase of the distension that developed during the Triassic-Carixian and which

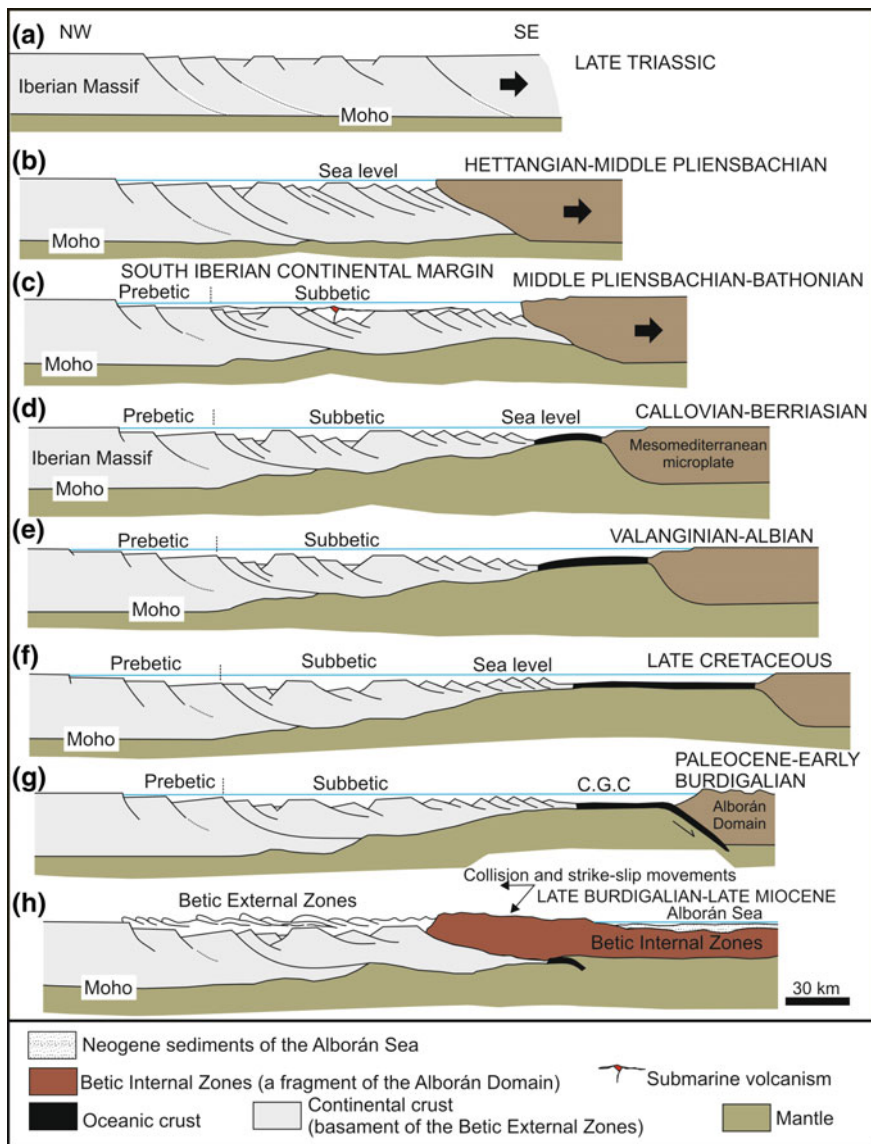


Fig. 2.4 Evolution of the South Iberian Continental margin from the first extensional stages until main deformation phases. C.G.C.: Campo de Gibraltar Complex (Actualized from Vera 2004)

is expressed by Cycle I comprising the rocks of the Triassic and the Liassic infra-Domerian (Fig. 2.4a, b).

B. *Main episode of intracontinental rifting (Cycle II)*. It was developed during the Domerian-Bathonian period. In the Subbetic, it shows remarkable variations of

facies and thicknesses from one palaeogeographic subdomain to other, but in all cases at the beginning of the cycle pelagic sedimentation began (Fig. 2.4c). During the cycle in some sectors were developed large-scale shallowing sequences that ended again with shallow platform limestones.

- C. *Expansive episode (Cycle III)*. It began when the first oceanic crust (or oceanic affinity) was formed between the Iberian Plate and the Meso-Mediterranean Plate. It started towards the boundary between Bathonian-Callovian (Vera 1988, 2001) and ended in the Upper Berriasian. During this episode it can be properly said that there is a relatively diversified and evolved South Iberian continental margin (Fig. 2.4d). In the greater part of the Prebetic there was a clear differentiation with respect to other areas adjacent to the Iberian Massif, reaching higher values of subsidence. In the Subbetic, there was a clear differentiation between subsident troughs and less subsident swells.
- D. *Rifting episode of the margin edge (Cycle IV)*. The Cycle IV was deposited from the upper Berriasian to the Upper Albian and is equivalent to the “tectosedimentary period without-extension” of Vilas et al. (2001) recognised in the Prebetic. It was a rifting phase that simultaneously affected the South Iberian Palaeomargin and other continental margins that surrounded the Iberian Massif. In the Subbetic, the upper part of this cycle (Barremian-Albian) is particularly well recognised in the Intermediate Domain (Fig. 2.4e) for the maximum development of turbidites (Ruiz-Ortiz 1980, 1981; de Gea et al. 2001).
- E. *Post-rift episode (Cycle V)*. It is characterised by the progressive disappearance of tectonic subsidence and the existence of a slow but persistent thermal subsidence (Vera 2001; Vilas et al. 2001). This episode began in the Late Albian and ended near the Cretaceous-Tertiary boundary (Figs. 2.3 and 2.4f) and during this period a homogenisation of the facies took place in wide sectors of the South Iberian Palaeomargin.
- F. *Convergent episode (Cycle VI)*. The transition from a passive margin to a convergent one occurred near the Cretaceous-Tertiary boundary (Vera 2001), although probably it began somewhat earlier, during the Campanian, as proposed Martín-Chivelet et al. (1997). During this period, the cycle VI comprising the sediments of the Lower Paleocene-Burdigalian was deposited (Fig. 2.4g). The end of this episode coincides with the beginning of the continental collision, during the Burdigalian, between the Alborán Domain and the South Iberian Palaeomargin.
- G. *Collision episode (Cycle VII)*. Between the Burdigalian and the beginning of the Upper Miocene, the displacement of the Alborán Domain towards the W was completed and the collision with the South Iberian Palaeomargin was blocked. The “Burdigalian Paroxysm” of Hermes (1985) coincided with the main deformation of the palaeomargin, which marked a true palaeogeographic revolution by raising the areas of its southernmost part and determining the individualisation of a subsident basin located at the deformation front. Also during this time interval (from Late Burdigalian to Early Tortonian) a remarkable extension occurred in the Alborán Sea, simultaneous to a remarkable shortening of the sedimentary cover of the South Iberian Palaeomargin with the

consequent structuration of the External Betic Zones (Sanz de Galdeano 1983, 1990, 1997; Vera 1988, 2000; Maldonado et al. 1992; Comas et al. 1992). Cycle VII corresponds to the sediments deposited in the South Iberian Palaeomargin from the beginning of the collision to the phase of intra-Tortonian tectonic deformation (Estévez et al. 1982). Since the structure of the Betic External Zones took place during this episode, the sedimentary rocks deposited therein can be considered as synorogenic. The area of greater depth and greater subsidence, in the western half, was located in the northern deformation-front of the Betic External Zones that progressed little by little towards the north. During this episode also occurred the deformation of a notable part of the Subbetic that produced the loss of internal coherence and the consequent formation of the Subbetic Chaotic Complexes.

- H. *Post-collision episode (Cycle VIII)*. During the Late Tortonian-Messinian-Pliocene the sedimentation occurred preferentially inside the Postorogenic Neogene Basins as differentiated subsidence areas, one of them, the most extensive, to the north of the cordillera (Guadalquivir Basin) and the others within the cordillera (intramontane basins) (Fig. 2.4h).

2.2 Sedimentary and Palaeogeographic Evolution of the Lower Jurassic

2.2.1 *The Gavilán Formation*

The Jurassic begins with the Gavilán Fm whose contact with the Triassic of the underlying Keuper facies. Three members are differentiated:

Lower member of dolomitised algal laminites (M1): it is constituted by massive dolomites (around 500 m thick), with remains of algal lamination. These facies, which are very uniform throughout the mountain range, have been interpreted as typical of tidal flat environments (García-Hernández et al. 1978, 1979; Andreo et al. 1991; Nieto 1997). Its top has been interpreted as a discontinuity related to the early stages of development of intracontinental rifting (Nieto et al. 1992; Vera 2001).

Intermediate member of pseudo-oolitic limestones (M2): it presents varying thicknesses (0–150 m) and very diverse facies: limestone of oncoids and ooids, limestone with *Lithiotis* or limestones with chert. This facies variability is probably related to a sudden change in the sedimentary conditions of the platform that divided it into more or less protected sectors and somewhat more open and energetic sectors, as well as into hemipelagic environments (García-Hernández et al. 1986; Andreo et al. 1991). It is a marine platform compartmentalised in small banks or swells, isolated by somewhat deeper sectors.

Top member of crinoidal limestones (M3): it is composed by calcarenites with abundant crinoid bioclasts and peloids, usually packstone or grainstone, interpreted as high-energy deposits of an external platform (Dabrio and Polo 1985).

The local differences among the members consist in the greater or lesser development, or in its case the absence of the more modern members. The upper member (M3) is not always present, whereas the massive dolomites of the lower member (M1), can extend vertically to cover almost all the formation in some outcrops due to the unequal extent of the dolomitisation that, according to Martín (1980), reached greater stratigraphic height in the limits between palaeogeographic subdomains.

The top of this cycle coincides with the more evident discontinuity of the Subbetic, record of the rupture of the carbonate platform and the drowning of the shallow environments (Fig. 2.5). Nieto et al. (2002) have described two phases of fracturing from the record of breccia deposits and other features related to the genesis of this discontinuity. The first levels situated on the discontinuity show condensed sedimentation rich in ammonites of the basal Domerian (Braga 1983), while in the Gavilán Fm several biozones of the Carixian (Lower Pliensbachian) have been dated (García-Hernández et al. 1979; Rivas 1979).

2.2.2 The Zegrí Formation

The Jurassic of the External Zones of the Betic Cordillera has been interpreted, from the perspective of basin analysis, as the recording of a rifting episode that led to the formation of a continental margin on the southern margin of the Iberian plate (e.g., García-Hernández et al. 1989; Vera 2001). The development of this rifting event meant, in its early stages, the fracturing and dismemberment of the enormous carbonate platform that during the Early Jurassic covered the entire area of the South Iberian Palaeomargin (Fig. 2.6) and extended widely to more northern sectors. In the early stages of rift evolution, the tectonic phase of the Early Pliensbachian had a very significant impact (Vera 2001; Nieto et al. 2002; Ruiz-Ortiz et al. 2004). During this phase the differentiation of the two great domains of the Betic External Zones, the Prebetic and the Subbetic, took place, and from that moment, they underwent different evolutions. In particular, in the Subbetic, the sedimentation in the Domerian is restarted, but with a marked pelagic character. Thus, the Zegrí Fm rocks deposited in a basin compartmentalised block rotated and tilted by faults. This caused important differences in the rate of subsidence that were recorded in the thickness, and more locally in the facies, of this lithostratigraphic unit. This formation is therefore the record of the first stages of the syn-rift stage, so the study of the distribution of thickness and facies is considered critical in order to quantify the process, not only in terms of sedimentation/subsidence rates, but also in relation to the size of the blocks, the lateral extension of the fractures and their spatio-temporal distribution.

The Zegrí Fm was defined by Molina (1987) in the Subbetic. Its age is generally comprised between the Middle Domerian (Upper Pliensbachian) and Lower Bajocian although in some places the bottom of the formation is of Early Domerian age and the top can reach the late Bajocian. This lithostratigraphic unit has two members (Fig. 2.5): (1) The lower member (Middle Domerian-Lower Toarcian) is a

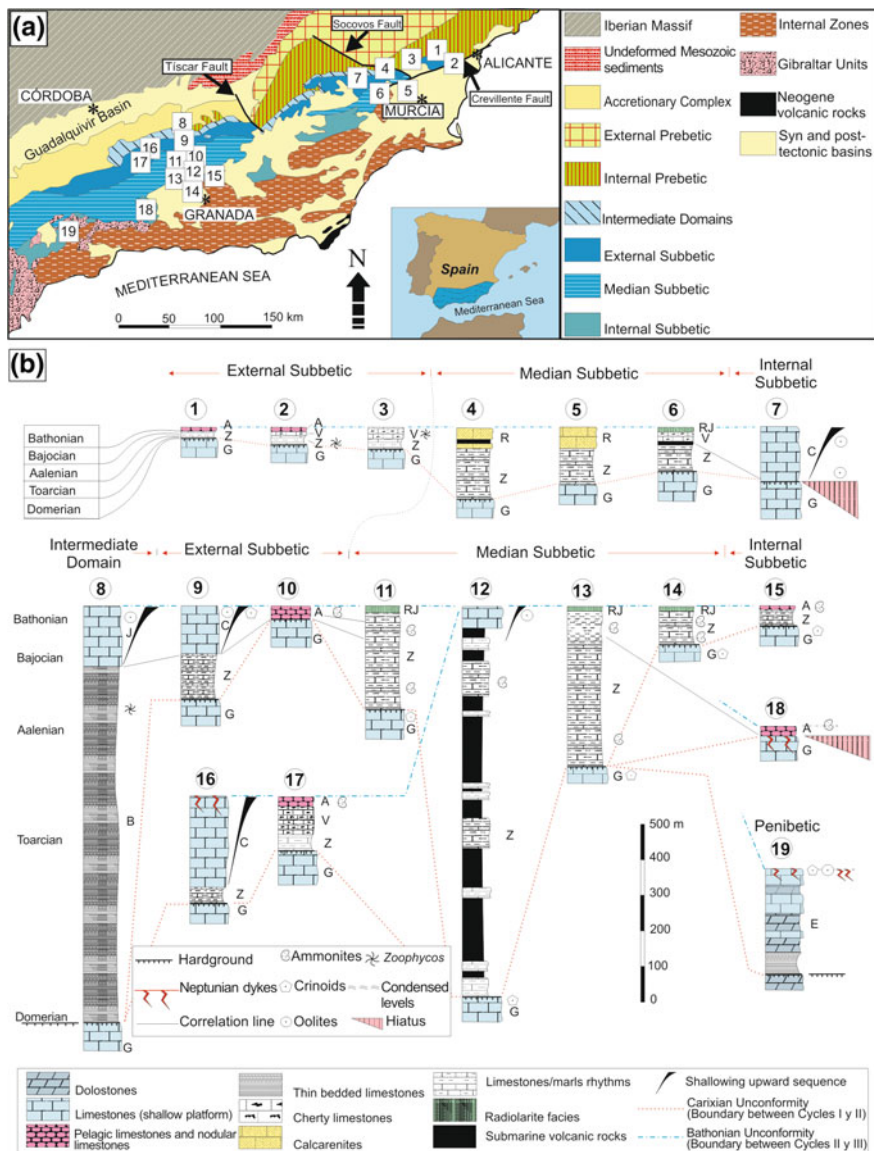


Fig. 2.5 Correlation for the Cycle II (see Fig. 2.1). **a** Geological sketch of the Betic Cordillera with location of the stratigraphic successions. **b** Correlation for the Cycle II Upper Pliensbachian to Bathonian for the Subbetic (modified from Vera et al. 2004). 1 Sierra de Reclot. 2 Sierra de Crevillente. 3 Sierra de Lúgar. 4 Bermeja Unit (Sierra de Ricote). 5 Garita Unit (Sierra de Ricote). 6 Sierra de Ponce. 7 Sierra del Gigante. 8 Jabalucz. 9 Grajales-Mentidero Unit. 10 Ventisquero Unit. 11 Noalejo. 12 Benalúa de las Villas. 13 Zegri. 14 Sierra Elvira. 15 Sierra Harana. 16 Camarena-Lanchares Unit. 17 Gaena Unit. 18 Sierra Gorda. 19 Torcal de Antequera

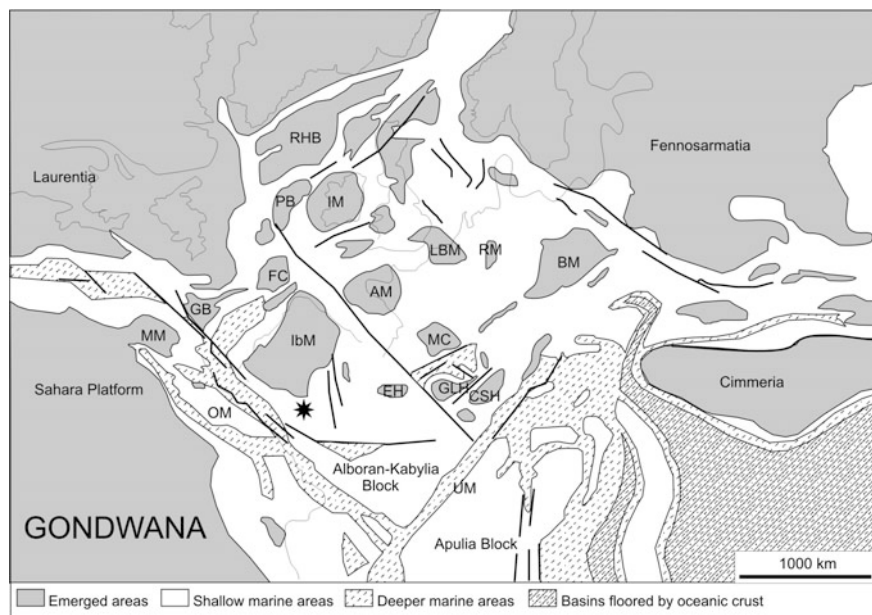


Fig. 2.6 Palaeogeographic reconstruction for the Toarcian in the westernmost Tethys based on Ziegler (1988) with location of the South Iberian Palaeomargin (star). Note AM Armorican Massif; BM Bohemian Massif; CSH Corsica-Sardinia High; EH Ebro High; FC Felmish Cap; GB Gran Bank; GLH Golf de Lyon High; IbM Ibeian Massif; IM Irish Massif; LBM London Brabant Massif; MC Massif Central; MM Moroccan Massif; OM Oran Massif; PB Porcupine Bank; RHB Rockall-Hatton Bank

rhythmite of marly limestones and marls, although locally only marls are present; and (2) The upper member, which is less potent, with mainly marly ammonitico rosso facies. The lateral and vertical changes in facies and thickness between both members are frequent. In some sectors this formation has very significant gaps affecting part or even the entire time interval (Domerian-Aalenian). The total thickness varies generally between a few metres and 250 m, although in some parts of the Median Subbetic can reach more than 500 m (Nieto et al. 2004).

This formation was likely deposited in a pelagic or hemipelagic environment below the base level of the storm surge, but close to it. The Toarcian Oceanic Anoxic Event (T-OAE) has been recognised in the Zegrí Fm (e.g., Jiménez et al. 1996; Reolid 2014) in the Serpentinum ammonite Zone (according to the Submediterranean ammonite biozonation, Fig. 2.7). In the central part of the Median Subbetic, submarine volcanic rocks are intercalated in the Zegrí Fm, in an WSW-ENE alignment, locally reaching accumulated thicknesses of several hundred metres. These volcanic rocks are mainly pillow lavas of a transitional-alkaline composition related to extensional crustal thinning. Based on geochemical data, Vera et al. (1997) indicated that these Jurassic submarine basic volcanic rocks are mainly ultrapotassic, with some showing shoshonitic affinities. Magmas were

		Boreal	Subboreal	Submediterranean	Mediterranean
TOARCIAN	Middle	<i>compactile</i>	<i>variabilis</i>	<i>gradata</i>	
		<i>braunianus</i>	<i>bifrons</i>		
	<i>commune</i>				
	Early	<i>falciferum</i>	<i>serpentinum</i>		<i>levisoni</i>
<i>antiquum</i>		<i>tenuicostatum</i>		<i>polymorphum</i>	
PLI.	Up.	<i>viligaensis</i>	<i>spinatum</i>	<i>emaciatum</i>	

Fig. 2.7 Uppermost Pliensbachian and Toarcian subdivisions and correlation of ammonite zones for Borela, Subboreal, Submediterranean and Mediterranean domains based on Elmi et al. (1997), Zakharov et al. (1997) and Page (2003)

generated in the upper mantle, passed through a thick continental crust, and were extruded at the sea-floor.

The lithostratigraphic equivalent in the Intermediate Domain is the Fm Baños (Ruiz-Ortiz 1980). In the section type has a thickness of 1000 m and is made up of thin-bedded limestones, among which centimetre marly levels are intercalated. Its deposition occurred in a pelagic environment of some tens to hundred metres deep (Ruiz-Ortiz 1980).

In the Penibetic, the Lower and Middle Jurassic is represented by a basal dolomite (Dolomía Jarastepar) on which the Endrinal Fm (Martín-Algarra 1987) is located. This formation is 200–300 m thick and likely misses the Upper Pliensbachian and Toarcian deposits equivalent to the Zegrí Fm in this palaeogeographic domain.

According to available biostratigraphic data (see Rivas 1972; Jiménez 1986; Molina 1987; Nieto 1997; among others), the top of the Zegrí Fm is heterochronous, with a large stratigraphic hiatus in wide sectors of the Subbetic, this hiatus covers at least the entire Aalenian (Ruiz-Ortiz et al. 1997). In some units this hiatus can extend from the Upper Toarcian to the Lower Bajocian.

The sedimentary rocks superimposed on the Zegrí Fm can be included in two large groups. First, those deposited in shallow carbonate platforms, which have been called Jabalcuz Fm (Intermediate Domain), Camarena Fm (Subbetic) and Endrinal Fm (Penibetic); and second, typical sediments of hemipelagic or pelagic environments, included in the Veleta, Ammonitic Rosso Superior, Jarropa and Ricote Fms, all of them of the Subbetic.

The similarity of the Zegrí Fm facies throughout the subbetic domain reveals that the fracture of the large liassic platform in the middle-upper Carixian and the generalised onset of pelagic sedimentation in the subbetic basin did not involve, on the contrary, substantial variations of the facies that were deposited from some areas to others. A limestone-marl rhythmite sedimentation is generalised and only in the areas closest to the Prebetic platform, in the Intermediate Domain (Baños Fm), the sedimentation is more calcareous. The rate of subsidence and accordingly the accumulated thickness in the Middle Jurassic is the only factor that makes a

difference between the incipient Subbetic subdomains that will end up being individualised, from the point of view of the nature of the facies.

The correlation between the sections of the Zegrí Fm analyzed in previous published papers is based mainly on lithostratigraphic criteria, since there is no precise dating that can reveal all the possible gaps within the formation as in the age of its top in each outcrop. On the other hand, the overlapping of overthrust nappes characteristic of the structure of the Betic Cordillera, and the lack of solidly argued palynospastic restitutions, makes difficult the elaboration of palaeogeographic reconstructions that otherwise, with the knowledge of the currently available stratigraphic architecture, could be realised. Even with the difficulties exposed, the few sections in which the Zegrí Fm shows a great contrast of thickness without significant tectonic translations between them, are located at such great distances (between 20 and 30 km).

The boundary faults of blocks and palaeogeographic subdomains would have directions around N 70° E (e.g., Nieto 1997). These faults were responsible of the changes in thickness that are detected in directions perpendicular to them. In addition, there would be other transverse faults (transfer faults) that would have directions close to the N-S. This type of faults would explain the thickness changes in an approximately E-W direction.

Nieto et al. (2002) identified gravitational deposits linked to small-slip and low lateral continuity faults, with approximately N-S directions., corresponding to outcrops with physical continuity belonging to a same subbetic subdomain (Intermediate Domain). In contrast, it is remarkable that uptodate there are not known deposits of breccias or other gravitational deposits in relation to what could be major faults, or margin faults, which would constitute the boundaries of the then incipient subbetic subdomains.

References

- Andreo B, García-Hernández M, Martín-Algarra A, Rey J, Vera JA (1991) La sedimentación carbonatada del Lías en la transversal de Vélez Rubio (Subbético Interno). *Rev Soc Geol Esp* 4:165–178
- Azema J, Foucault A, Fourcade E, García-Hernández M, González-Donoso JM, Linares A, Linares D, López-Garrido AC, Rivas P, Vera JA (1979) Las microfacies del Jurásico y Cretácico de las Zonas Externas de las Cordilleras Béticas. Secretariado de Publicaciones de la Universidad de Granada
- Blumenthal M (1927) Versuch einer tektonischen Gliederung der betischen Cordillera von Central-und Südwest (Andalusien). *Eclogae Geol Helv* 20:487–532
- Braga JC (1983) Ammonites del Domerense de la Zona Subbética (Cordilleras Béticas, Sur de España). Ph.D. Thesis, Universidad de Granada
- Comas MC, García-Dueñas V, Jurado MJ (1992) Neogene tectonic evolution of the Alboran Basin from MCS data. *Geo-Mar Lett* 12:144–149
- Dabrio CJ, Polo D (1985) Interpretación sedimentaria de las calizas de crinoides del Carixiense Subbético. *Mediterr, Ser Geol* 4:55–77

- de Gea GA, Aguado R, Ruiz-Ortiz PA (2001) Precisiones bioestratigráficas y cartográficas sobre el Cretácico de la Unidad de Cárceles-Carlucu. Cordilleras Béticas. Sur de Bedmar. *Geotemas* 3 (1):169–174
- Elmi S, Rulleau L, Gabilly J, Mouterde R (1997) Toarcien. In: Carieu E, Hantzpergue P (coord) *Biostratigraphie du Jurassique Ouest-Européen et Méditerranéen*, vol 17. Bulletin Centre Recherche Elf Exploration Production Mémoire, pp 25–36
- Estévez A, Rodríguez-Fernández J, Sanz de Galdeano C, Vera JA (1982) Evidencia de una fase compresiva de edad Tortonense en el sector central de las Cordilleras Béticas. *Estud Geol* 38:55–60
- Fallot P (1945) Estudios geológicos en la Zona Subbética entre Alicante y el río Guadiana Menor. Memorias del Instituto Lucas Mallada, CSIC, Madrid
- Fallot P (1948) Les Cordillères Bétiques. *Estud Geol* 8:83–172
- Fontboté JM (1970) Sobre la historia preorogénica de las Cordilleras Béticas. *Cuad Geol Univ Granada* 1:71–78
- García-Dueñas V (1967) Unidades paleogeográficas en el sector central de la Zona Subbética. *Notas Comun Inst Geol Min Esp* 101–102:73–100
- García-Hernández M, González-Donoso JM, Linares A, Rivas P, Vera JA (1978) Características ambientales del Lías inferior y medio en la Zona Subbética y su significado en la interpretación general de la cordillera. In: Reunión sobre la geodinámica de la Cordillera Bética y Mar de Alborán. Universidad de Granada, pp 125–157
- García-Hernández M, Rivas P, Vera JA (1979) El Carixiense en la Zona Subbética. *Cuad Geol Univ Granada* 10:375–382
- García-Hernández M, López-Garrido AC, Rivas P, Sanz de Galdeano C, Vera JA (1980) Mesozoic paleogeographic evolution in the external zones of the Betic Cordillera (Spain). *Geol Mijnbouw* 59:155–168
- García-Hernández M, Lupiani E, Vera JA (1986) La sedimentación liásica en el sector central del Subbético Medio: registro de la evolución de un rift intracontinental. *Acta Geol Hisp* 21:329–337
- García-Hernández M, López-Garrido AC, Martín-Algarra A, Molina JM, Ruiz-Ortiz PA, Vera JA (1989) Las discontinuidades mayores del Jurásico de las Zonas Externas de las Cordilleras Béticas: Análisis e interpretación de los ciclos sedimentarios. *Cuad Geol Ibérica* 13:35–52
- Gibbons W, Moreno T (eds) (2002) *The geology of Spain*. Geological Society, London
- Hermes JJ (1985) Algunos aspectos de la estructura de la Zona Subbética (Cordilleras Béticas, España meridional). *Estud Geol* 41:157–176
- Jiménez AP (1986) Estudio paleontológico de los ammonites del Toarciense inferior y medio de las Cordilleras Béticas (Dactylioceratidae e Hildoceratidae). Ph.D. Thesis, Universidad de Granada
- Jiménez AP, Jiménez de Cisneros C, Rivas P, Vera JA (1996) The early Toarcian anoxic event in the westernmost Tethys (Subbetic): paleogeographic and paleobiogeographic significance. *J Geol* 104:399–416
- Maldonado A, Campillo AC, Mauffret A, Alonso B, Woodside J, Campos J (1992) Alboran Sea Late Cenozoic tectonic and stratigraphic events. *Geo-Mar Lett* 12:179–186
- Martín JM (1980) Las dolomías de las cordilleras Béticas. Ph.D. Thesis, Universidad de Granada
- Martín-Algarra A (1987) Evolución alpina del contacto entre las Zonas Internas y Las Zonas Externas de la Cordillera Bética (sector central y occidental). Ph.D. Thesis, Universidad de Granada
- Martín-Algarra A, Sánchez-Navas A (2000) Bacterially mediated authigenesis in Mesozoic stromatolites from condensed pelagic sediments (Betic Cordillera, Southern Spain). In: Glenn CR, Lucas J, Prévôt-Lucas L (eds) *Marine authigenesis: from global to microbial*. SEPM Special Publication 66, pp 499–525
- Martín-Algarra A, Vera JA (1982) Penibético, las unidades del Campo de Gibraltar, las zonas Internas y las unidades implicadas en el contacto entre Zonas Internas y Zonas Externas. In: García A (ed) *El Cretácico de España*. Editorial Complutense, Madrid, pp 603–632

- Martín-Algarra A, Vera JA (1989) La serie estratigráfica del Penibético. In: Libro homenaje a Rafael Soler. AGGEP, Madrid, pp 67–76
- Martín-Algarra A, Vera JA (1994) Mesozoic pelagic phosphate stromatolites from the Penibetic (Betic Cordillera, Southern Spain). In: Bertrand-Sarfati J, Monty CLV (eds) Phanerozoic Stromatolites II. Kluwer Academic Publications, Dordrecht, pp 345–391
- Martín-Chivelet J, Giménez R, Luperto-Sinni E (1997) La discontinuidad del Campaniense basal en el Prebético: ¿Inicio de la convergencia alpina en la Margen Bética? *Geogaceta* 22:121–124
- Molina JM (1987) Análisis de facies del Mesozoico en el Subbético Externo (Provincia de Córdoba y Sur de Jaén). Ph.D. Thesis, Universidad de Granada
- Molina JM, Nieto LM (2003) Calcarenitas y calizas del Oligoceno superior – Mioceno inferior discordantes sobre el Mesozoico en el Subbético al S. de Jaén. *Geotemas* 5:171–174
- Molina JM, Vera JA, Aguado R (2003) La Formación Majalcorón (Calcarenitas con *Microcodium*, Paleoceno, Subbético): definición y descripción. *Geotemas* 5:175–179
- Molina JM, Vera JA, Aguado R (2006) Reworked *Microcodium* calcarenites interbedded in pelagic sedimentary rocks (Paleocene, Subbetic, southern Spain): paleoenvironmental reconstruction. In: Alonso-Zarza AM, Tanner LH (eds) Paleoenvironmental record and applications of calcretes and palustrine carbonates. Geological Society of America Special Paper 416, pp 189–202
- Nieto LM (1997) La Cuenca subbética mesozoica en el sector oriental de las Cordilleras Béticas. Ph.D. Thesis, Universidad de Granada
- Nieto LM, Molina JM, Ruiz-Ortiz PA (1992) Influencia de la tectónica de fractura y del diapirismo en la sedimentación del Jurásico y Cretácico basal al sur de la provincia de Jaén (Zona Subbética). *Rev Soc Geol Esp* 5:95–111
- Nieto LM, Ruiz-Ortiz PA, Rey J (2002) La ruptura de la plataforma carbonatada liásica en la Unidad de Jabalcuz (Dominio Intermedio, prov. Jaén). *Geogaceta* 32:279–281
- Nieto LM, Molina JM, Ruiz-Ortiz PA (2004) La Formación Zegri: registro de los primeros estadios de una etapa sin-rift en el Jurásico de las Zonas Externas Béticas. *Geotemas* 6:157–160
- Nieto LM, Reolid M, Molina JM, Ruiz-Ortiz PA, Jiménez-Millán J, Rey J (2012) Evolution of pelagic swells from hardground analysis (Bathonian–Oxfordian, Eastern External Subbetic, southern Spain). *Facies* 58:389–414
- O’Dogherty L, Sandoval J, Vera JA (2000) Ammonite faunal turnover tracing sea-level changes during the Jurassic (Betic Cordillera, southern Spain). *J Geol Soc London* 157:723–736
- Page KN (2003) The Lower Jurassic of Europe: its subdivision and correlation. *Geol Surv Den Greenl Bull* 1:23–59
- Pérez-López A, Sanz de Galdeano C (1994) Tectónica de los materiales triásicos en el sector central de la Zona Subbética (Cordillera Bética). *Rev Soc Geol Esp* 7:141–153
- Pérez-Valera F, Sánchez-Gómez M, Pérez-López A, Pérez-Valera LA (2017) An evaporite-bearing accretionary complex in the northern front of the Betic-Rif Orogen. *Tectonics*. doi:10.1002/2016TC004414
- Reolid M (2014) Stable isotopes on foraminifera and ostracods for interpreting incidence of the Toarcian Oceanic Anoxic Event in Westernmost Tethys: role of water stagnation and productivity. *Palaeogeogr Palaeoclimatol Palaeoecol* 395:77–91
- Reolid M, Molina JM (2010) Serpulid-*Frutexites* assemblage from shadow-cryptic environments in jurassic marine caves, Betic Cordillera, Southern Spain. *Palaios* 25:468–474
- Rivas P (1972) Estudio paleontológico-estratigráfico del Lías (Sector Central de las Cordilleras Béticas). Ph.D. Thesis, Universidad de Granada, Short Publication 29, p 77
- Rivas P (1979) Zonación del Carixiense en la Zona Subbética. *Cuad Geol Univ Granada* 10:383–387
- Ruiz-Ortiz PA (1980) Análisis de facies del Mesozoico de las Unidades Intermedias (Entre Castril–prov. Granada y Jaén). Ph.D. Thesis, Universidad de Granada
- Ruiz-Ortiz PA (1981) Sedimentación turbidítica en el Cretácico de las Unidades Intermedias, Zonas Externas de las Cordilleras Béticas. En: Programa Internacional de Correlación

- Geológica, vol 2. Real Academia de Ciencias Exactas, Físicas y Naturales, Madrid, pp 261–279
- Ruiz-Ortiz PA, Nieto LM, Castro JM, Molina JM, Rey J (1997) Discontinuidades mayores y otros eventos jurásicos en el Subbético Externo. Correlación con otros dominios de las Cordilleras Béticas. Sur de España. I Congreso Latinoamericano de Sedimentología, Isla Margarita, Venezuela, Memorias 2, pp 239–248
- Ruiz-Ortiz PA, Bosence DWJ, Rey J, Nieto LM, Castro JM, Molina JM (2004) Tectonic control of facies architecture, sequence stratigraphy and drowning of a Liassic carbonate platform (Betic Cordillera, Southern Spain). *Basin Res* 16:235–257
- Sanz de Galdeano C (1983) Los accidentes y fracturas principales de las Cordilleras Béticas. *Estud Geol* 39:157–165
- Sanz de Galdeano C (1990) Geologic evolution of the Betic Cordilleras in the western Mediterranean, Miocene to the present. *Tectonophysics* 172:107–119
- Sanz de Galdeano C (1997) La Zona Interna Bético-Rifeña. Monografías Tierras del Sur, Universidad de Granada, p 316
- Soria JM (1994a) Sedimentación y tectónica durante el Mioceno de Sierra Arana Mencil y su relación con la evolución geodinámica de la Cordillera Bética. *Rev Soc Geol Esp* 7:193–213
- Soria JM (1994b) Rocas volcanoclasticas submarinas de edad Burdigaliense inferior en el sector del Mencil (Zona Subbética, Cordillera Bética central): contexto sedimentario y tectónico. *Estud Geol* 50:169–178
- Soria JM (1998) La cuenca de antepaís norbética en la Cordillera Bética central (sector del Mencil): evolución tectosedimentaria e historia de la subsidencia. *Rev Soc Geol Esp* 11:23–31
- Vera JA (1986) Las Zonas Externas de las Cordilleras Béticas. En: *Geología de España, Libro jubilar J.M. Ríos 2*. IGME, Madrid, pp 218–251
- Vera JA (1988) Evolución de los sistemas de depósito en el Margen Ibérico de la Cordillera Bética. *Rev Soc Geol Esp* 1:373–391
- Vera JA (2000) El Terciario de la Cordillera Bética: Estado actual de conocimientos. *Rev Soc Geol Esp* 13:345–373
- Vera JA (2001) Evolution of the Iberian Continental Margin. *Mém Mus Natl d’Hist Nat Paris* 186:109–143
- Vera JA (2004) *Geología de España*. Sociedad Geológica de España–IGME, Madrid
- Vera JA, Molina JM (1999) La Formación Capas Rojas: caracterización y génesis. *Estud Geol* 55:45–66
- Vera JA, García-Hernández M, López-Garrido AC, Comas MC, Ruiz-Ortiz PA, Martín-Algarra A (1982) El Cretácico de la Cordillera Bética. In: García A (ed) *El Cretácico de España*. Editorial Complutense, Madrid, pp 515–632
- Vera JA, Molina JM, Montero P, Bea F (1997) Jurassic guyots on the Southern Iberian Continental Margin: a model of isolated carbonate platforms on volcanic submarine edifices. *Terra Nova* 9:163–166
- Vilas L, Dabrio CJ, Peláez JR, García-Hernández M (2001) Dominios sedimentarios generados durante el período extensional Cretácico inferior entre Cazorla y Hellín (Béticas Externas), su implicación en la estructura actual. *Rev Soc Geol Esp* 14:113–122
- Zakharov VA, Bogomolov YI, Ilyna VI, Konstatinov AG, Kurushin NI, Lebedeva NK, Meledina SV, Nikitenko BL, Sobolev ES, Shurygin BN (1997) Boreal zonal standard and biostratigraphy of the Mesozoic of Siberia. *Geol Geofiz* 38:99–128
- Ziegler PA (1988) Evolution of the Arctic-North Atlantic and the Western Tethys. *AAPG Memoir* 43:198

Chapter 3

External Subbetic Outcrops

3.1 Fuente Vidriera Section

The Fuente Vidriera (FV) section is located on a valley slope (38° 03' 19.8" N; 02° 07' 01.7" W), 15 km west of the village of Barranda (Murcia Province), near Caravaca de la Cruz (Fig. 3.1). The study section pertains to the Upper Pliensbachian to uppermost Toarcian of the Zegrí Formation, and contains alternating marls and marly limestones in the lower part with nodular marly limestones in the upper part (Rey and Delgado 2002). During the Toarcian, the FV succession was deposited in the westernmost end of the Tethys, in a passage between the Western Tethys and the proto-Atlantic, at an approximate palaeolatitude of 20° N, near the Iberian Meseta (Fig. 2.6).

The studied Lower Toarcian section contains an approximately 30-m-thick rhythmic succession of soft and hard marlstones, from a calcilutite bed containing *Dactylioceras* (*Eodactylioceras*) *polymorphum*, to a succession of limestone beds just below the *Hildoceras bifrons* Biozone of the Middle Toarcian (Fig. 3.2). Biostratigraphic zonation within the Lower Toarcian of the FV section was mainly obtained based on stratigraphic correlation, due to the scarcity of index fossils (Jiménez 1986; Jiménez and Rivas 2007). Thus, at the FV section the *Dactylioceras polymorphum* (approx. correlated with the *Dactylioceras tenuicostatum*, or *Dactylioceras semicelatum* Biozone) and *Harpoceras serpentinum* (approx. correlated with the *Harpoceras serpentinus*, or *Harpoceras falciferum* Biozone) biozones could be distinguished, although their boundaries are imprecise (Jiménez 1986; Jiménez et al. 1996).

This section was studied from different approaches, as ichnology (Rodríguez-Tovar and Uchman 2010), geochemical analysis for redox, palaeoproductivity and detrital proxies (Rodríguez-Tovar and Reolid 2013), stable isotopes from microfossils (Reolid 2014a) and analysis of pyrite framboids (Gallego-Torres et al. 2015).

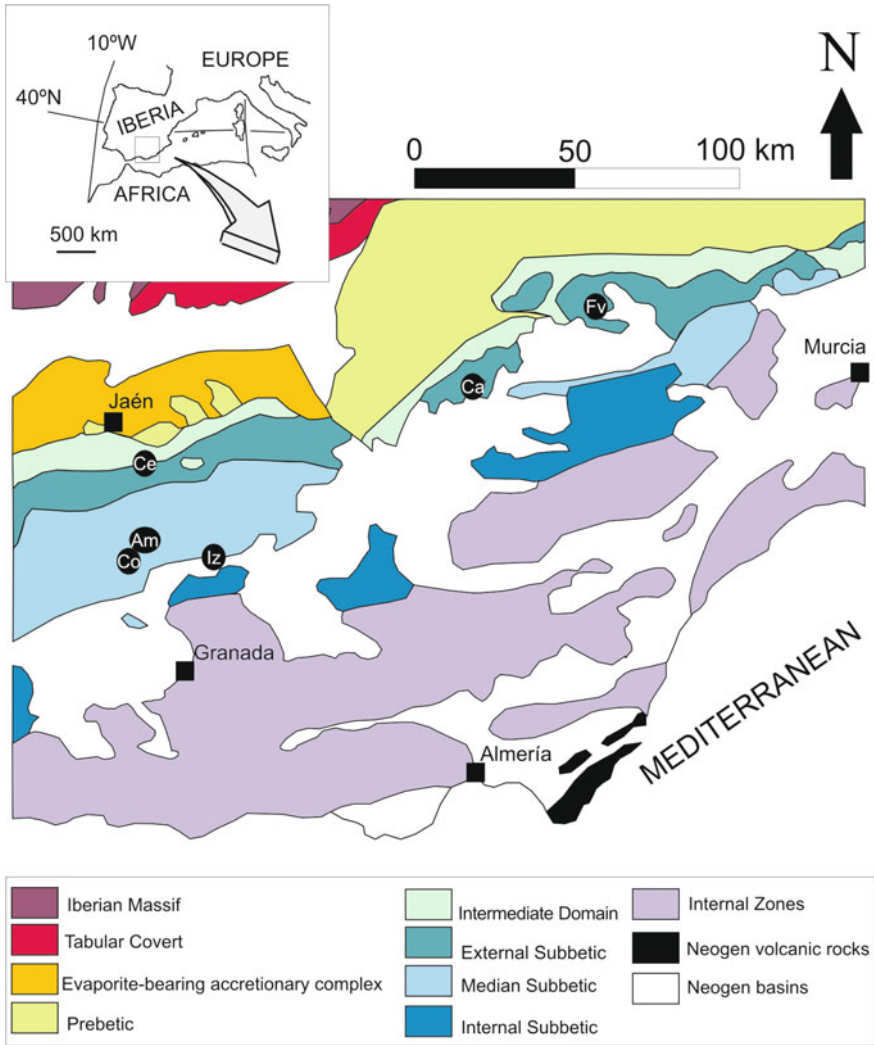


Fig. 3.1 Location of the studied reference sections for the External and Median Subbetic. *Note Ce* La Cerradura; *Am* Arroyo Mingarrón; *Co* Colomera; *Po* Poloria; *Iz* Iznalloz; *Ca* Cueva del Agua; *Fv* Fuente Vidriera

3.1.1 Mineralogy

The studied Uppermost Pliensbachian-Lower Toarcian section is made up of bioturbated soft and hard marlstones with a variable carbonate content (mean value of 42% for soft marls and 54% for indurated marls; Fig. 3.3). Only the sampling bed FV-18 (Figs. 3.2 and 3.3c) presents thin lamination and trace fossils are absent

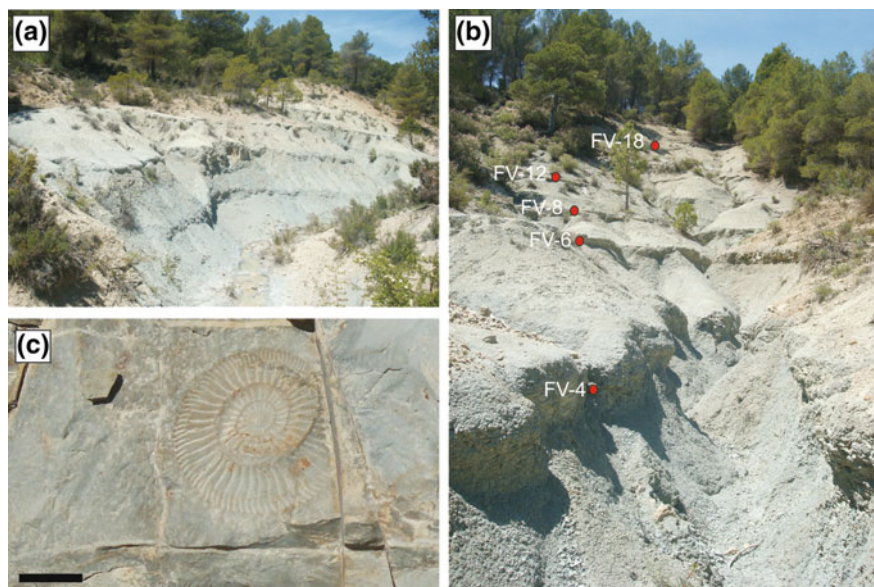


Fig. 3.2 Field appearance of the Lower Toarcian of the Fuente Vidriera section (**a** and **b**), and *Dactylioceras* (**c**) from the base of *Polymorphum* Zone (Scale bar 1 cm)

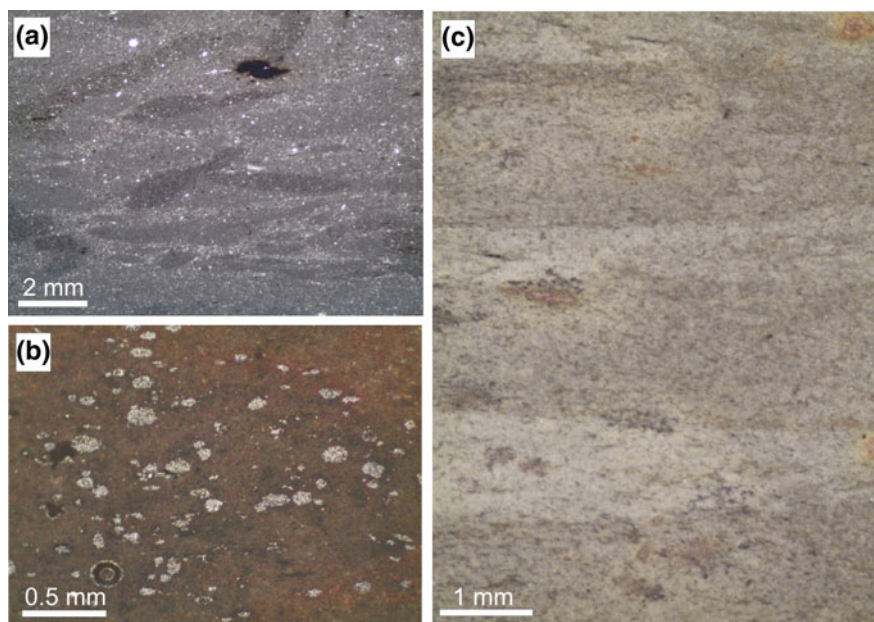


Fig. 3.3 Microfacies from the Fuente Vidriera section. **a** Trace fossils from hard marls. **b** Pyrite framboids (*white masses*) under magnification glasses. **c** Thin laminated marls from FV-18 bed

(Rodríguez-Tovar and Uchman 2010). In thin section they correspond to mudstones with scarce bioclasts (benthic foraminifera, ostracods, small gastropods and echinoderm fragments; Fig. 3.3). A detailed analysis of the micrite under SEM shows nannoplankton remains to be the main carbonate component, in addition to quartz grains, clay minerals and sulphides. Preliminary mineralogical analysis reveals a similar composition in marlstone levels of the FV section, consisting essentially of calcite, quartz and clay minerals (illite, smectite and interstratified illite/smectite, and minority chlorite).

Different occurrences of pyrite (Fig. 3.4) are identified according to classification of Wang et al. (2012): biomorphic aggregates and abiological aggregates. Biomorphic aggregates are represented by pyrite radiolarian moulds and pyrite hexactinellid moulds (see Reolid 2014b), and pyrite laminae growing within coal wood fragments (Fig. 3.4a, b). Abiological aggregates are constituted mainly by pyrite frambooids, with different organisations. Pyrite frambooids are densely packed aggregates of pyrite crystals with a spherical shape. Different types of abiological aggregates are identified: (a) disperse single pyrite frambooids (Fig. 3.4c), (b) polyframbooid aggregates related to trace fossils (Fig. 3.4d, e), and (c) secondary fissures infillings composed by irregular euhedral crystal aggregates (Fig. 3.4f).

Two populations of frambooids are distinguished according to size: frambooids <15 μm and frambooids in the range 60–220 μm . The small-size population corresponds to single pyrite frambooids that appear disperse in the sediment and locally forming small lentoid frambooidal aggregates and dumbbell-shaped aggregates with a length <60 μm . Frambooids are dominated by the submicron-sized octahedral euhedral crystals and the crystals are sometimes only aggregated whereas in other cases they are joined with pyrite cement.

The largest pyrite frambooids or macroframbooids (s. Wei et al. 2015) are commonly located in large polyframbooid aggregates commonly related to trace fossils and locally coal wood fragments (see Gallego-Torres et al. 2015). The polyframbooid aggregates related to trace fossils are dumbbell-shaped aggregates and lenticular-shaped aggregates (s. terminology of Pingkang et al. 2012) with a length of 70–200 μm . The pyrite crystals are almost exclusively octahedron with sizes reaching 8 μm and they are commonly joined by pyrite cement. Large pyrite frambooids are locally oxidised to goethite.

The proportion of pyrite frambooids <5 μm in this population along the studied interval (uppermost Pliensbachian-Lower Toarcian) ranges from 13.5 to 19.0%. As a whole, frambooids >10 μm are scarce, 98.5% of all measured frambooids are <10 μm in size (see more details in Gallego-Torres et al. 2015).

3.1.2 Trace Fossils

Ichnological analysis of the section shows a relatively abundant and moderately diverse trace-fossil assemblage (Fig. 3.5) composed of *Alcyonidiopsis* isp., *Chondrites* isp., *Nereites* isp., *Palaeophycus heberti*, *Planolites* isp., *Teichichnus*

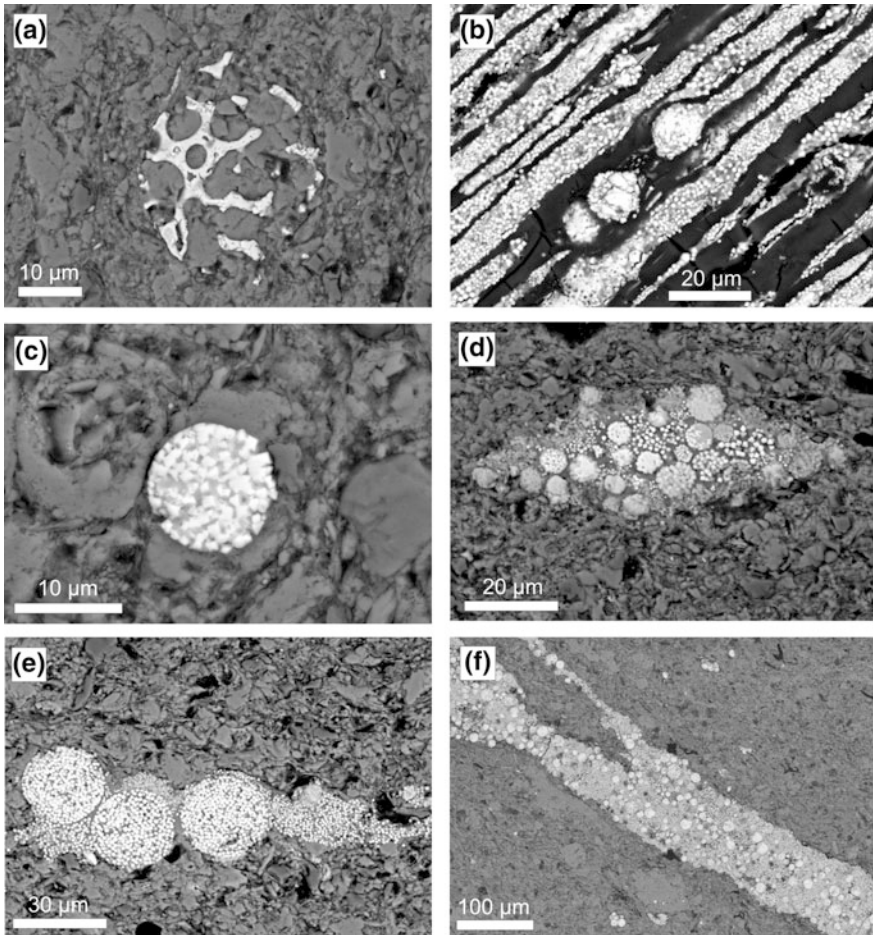
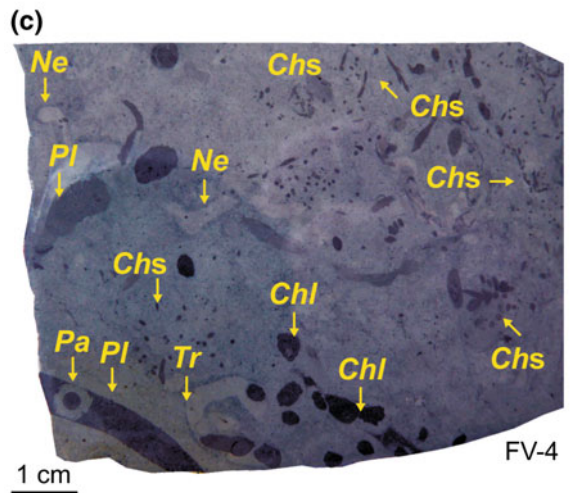
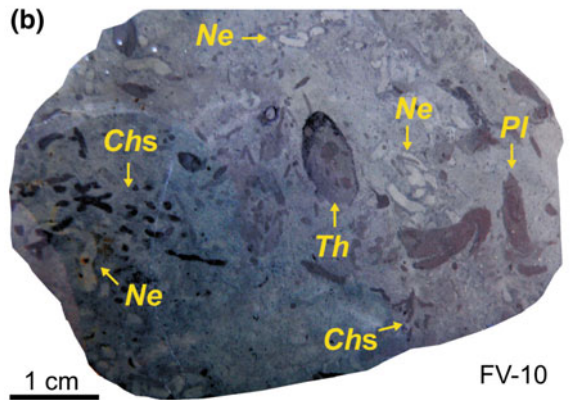
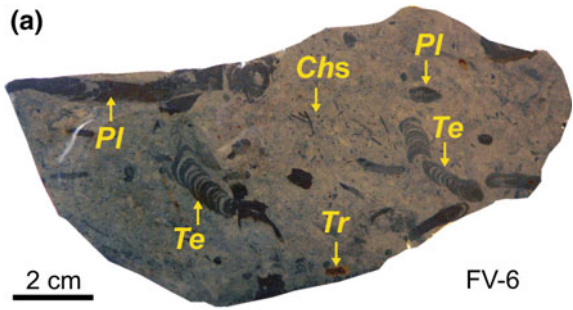


Fig. 3.4 Backscattered electron images of pyrite from thin sections from Fuente Vidriera. **a** Pyrite radiolarian mould. **b** Pyrite laminae developed within a coal wood fragment (FV-20). **c** Single pyrite framboid (FV-14). **d** Lenticular-shape pyrite polyframboid aggregate (FV-14). **e** Dumbbell-shape pyrite polyframboid aggregate (FV-14). **f** Polyframboid aggregates infilling a small trace fossil (*Chondrites*-like, FV-3). Modified from Gallego-Torres et al. (2015)

isp., *Thalassinoides* isp., and *Trichichnus linearis*, with only local lamination in FV-18 (Rodríguez-Tovar and Uchman 2010). The trace-fossil assemblage is generally homogenous, without significant changes in trace-fossil abundance and composition. *Chondrites*, especially the smaller forms, and *Trichichnus* are the most abundant ichnotaxa; *Planolites*, *Thalassinoides*, and *Nereites* are less common; and *Palaeophycus* and *Teichichnus* are comparatively rare. All of these ichnotaxa occur throughout the section and in all lithofacies.

Fig. 3.5 Polished slabs from Fuente Vidriera illustrating trace fossils. Note *Pl* *Planolites* isp. *Pa* *Palaeophycus* isp.; *Chs* *Chondrites* isp. (small); *Chl* *Chondrites* isp. (large); *Ne* *Nereites* isp.; *Te* *Teichichnus* isp.; *Th* *Thalassinoides* isp.; *Tr* *Trichichnus* isp. Pictures by Uchman and Rodríguez-Tovar



Some trace fossils display repetitive crosscutting relationships, *Palaeophycus* crosscuts *Planolites* and *Thalassinoides*, *Thalassinoides* crosscuts *Nereites*, and *Chondrites* and *Trichichnus* crosscut all other trace fossils. Small *Chondrites*

crosscut the larger ones, and *Trichichnus* crosscuts both of them. Thus, a well-developed endobenthic multi-tiered community is characterised by: (a) an upper tier represented by homogenised sediment—individual burrows difficult to discern, (b) a middle tier with a relatively diverse trace-fossil assemblage of mainly vagile deposit feeders—*Nereites* and *Thalassinoides* record the activity of mobile organisms in the uppermost part of this tier, whereas *Alcyonidiopsis*, *Planolites*, *Teichichnus*, and *Palaeophycus* indicate the activities of mobile deposit feeders, and carnivorous or omnivorous invertebrates at a slightly deeper level, and (c) a lower tier with activities of semisessile deposit feeders, comprising small and large *Chondrites* as well as *Trichichnus*.

3.1.3 Foraminiferal and Ostracod Assemblages

The recorded foraminiferal taxa are exclusively benthic, belonging to the suborders Involutinina, Lagenina, Milionina, Robertinina, Spirillinina, and Textulariina (Fig. 3.6). The benthic assemblage consists predominantly of calcareous forms (mean value 82%) and scarce agglutinated shell type forms, comprising 32 genera. The calcareous group includes forms with three wall types: calcitic perforated, represented by Lagenina, Involutinina, and Spirillinina; porcelaneous Milionina; and aragonitic, represented by Robertinina. Textulariina represent the agglutinated foraminifera. In the average composition of the foraminiferal assemblage the following genera prevail: *Dentalina* (25%), *Eoguttulina* (15%), *Spirillina* (9%), *Reinholdella* (8%), *Lenticulina* (6%), *Ammobaculites* (4%) and *Trochammina* (3%). The abundance of foraminifera generally ranges between 500 and 1500 specimens/100 g and in ostracods is usually lower than 500 specimens/100 g (Fig. 3.7). However, three maxima are reached in foraminiferal abundance with more than 2500 specimens/100 g (FV-4, FV-13 and FV-19). Especially relevant is the bed FV-18 where minimum values of abundances of foraminifera are reached (167 foraminifera/100 g). Regarding the diversity values calculated from foraminiferal assemblages, the α -diversity presents values between 4 and 7, except in beds FV-8 (3.2) and FV-18 (2.0) where lowest values are recorded (Reolid 2014a). Foraminiferal preservation is characterised by micritic infilling. The aragonitic shells of *Reinholdella* are frequently preserved as epigenised calcite shells. Processes of bioerosion or abrasion/dissolution were not identified. Analysis of taphonomic features from the foraminiferal assemblage evidences good preservation and a virtual lack or low incidence of reworking, this being an autochthonous or para-autochthonous assemblage. Therefore, the foraminiferal assemblages can be interpreted as a primary signal, linked with the palaeoenvironmental and palaeoecological conditions.

Respect to the ostracods (Fig. 3.8), the top of the Pliensbachian is dominated by Family Pontocypridae (41%, mainly *Liasina lanceolata*) and secondarily Family Healdiidae (28%, mainly *Ogmoconcha contractula* and *O. amalthei*) and Bairdiidae (24%). The Polymorphum Zone begins with high values of Family Bairdiidae

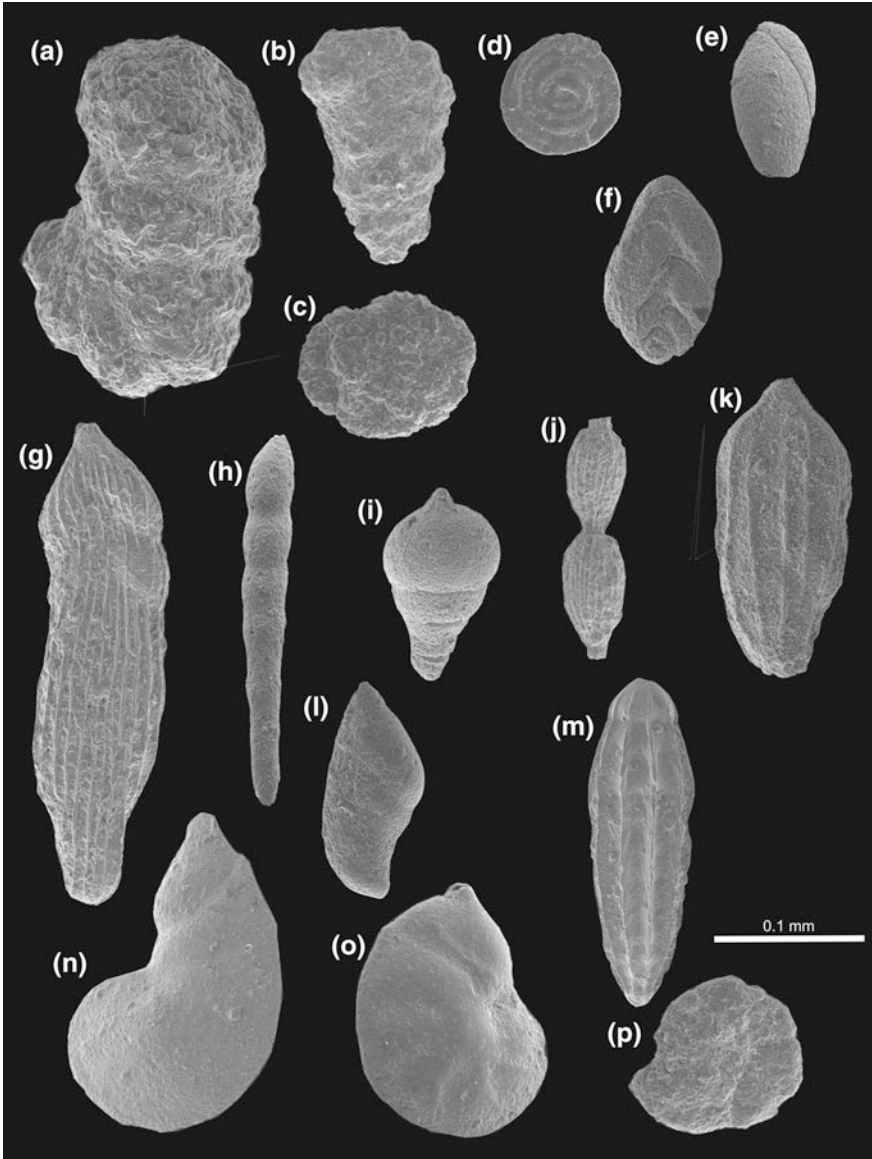


Fig. 3.6 Secondary electron images of foraminifera from Fuente Vidriera section. **a** *Ammobaculites*. **b** *Textularia*. **c** *Trochammina*. **d** *Spirillina*. **e** *Eoguttulina*. **f** *Berthelinella*. **g** *Lingulina*. **h** *Dentalina*. **i** *Pseudonodosaria*. **j** *Nodosaria*. **k** *Ichtyolaria*. **l** *Planularia*. **m** *Marginulina*. **n** *Marginulinopsis*. **o** *Lenticulina*. **p** *Reinholdella*

(28%) and Family Cytherellidae (27%, mainly *Cytherella toarcensis*) and secondarily by families Healdiidae (20%) and Pontocypridae (15%). The ostracod assemblage of the lower part of the Serpentinum Zone is characterised by high

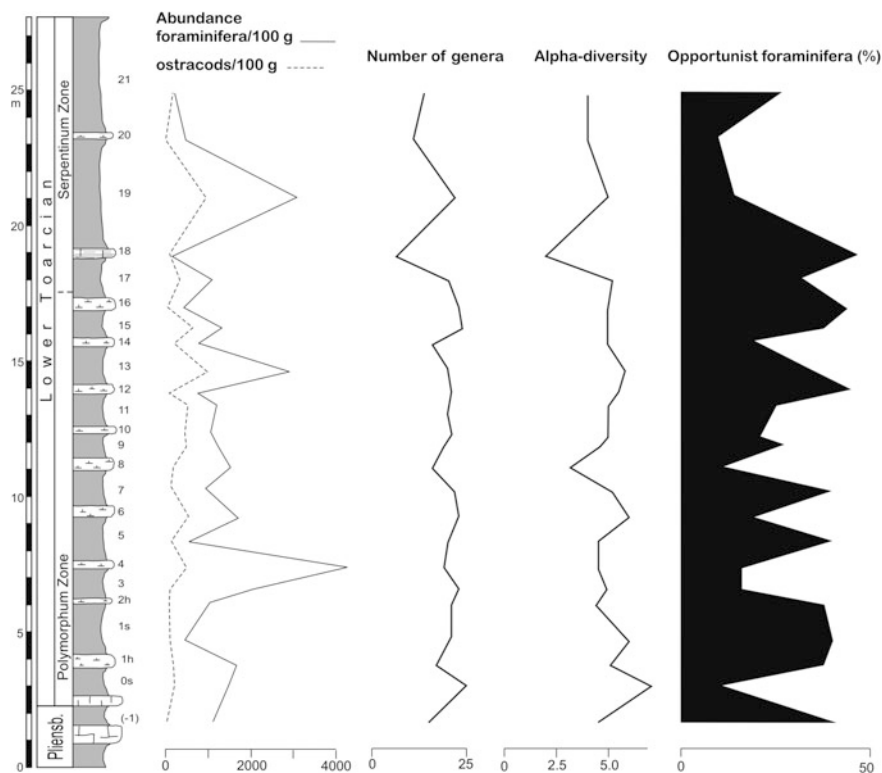


Fig. 3.7 Fuente Vidriera section and the stratigraphic distribution of abundance (specimen/100 g) of foraminifera and ostracods, diversity (number of genera and α -diversity) and proportion of opportunistic foraminifera

values of Family Cytherellidae (75%), followed by Pontocypridae (14%), Healdiidae (6%) and Bairdiidae (4%). Family Healdiidae disappears during the microfossil barren interval and the negative carbon isotopic excursion (CIE). The abundance of ostracods presents two relative maximums reaching almost 1000 specimens/100 g (FV-13 and FV-19). The minimum values of abundances of ostracods are reached at FV-18 bed (118 ostracods/100 g; Fig. 3.7). Both disarticulated and articulated valves were recorded frequently.

Radiolarids (*Spumellaria* and *Nassellaria*) are scarce and only preserved as pyritised casts (Reolid 2014b).

The abundance and diversity of foraminiferal assemblages throughout the section reveal an important decrease in the number of foraminifera per 100 g and in α -diversity in sampling layer FV-18 (Fig. 3.7). The presence of ostracods also decreases in this level within the lower part of the Serpentinum Zone.

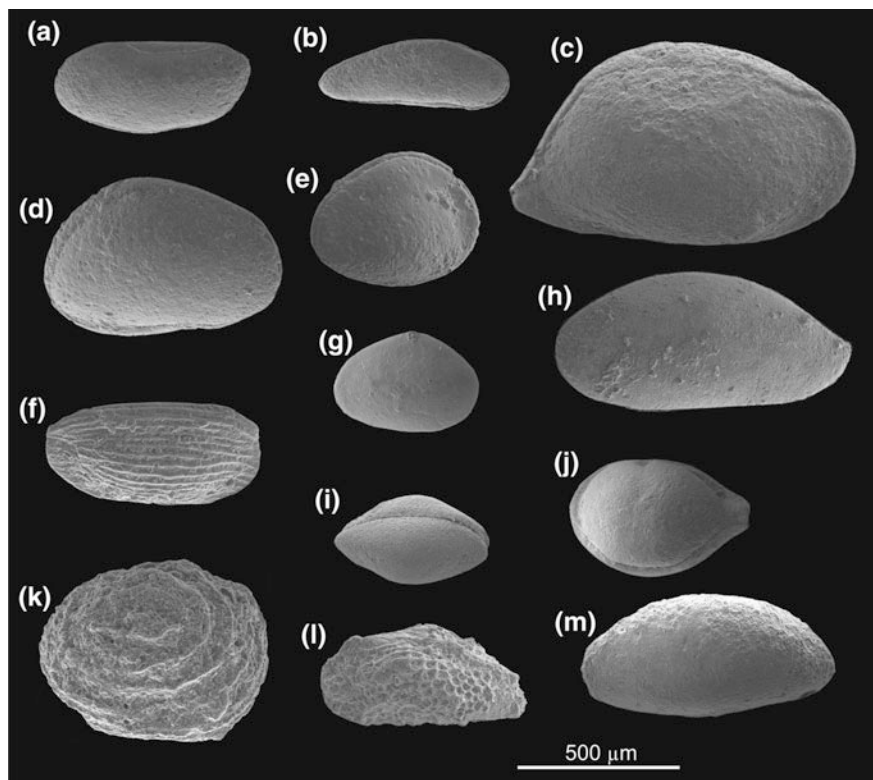


Fig. 3.8 Secondary electron images of ostracods from Fuente Vidriera section. **a** *Pontocyprrella*. **b** *Liasina*. **c** *Bairdia*. **d** and **e** *Ogmococoncha*. **f** *Monoceratina*. **g** *Ogmococoncha*. **h** *Bairdia*. **i** *Ogmococonchella*. **j** *Bairdia*. **k** *Polycope*. **l** *Rutlandella*. **m** *Isobithocypris*

3.1.4 Stable Isotopes

Isotopic values from bulk rock

The $\delta^{13}\text{C}$ values obtained from whole sample undergo a progressive increase from the Upper Pliensbachian to level FV-8, from 0.05 to 1.41‰ (Fig. 3.9). Later, the $\delta^{13}\text{C}$ values show a slight drop, and then increase just until FV-14, where they reach 1.91‰. After this maximum, the values gradually diminish to the top of the studied interval.

The $\delta^{18}\text{O}$ values present a more irregular pattern, with short fluctuations between -4.08 and -3.08 ‰ (Fig. 3.9). The values decrease slightly from FV-12 to the top (<4 ‰). The $\delta^{18}\text{O}$ value in FV-18 is slightly higher (-3.39 ‰).

Isotopic values from foraminifera and ostracods

The genera of foraminifera selected for isotopic analyses, *Lenticulina* and *Dentalina*, represent different microhabitats and are common foraminifera in the

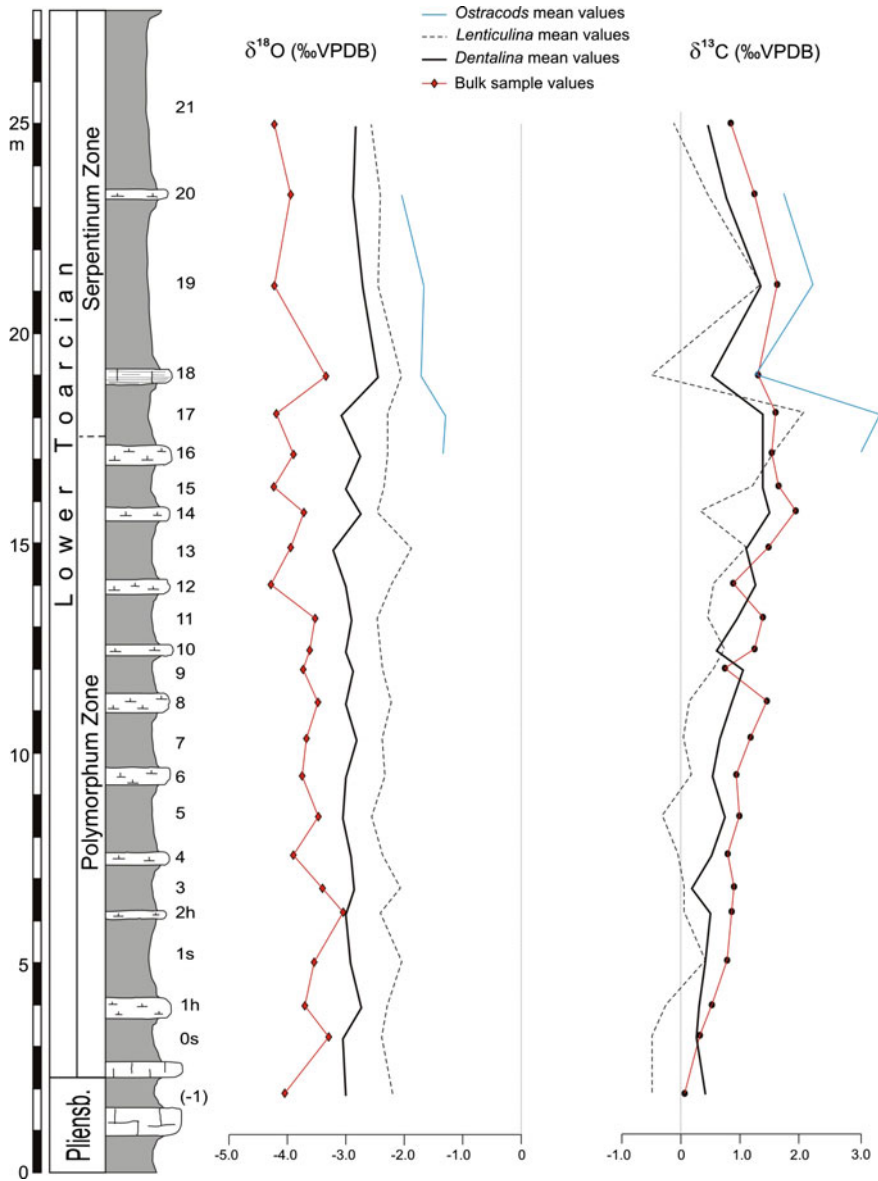


Fig. 3.9 Stratigraphic distribution of the $\delta^{13}\text{C}$ and $\delta^{18}\text{O}$ from bulk sample, and the mean values of $\delta^{13}\text{C}$ and $\delta^{18}\text{O}$ from *Dentalina*, *Lenticulina* and bairdioid ostracods. Modified from Reolid (2014a)

fossil assemblage. *Lenticulina* is an opportunist form with an epifaunal to deep infaunal microhabitat related to redox fluctuations within the sediment (Tyszka 1994; Reolid et al. 2008, 2012b; Reolid and Martínez-Ruiz 2012; Rita et al. 2016). *Dentalina* is a specialist adapted to shallow infaunal lifestyle (e.g., Rey et al. 1994;

Reolid et al. 2013a). The ostracod *Bairdia* has been selected also for isotopic analyses. Bairdioids require open-marine conditions and present high palaeoecologic tolerance (Fohrer and Samankassou 2005). *Bairdia* is a shallow infaunal to epifaunal form (Sohn 1960) with opportunist behaviour (Fohrer and Samankassou 2005).

The mean values of $\delta^{13}\text{C}$ on *Dentalina* tests show increasing values from Upper Pliensbachian (0.41‰) to bed FV-14 (1.50‰), with subsequent constant values up to bed FV-17. The bed FV-18 presents a decreasing $\delta^{13}\text{C}_{Dentalina}$ value (0.55‰ with a diminishing of -0.81‰ ; Fig. 3.9).

The mean values of $\delta^{13}\text{C}$ obtained on *Lenticulina* tests show a trend similar to that of $\delta^{13}\text{C}_{Dentalina}$ yet more accentuated (Fig. 3.9). Values in the Upper Pliensbachian go from slightly lower $\delta^{13}\text{C}$ values (-0.50‰) than in $\delta^{13}\text{C}_{Dentalina}$ increasing to bed FV-17 (2.07‰). The bed FV-18 features an important negative isotopic excursion on values of $\delta^{13}\text{C}_{Lenticulina}$ (-0.49‰ , a drop of -2.56‰). After bed FV-18, the $\delta^{13}\text{C}_{Lenticulina}$ recovers. Values of $\delta^{13}\text{C}_{Lenticulina}$ and $\delta^{13}\text{C}_{Dentalina}$ are usually lower than $\delta^{13}\text{C}$ from the bulk rock.

As an overall pattern, values of $\delta^{13}\text{C}_{\text{ostracods}}$ are higher than in foraminifera and the bulk rock, but show an abrupt negative fluctuation in bed FV-18 parallel to the curve traced by $\delta^{13}\text{C}_{Lenticulina}$.

Regarding $\delta^{18}\text{O}$, the values from both *Dentalina* and *Lenticulina* show minor fluctuations in the studied interval (Fig. 3.9), with a mean difference of 0.56‰; $\delta^{18}\text{O}_{Dentalina}$ (-3.22 to -2.45‰) was lower than $\delta^{18}\text{O}_{Lenticulina}$ (-2.56 to -2.02‰). The $\delta^{18}\text{O}$ values obtained from the bulk rock (-4.28 to -3.08‰) present a curve with stronger fluctuations than the values obtained on foraminiferal shells, which were the most negative. A short increase in $\delta^{18}\text{O}$ values was seen for bed FV-18. The $\delta^{18}\text{O}_{\text{ostracods}}$ values are higher than those obtained on foraminifera and bulk rock.

3.1.5 Geochemical Proxies

Detrital proxies—Together with the mineral composition of the studied succession, some element/Al ratios (Si/Al, K/Al, Rb/Al, Ti/Al, and Zr/Al), have been used as proxies for the reconstruction of detrital input, with the differentiation between fluvial contribution (K/Al and Rb/Al, Chester et al. 1977), and eolian transport (Zr/Al, Si/Al and Ti/Al, Pye 1987). Respect to the geochemical proxies used for the reconstruction of detrital input, K/Al, Rb/Al, and Si/Al show only minor changes (Fig. 3.10). Conversely, the Ti/Al and above all Zr/Al ratios temporarily manifest some increases. The Zn/Al ratios exhibit its highest values in the upper part of the section, around sample FV-18, though other significant increases are noted in the middle (samples FV-7 and FV-8; K/Al), and lower parts (samples FV-1 and FV-2; Ti/Al and Zr/Al) (Rodríguez-Tovar and Reolid 2013).

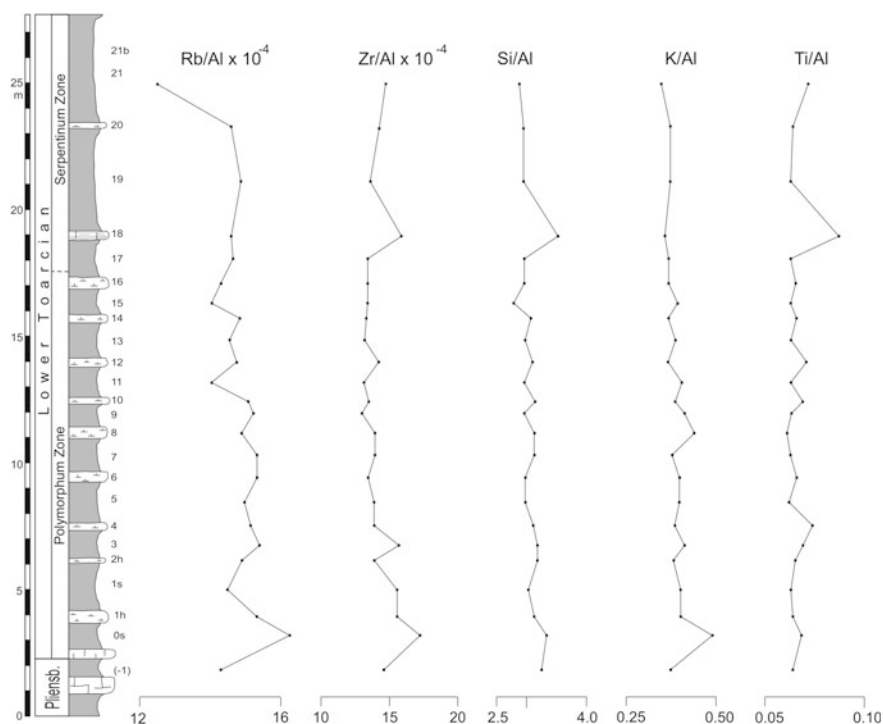


Fig. 3.10 Stratigraphic distribution of detrital proxies for eolian (Zr/Al, Si/Al and Ti/Al) and fluvial (K/Al and Rb/Al) inputs. Modified from Rodríguez-Tovar and Reolid (2013)

Palaeoproductivity proxies—The geochemical proxies commonly used to interpret relative fluctuations in productivity are P/Ti ratio (Latimer and Filippelli 2001; Robertson and Filippelli 2008; Reolid and Martínez-Ruiz 2012; Reolid et al. 2012a, b) and Sr/Al ratio (Sun et al. 2008). Specially important is the relationship of uranium with organic matter in the sediment (Baturin 2002), as uranium may form a complex with dissolved fulvic acid in hemipelagic sediments (Nagao and Nakashima 1992). In this sense, high values of U/Al ratio would be congruent with high values in other palaeoproductivity proxies. Stratigraphic distribution of these proxies indicates peaks with relatively high values of Sr/Al, Ba/Al, U/Al and P/Ti ratios, as well as high total organic carbon (TOC) (Fig. 3.11). The Sr/Al, U/Al, P/Ti and TOC clearly increase in FV-18. In the case of the Sr/Al ratio, the trends seen for soft and hard marlstones levels differ, with values generally higher in hard marlstones than in soft marlstones. In both cases, maximum values are in FV-8 and FV-18. In the case of P/Ti, no significant differences exist between the highest values with respect to the background. TOC manifests minor fluctuations throughout the section (usually <0.4 wt%), with the exception of bed FV-18, where TOC is nearly 1% (0.987 wt%) (Rodríguez-Tovar and Reolid 2013).

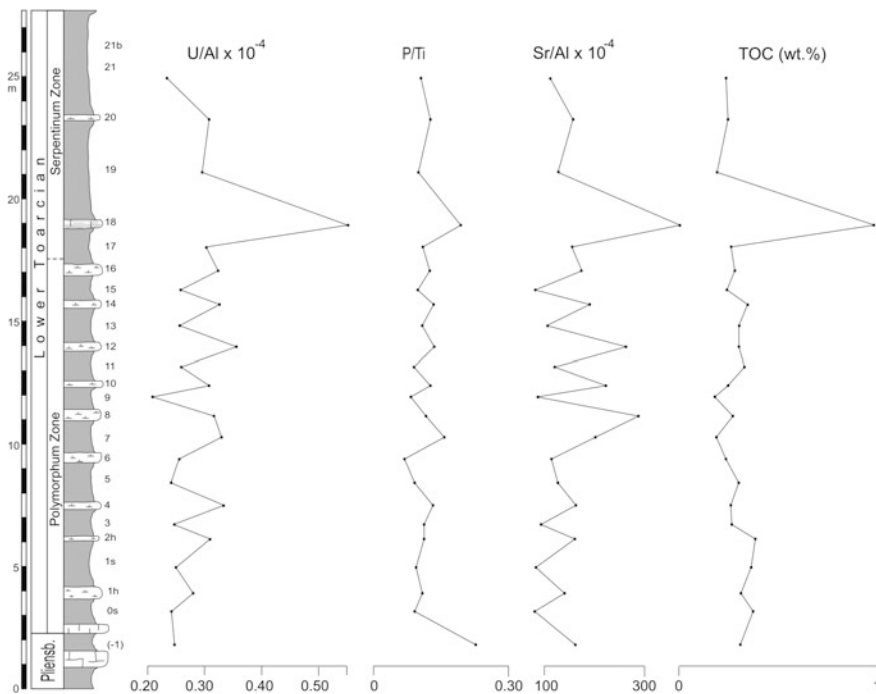


Fig. 3.11 Stratigraphic distribution of selected palaeoproductivity proxies. Data obtained retrieved from Rodríguez-Tovar and Reolid (2013) and Reolid (2014a)

Redox proxies—Diverse geochemical ratios, Co/Al, Cu/Al, Cr/Al, V/Al, Ni/Al, Mo/Al, and U/Th, have been selected focusing on those which tend to be less soluble under reducing conditions (Rodríguez-Tovar and Reolid 2013; Reolid et al. 2015a). They have been extensively used as redox proxies to interpret palaeoxygenation conditions at time of sediment deposition (Wignall and Myers 1988; Nagao and Nakashima 1992; Calvert and Pedersen 1993; Powell et al. 2003; Siebert et al. 2003; Gallego-Torres et al. 2007, 2010; Jiménez-Espejo et al. 2007; Yilmaz et al. 2010; Reolid et al. 2012a, b). Some redox-sensitive metals are delivered to the sediment in association with organic matter (Ni, Cu, and Zn). These redox-sensitive elements tend to coprecipitate with sulfides (mainly pyrite) and are not usually remobilised during diagenesis in the absence of post-depositional replacement of oxydizing agents (Tribouillard et al. 2006). In the case of the manganese, high concentrations indicate an oxidation front that penetrates the sediments (e.g., Martínez-Ruiz et al. 2000, 2003). Their stratigraphic evolution shows some fluctuations along the succession (Fig. 3.12), the most significant ones being found in samples FV-8 and FV-18. In FV-8, relatively high values are registered for Ni/Al, V/Al, Cu/Al, Mo/Al, and Co/Al, but without changes in Mn/Al (Rodríguez-Tovar and Reolid 2013). In this level, analysis of grains from sieved samples revealed Cu and Fe sulfides including pyrite, chalcopyrite and covellite. In FV-18, high values

are recognised for Cr/Al, Mn/Al, Ni/Al, V/Al, and U/Th, while other redox proxies do not increase (Co/Al, Cu/Al, and Mo/Al). A maximum in Mn/Al, together with an increase in Fe/Al, are registered at this sample level. Analysis of grains from sieved samples reveals common goethite grains in sample FV-18 with the shape of pyrite crystals (large framboids and euhedral cubic crystals); whereas in sample FV-19 pyrite is totally absent, and goethite grains are very common in the >200 µm fraction.

3.1.6 Interpretation

The T-OAE record from the Fuente Vidriera section

The selected Lower Jurassic section represents a deep-marine setting in a passage between the Western Tethys and the Atlantic Tethys (Fig. 2.6), revealing of special interest to interpret the Early Toarcian Oceanic Anoxic Event at the westernmost end of the Tethys.

Trace fossil analysis evidences a well-developed endobenthic multitiered community interpreted based on the presence of a relatively abundant, diverse, and continuous trace-fossil assemblage in the section, composed by *Alcyonidiopsis*, *Chondrites*, *Nereites*, *Palaeophycus*, *Planolites*, *Teichichnus*, *Thalassinoides*, and *Trichichnus*, with only local lamination (FV-18) (Rodríguez-Tovar and Uchman 2010). Oxidic or slightly dysoxic bottom waters were inferred, as well as the absence of anoxic conditions attending to trace fossils (Rodríguez-Tovar and Uchman 2010). In this work we follow the recommendation of Tyson and Pearson (1991) for oxygenation levels: oxidic (8.0–2.0 ml/l O₂), dysoxic (2.0–0.2 ml/l O₂), suboxic (0.2–0.0 ml/l O₂) and anoxic (0.0 ml/l). Thus, in view of ichnological evidence, minor incidence of the T-OAE on the macro-endobenthic environment in this part of the westernmost Tethys was interpreted, and the worldwide anoxic phenomena related to the T-OAE, determining significant biotic changes, including global mass extinctions, was not recognised by the ichnofossil assemblages. However, the record of laminated bed without trace fossils (bed FV-18) points to adverse conditions for infauna temporarily. The record of thinly laminated marls and marly limestones has been related to anoxic conditions in Lower Toarcian deposits from other regions (Parisi et al. 1996; Hermoso et al. 2009; Izumi et al. 2012).

Data obtained from the ratios of the detrital proxies through the Fuente Vidriera section allow the interpretation of the incidence of the detrital input, and the main source of detrital material, as eolian (Zr/Al, Si/Al and Ti/Al, Pye 1987) or fluvial (K/Al and Rb/Al, Chester et al. 1977) contribution (Fig. 3.10). According to the absence of significant variations in the K/Al, Rb/Al, and Si/Al ratios, a context of uniform detrital input could be inferred. This interpretation accords with the generalised homogeneous lithology through the studied succession, mainly consisting of a rhythmic succession of soft and hard marlstones, and the absence of significant sedimentary structures (except for bed FV-18 characterised by the presence of

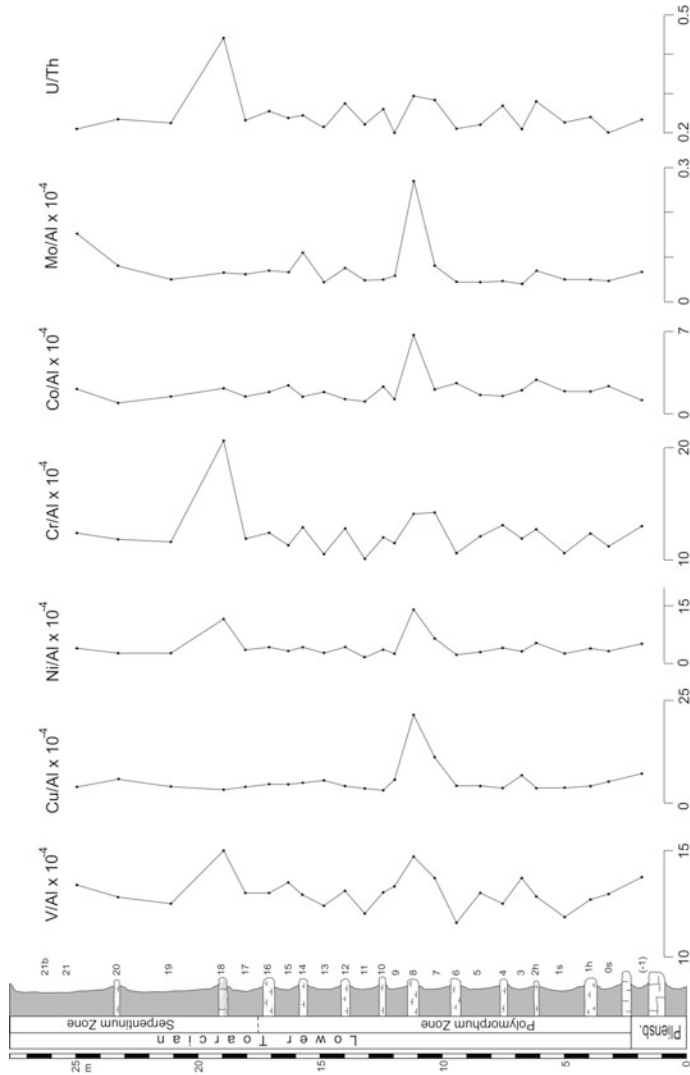


Fig. 3.12 Stratigraphic distribution of selected redox proxies. Data obtained from Rodríguez-Tovar and Reolid (2013) and Reolid (2014a)

primary lamination). However, the punctual but simultaneous significant increases in the Ti/Al and—especially—Zr/Al ratios registered throughout the section (FV-18) may be associated to short periods of aggravation in the transport of siliciclastic material to the basin. These detrital proxies are associated with both fluvial and eolian processes that could be, at least in part, directly related. This could be understood as the response to a unique phenomenon, as climatic changes increasing the input from the source area, or as a relative sea-level fall extending this area, or the combination of both. However, a phase of generalised transgression has been widely interpreted for the Early Toarcian (e.g., Hallam 1986, 1987; Gómez and Goy 2000, 2005; Bodin et al. 2010). The highest values in the detrital proxies, usually registered in the upper part of the section (FV-18), reveal a major incidence of the involved phenomena during this time, concomitant with higher fluvial and eolian activity. During sea-level evolution, the registered significant increases in the detrital proxies could be associated to punctual climatic changes.

Stratigraphic changes of the selected geochemical palaeoproductivity proxies reveal a similar pattern (Figs. 3.11 and 3.13), with a generalised increment in sample FV-18 (in Sr/Al, U/Al, and P/Ti). This fluctuated increase suggests a local addition of nutrients in the middle part of the section with respect to the sediments below and above this interval, associated with intermittent processes.

The overall TOC values for the entire succession would lie in the lower range of those registered in the Tethyan Toarcian sections. In northern European sections, TOC values typically range from 5 to 15 wt% (Sælen et al. 2000; Röhl et al. 2001; Bucefalo-Palliani et al. 2002; Mailliot et al. 2006; Hesselbo et al. 2007; McArthur et al. 2008; Bodin et al. 2010; Tyszka et al. 2010; García Joral et al. 2011); in southern European sites (Tethyan region) the usual values are some 0.5–3 wt% TOC (Jenkyns 1985, 1988; Jenkyns et al. 2002; Hesselbo et al. 2007; Sabatino et al. 2009; Bodin et al. 2010; Tyszka et al. 2010; Reolid 2014a). As McArthur et al. (2008) affirm that black shales are exceptionally rich in organic matter (5 wt% or more carbon content), the sediments studied here should not be considered true black shales. Yet most shales documented from southern European sites have less than 5 wt% TOC and are nonetheless considered to constitute black shales. Low overall TOC values here presented suggest lower concentrations of organic matter. In this context of low overall TOC values, of special interest is the TOC maximum registered in sample FV-18, with a value (0.987 wt%) over 3 times the mean of the rest of the section. Such a significant increase in TOC underlines punctual and abrupt concentrations in organic matter with respect to the sediments just above and below the record, suggesting that a brief phenomenon occurred suddenly in the Serpentinum Zone. Moreover, the Mn/Al ratio indicates that the oxidation front penetrates this potentially high productivity level, consuming part of the organic matter originally present in the sediment.

The generalised absence of high values in the ratios of the selected redox-sensitive trace metals through the studied interval suggests predominating oxic to slightly dysoxic bottom waters, discarding anoxic conditions (Rodríguez-Tovar and Reolid 2013). However, occasionally, punctual enrichments in redox sensitive elements are observed in levels FV-8 (V/Al, Cu/Al, Ni/Al Cr/Al, Co/Al, and Mo/Al ratios) and

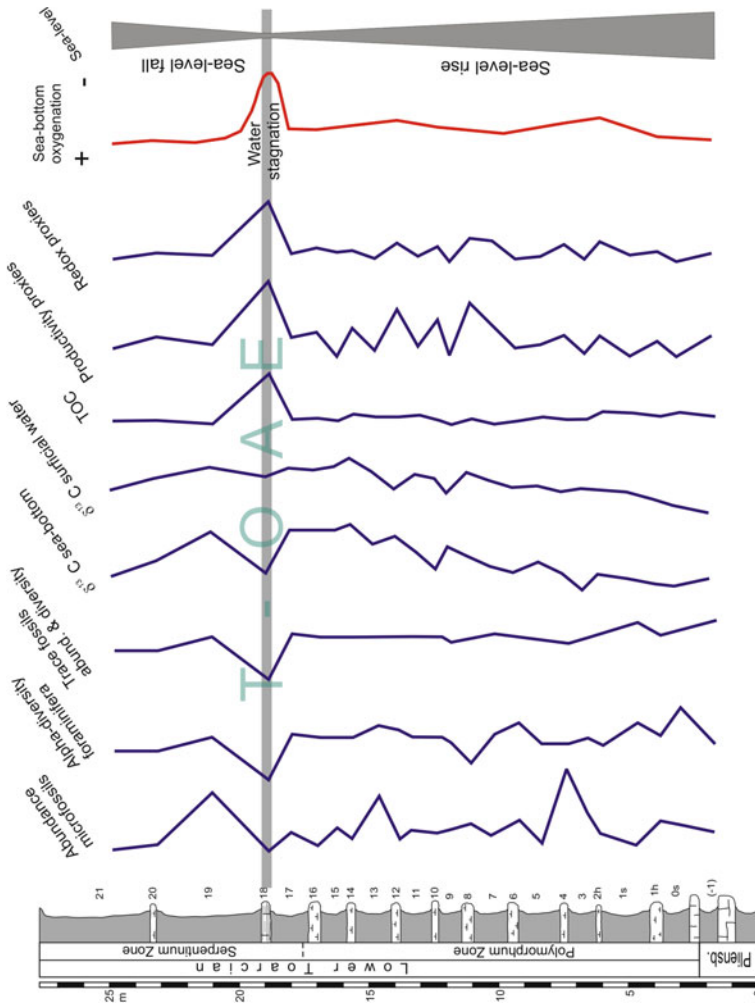


Fig. 3.13 Interpretation of environmental conditions according to the geochemical and palaeontological data in the Fuente Vidriera section and location of the oxygen depleted conditions related to the T-OAE

FV-18 (V/Al, Ni/Al, Cr/Al, U/Th and U/Al ratios). These local concentrations would point to decreasing oxygen conditions. U-based proxies suggest that the deposition of the bed FV-18 was in rather depleted oxygen conditions (Fig. 3.13).

The presence of pyrite framboids is congruent with reducing conditions because they form at the redox boundary where oxygen-bearing and hydrogen sulphide-bearing waters are in contact. In oxygenated bottom water settings, pyrite framboid growth occurs in the upper sediment column. In dysoxic to anoxic conditions, there is increased H₂S in the pore-water and the redox boundary is shallow in the sediment-water interface. Pyrite framboids of small-size have a mean of 6.3–7.1 μm in diameter in Fuente Vidriera section. According to Wilkin et al. (1996) and Dustira et al. (2013), a mean framboid size around 7.7 μm indicates oxic conditions within the sediment, 5–7.7 μm corresponds to dysoxic-anoxic conditions within the sediment, and <5 μm indicates euxinic conditions (affecting water column). The presence of a large-size pyrite population clearly supports the absence of anoxic or euxinic conditions in the water column.

In a context of uniform detrital input determining a very homogeneous rhythmic succession of soft and hard marlstones, minor increases in the detrital proxies reveal several short periods of aggravation in the transport of siliciclastic material to the basin. Among these, the most significant increase in fluvial and eolian detrital proxies is registered in the upper part of section FV-18. This finding can be related to a significant variation in the palaeo-depositional context, probably involving climatic changes. Associated with the higher fluvial and eolian activity, a comparatively increase in concentration in organic matter is punctually registered, as derived from the comparatively higher TOC values of sample FV-18. In the rest of the succession, minor inputs of detrital material are registered in conditions of low concentration, without significant variations, in organic matter content. This generalised low concentration of organic matter content is associated to oxic or slightly dysoxic bottom-waters, sufficient to maintain a fairly abundant and moderately diverse endobenthic multitiered community (Rodríguez-Tovar and Uchman 2010), as is corroborated by the absence of high concentrations of the selected redox-sensitive trace metals (Rodríguez-Tovar and Reolid 2013).

Occasionally, the comparatively higher concentration of organic matter registered in sample FV-18 would be associated with a sharp decrease in oxygenation, as revealed by increasing values of redox proxies, the absence of bioturbation and the presence of lamination (Rodríguez-Tovar and Uchman 2010; Fig. 3.13). The highest concentrations of organic matter in the sediment associated with high values of certain element ratios support a link among TOC, palaeoxygenation conditions and the concentration of these elements (Fig. 3.13). The highest values of TOC at FV-18 can be interpreted in the framework of a complex interaction of processes. Organic matter deposition could be likely related to: (a) phytodetrital inputs from emerged areas correlated to increasing detrital proxies; (b) an increase in marine surface productivity as indicated by high Sr/Al and P/Ti values; and (c) oxygen depletion at the sea-bottom favouring the preservation of organic matter. The FV-8 level probably represents less accentuated oxygen depletion than in FV-18.

The abundance of foraminifera, the size of specimens, and the diversity of the assemblage severely decrease in the FV-18 bed (Figs. 3.7 and 3.13), constituting an almost barren interval for microbenthic organisms. The abundance of ostracods also severely decreases in this bed. Depleted oxygen conditions in other sections related to the T-OAE have been evidenced by decrease in the abundance and diversity of foraminifera (Nikitenko et al. 2013; Reolid et al. 2014a; Rita et al. 2016) or the presence of a benthic barren interval (Sebane et al. 2007; Reolid et al. 2012a, b).

During the development of the T-OAE worldwide, in the westernmost end of the Tethys local conditions would have assuaged the impact of this global phenomenon as reflected by the obtained geochemical data and the correlation with the ichnological information.

We cannot discard that the restricted oxygen conditions occurred in a phase of generalised transgression that involved water stratification. According to Hallam (1986, 1987) and Haq et al. (1987), among others, during the Early Toarcian a sea-level rise took place, causing maximum confinement of bottom waters of the deep sub-basins in the Western Tethys. The configuration of the Subbetic during the Toarcian in troughs and swells (Reolid et al. 2014b, 2015b), with an intricate physiography, resulted in different sub-basins, disfavoured bottom water circulation.

The negative carbon isotopic excursion

The Early Toarcian was characterised by large perturbations of the carbon cycle, and a pronounced negative carbon isotope excursion (e.g., Jenkyns et al. 2002; Cohen et al. 2004; Hesselbo et al. 2007; Suan et al. 2008; Hermoso et al. 2009; Bodin et al. 2010; Littler et al. 2010; Reolid et al. 2012a, 2013a, b; Sandoval et al. 2012). However, the $\delta^{13}\text{C}$ negative shift is not always observed in the bulk marine carbonate or in belemnite carbonates from every locality (e.g., Jenkyns et al. 1991; Jenkyns and Clayton 1997; McArthur et al. 2000; van de Schootbrugge et al. 2005a). The magnitude of the $\delta^{13}\text{C}$ negative excursion fluctuates with palaeogeography in the Tethys Ocean (e.g., Morard et al. 2003; van de Schootbrugge et al. 2005b; Hermoso et al. 2009). In the Fuente Vidriera section the $\delta^{13}\text{C}$ values from bulk carbonate do not show the characteristic carbon isotopic excursion, which is however evident in the shells of microfossils analysed (Fig. 3.9). The amplitude of the carbon isotopic excursion is higher in shells of *Lenticulina* and ostracods. The amplitude of the carbon isotopic excursion is $\sim -2.6\text{‰}$ for $\delta^{13}\text{C}_{\text{Lenticulina}}$, -2.0‰ for $\delta^{13}\text{C}_{\text{ostracods}}$, and -0.8‰ for $\delta^{13}\text{C}_{\text{Dentalina}}$. That is, the carbon isotopic excursion is mainly identified in bottom-waters and sediment pore-water.

Role of water stagnation versus productivity

The values of $\delta^{13}\text{C}$ obtained from the bulk rock and the benthic microfossils reflect the isotopic signals of different environments. In the bulk rock, $\delta^{13}\text{C}$ values would mainly signal surficial water of the euphotic zone, due to nanofossils. The coccoliths are easily observed under SEM, also forming the tests of agglutinated foraminifera such as *Ammobaculites* and *Trochammina*. The values of $\delta^{13}\text{C}$ from calcitic microfossil tests such as *Dentalina*, *Lenticulina* and ostracods hence

represent the isotopic composition of the bottom sea-water and the sediment pore-water.

Throughout the section, the values of $\delta^{13}\text{C}$ from the bulk rock are considerably higher than those obtained from foraminifera. Because photosynthesis shows a preference for ^{12}C (and calcareous nannoplankton have strong vital effects; Ziveri et al. 2012), surficial sea-water is rich in ^{13}C . Hence, the tests of nannoplankton formed are depleted in ^{12}C and comparatively enriched in ^{13}C . The bottom sea-water is comparatively rich in ^{12}C with respect to the surficial sea-water of the euphotic zone; that is, the $\delta^{13}\text{C}$ is lower. The shells of benthic foraminifera formed in equilibrium with the bottom sea-waters have a $\delta^{13}\text{C}$ lower than the signal of the bulk rock, which mainly consists of nannoplankton. In light of the above observations, it makes sense that the record in the studied section shows higher values for $\delta^{13}\text{C}$ from the bulk rock than from benthic foraminifera. However, the $\delta^{13}\text{C}$ of ostracods with inferred shallow-infaunal to epifaunal lifestyle is higher than the $\delta^{13}\text{C}$ of the bulk sediment. This is most likely due to a strong vital effect of ostracods (Reolid 2014a). A similar situation occurs with the $\delta^{13}\text{C}$ bulk signal coming from calcareous nanofossils, with strong vital effects, which has values lower than those of co-occurring surface-dwelling planktic foraminifera (Ennyu et al. 2002; Ziveri et al. 2012; Wendler et al. 2013).

Higher productivity in bed FV-18, as opposed to other layers, is reflected by the greater difference between the $\delta^{13}\text{C}$ value of the surficial sea-water represented by the bulk rock and the $\delta^{13}\text{C}$ values of the sea-bottom represented by the foraminiferal tests (see Reolid 2014a). Analysis of selected palaeoproductivity proxies (U/Al, P/Ti, and TOC) is congruent with the data on $\delta^{13}\text{C}$ previously described and reveals a generalised increment in bed FV-18 (in Sr/Al, U/Al, and P/Ti) related to increasing productivity (Fig. 3.13). The peaks of palaeoproductivity proxies are not very intense and TOC values are not very high and therefore, the role of productivity is not totally clear (Rodríguez-Tovar and Reolid 2013).

The $\delta^{13}\text{C}_{\text{Lenticulina}}$ shows an abrupt negative excursion in bed FV-18 related to the dysoxic-anoxic event, underlined by the increase in redox proxies and wider difference with respect to the bulk rock $\delta^{13}\text{C}$. In this bed, the fact that the $\delta^{13}\text{C}$ of the bulk rock is constant indicates that the heightened productivity reflected by the P/Ti and U/Al really was not very important in the euphotic zone. Given high productivity in the euphotic zone, bulk $\delta^{13}\text{C}$ would increase as surficial waters became enriched in ^{13}C , whereas bottom sea-waters would be impoverished in ^{13}C . In this sense, the increase of organic matter at sea-bottom and the oxygen restricted conditions (indicated by the redox proxies) are related to water stagnation. The degree of oxygenation at bottom was reduced by the decaying organic matter accumulated as well as the lack of water circulation. The flux of ^{12}C -enriched organic matter to the seafloor resulted in a carbon isotopic gradient between surface (represented by bulk sediment rich in coccoliths) and bottom water in the presence of a stratified water column; differences are more accentuated during dysoxic conditions in infaunal microhabitats, as evidenced by bed FV-18 (base of the Serpentinum Zone).

The $\delta^{18}\text{O}$ of the bulk samples presents stronger fluctuations and lower values than $\delta^{18}\text{O}_{\text{Dentalina}}$ and $\delta^{18}\text{O}_{\text{Lenticulina}}$. The stratigraphic differences between $\delta^{18}\text{O}_{\text{Dentalina}}$ and $\delta^{18}\text{O}_{\text{Lenticulina}}$ would correspond to a vital effect, as the absence of peaks and stratigraphic trends in the interval studied suggests that no important fluctuations in temperature took place in the bottom sea-water. However, the $\delta^{18}\text{O}$ of the bulk rock reflects warmer temperatures than bottom sea-waters and variations.

3.2 Cueva del Agua Section

The Cueva del Agua (CA) section is located in a ravine with the same name (37° 54' 20.1" N; 02° 32' 61.0" W), 11 km northwest of the village of Huescar (Granada Province), (Fig. 3.1). The Zegrí Formation in the Cueva del Agua section is constituted by around 200 m-thick of an alternance of grey marls and marly-limestones with peloidal and bioclastic mudstones to wackestones with ammonites (Fig. 3.14). Locally grainstones of bioclasts and peloids occur, usually showing wavy lamination type hummocky cross stratification (HCS) and parallel laminations. The upper part of the alternance of grey marls and marly-limestones corresponds to the Lower Toarcian (Polymorphum Zone; Jiménez 1986; Mira 1987). Over this lithofacies there are 16 m of dark marls corresponding to the Polymorphum Zone and lower part of the Serpentinum Zone. Finally, there are 13 m of thin bedded limestones of the Serpentinum Zone (Jiménez 1986).

3.2.1 Facies and Microfacies

The studied interval begins at the top of the alternance of grey marls and marly limestones (Fig. 3.15a, b) where ammonite assemblage is composed by *Canavaria elisa*, *Emaciatoceras emaciatum*, *E. imitator*, *E. lotti*, *Lioceratoides aradasi*, and *Protogrammoceras bassanii* (Emaciatum Zone, Upper Pliensbachian) followed by the first record of *Dactylioceras (Eodactylioceras) polymorphum* of the Polymorphum Zone (Lower Toarcian). The ammonoids are more common at the top of the Pliensbachian. The limestone beds are around 20–30 cm thick and they are densely bioturbated at the top by *Planolites*, *Thalassinoides* and *Chondrites*. The microfacies are mudstones.

The dark marls are approximately 16 m thick (Figs. 3.14 and 3.15c–e), but their lower part is poorly exposed in the outcrop. Jiménez (1986) defined the Polymorphum-Serpentinum zone boundary within this lithofacies, but more recent studies (Reolid et al. 2013b) have not recorded ammonites in this lithofacies. These marls display some limestone interlayers progressively more abundant to the top. The clay-richest interval is 50 cm thick and is located 8.4 m below the base of the thin bedded limestones (Fig. 3.15d, e). The clay rich interval is characterised by

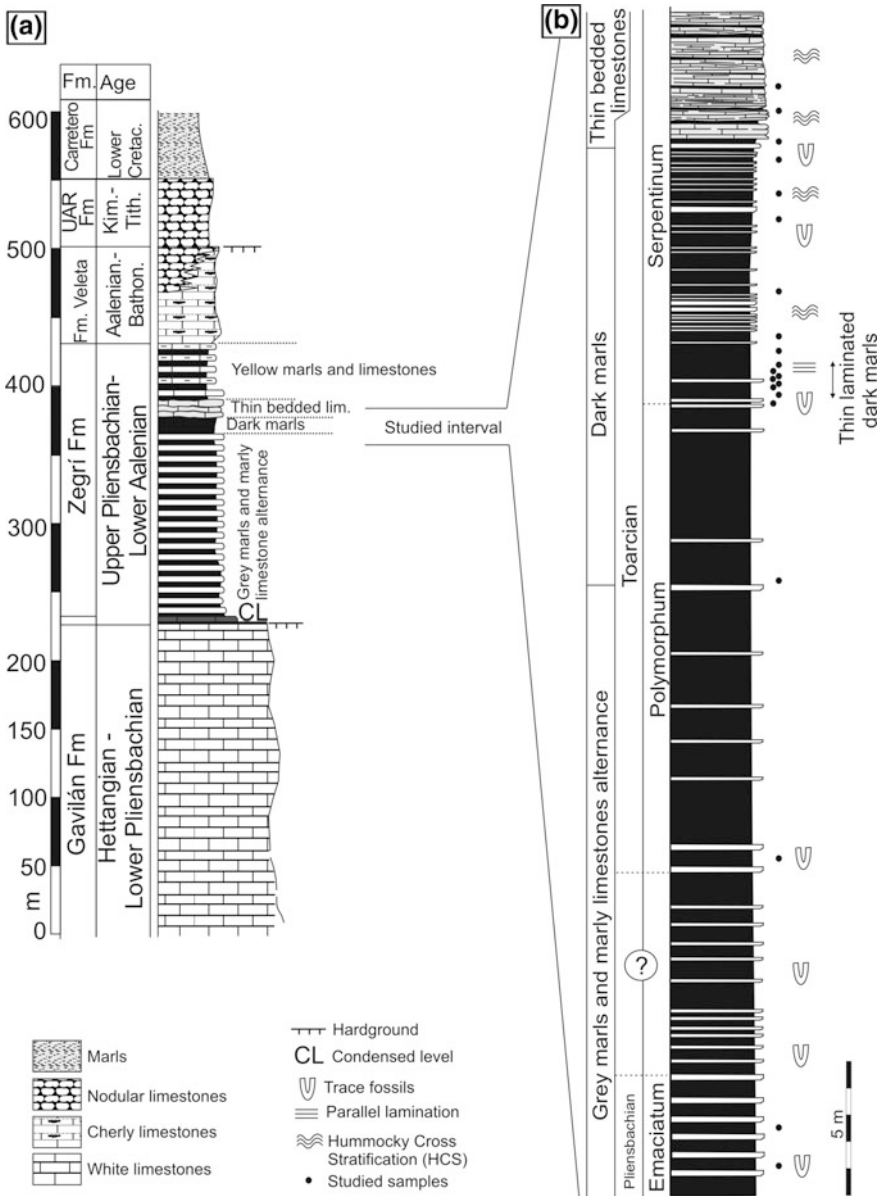


Fig. 3.14 Stratigraphy of the Cueva del Agua section. **a** General column of the Jurassic of the External Subbetic in the Huescar sector (North of Granada province). **b** Cueva del Agua section with distribution of lithofacies, ammonite zones and samples

the dark colour and the thin laminated fabric without trace fossils (Fig. 3.15e). In the directly underlying levels of the dark marl only scarce *Chondrites* are recorded. The pyrite framboids are abundant in the 100–50 μm fraction. Microfossils are

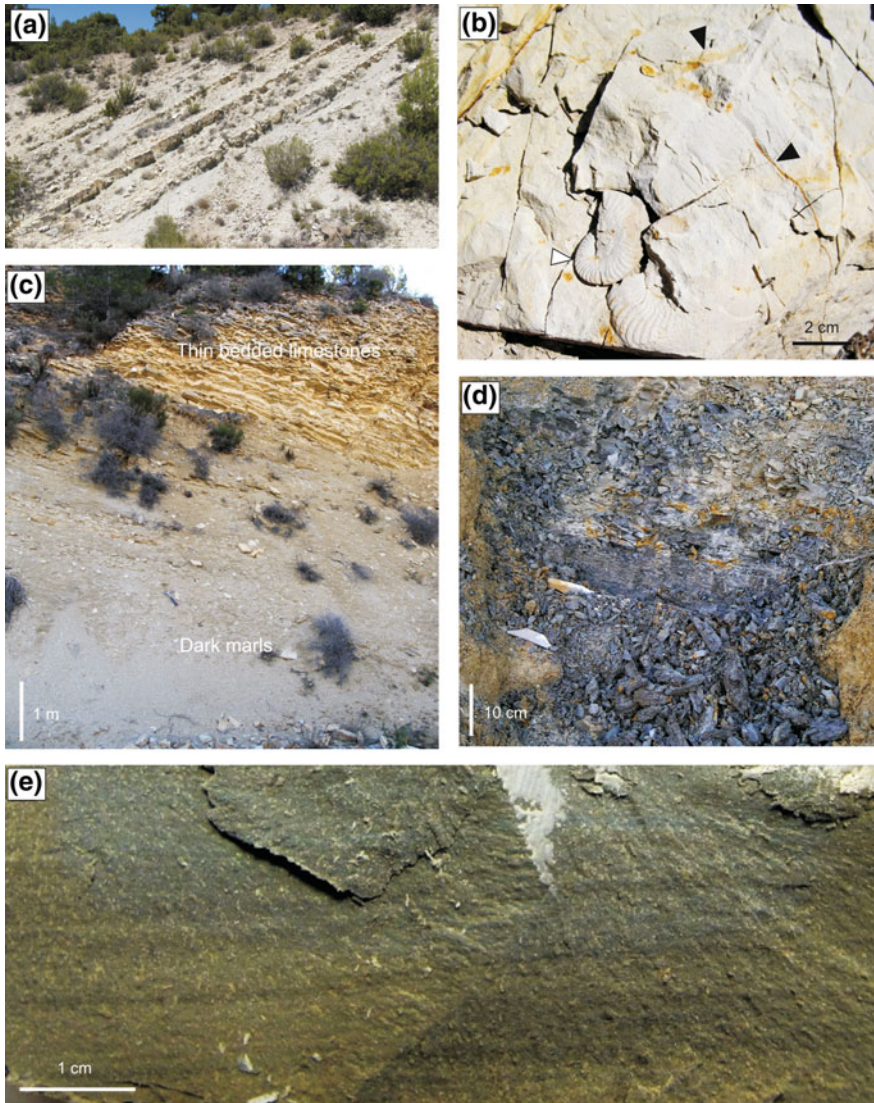


Fig. 3.15 Field view of the Cueva del Agua outcrop. **a** Marls and marly limestone alternance of the Upper Pliensbachian. **b** Ammonites (*Protogrammoceras bassanii*, white arrow) and trace fossils (black arrows) at top of a marly limestone bed of the Upper Pliensbachian. **c** Field view of the dark marls and the thin bedded limestones. **d** Detail of the dark marls. **e** Close view of the laminated dark marls

scarce in the thin laminated interval of the dark marl lithofacies. The ferruginous moulds of gastropods (<1 mm) are very abundant. They are made out of hematites, but the analysis of microstructure under SEM indicates that they were originally

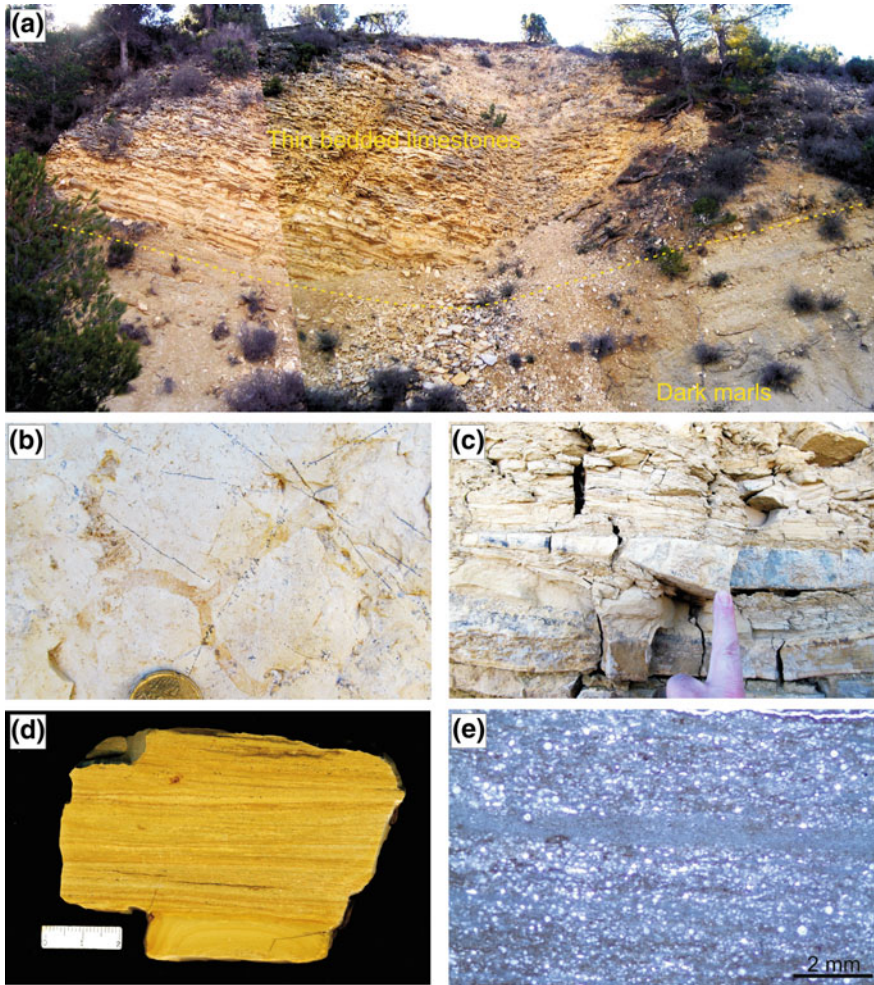


Fig. 3.16 Thin bedded limestones. **a** Field view of the outcrop. **b** *Thalassinoides* in the base of a limestone layer. **c** Detail of a layer with HCS. **d** Polished slab of a fragment of thin bedded limestone showing thin parallel lamination. **e**. Microfacies with abundant radiolarians

cubic and octahedral crystals of pyrite. In this interval the phosphatic fossil remains of indeterminate origin as well as Mn oxides are very common.

Over the thin laminated interval of the clay rich dark marls the trace fossils are progressively more abundant, mainly *Chondrites* and secondarily *Planolites* (<6 mm in diameter). In the upper part of the dark marls, yellow layers with a diversified foraminiferal assemblage occur (see below).

At the upper part of the dark marls the limestone beds are progressively more common, consisting of thin calcarenites and calcilimolites. These thin levels are the precursors of the thin bedded laminated limestones (Fig. 3.16). This lithofacies is

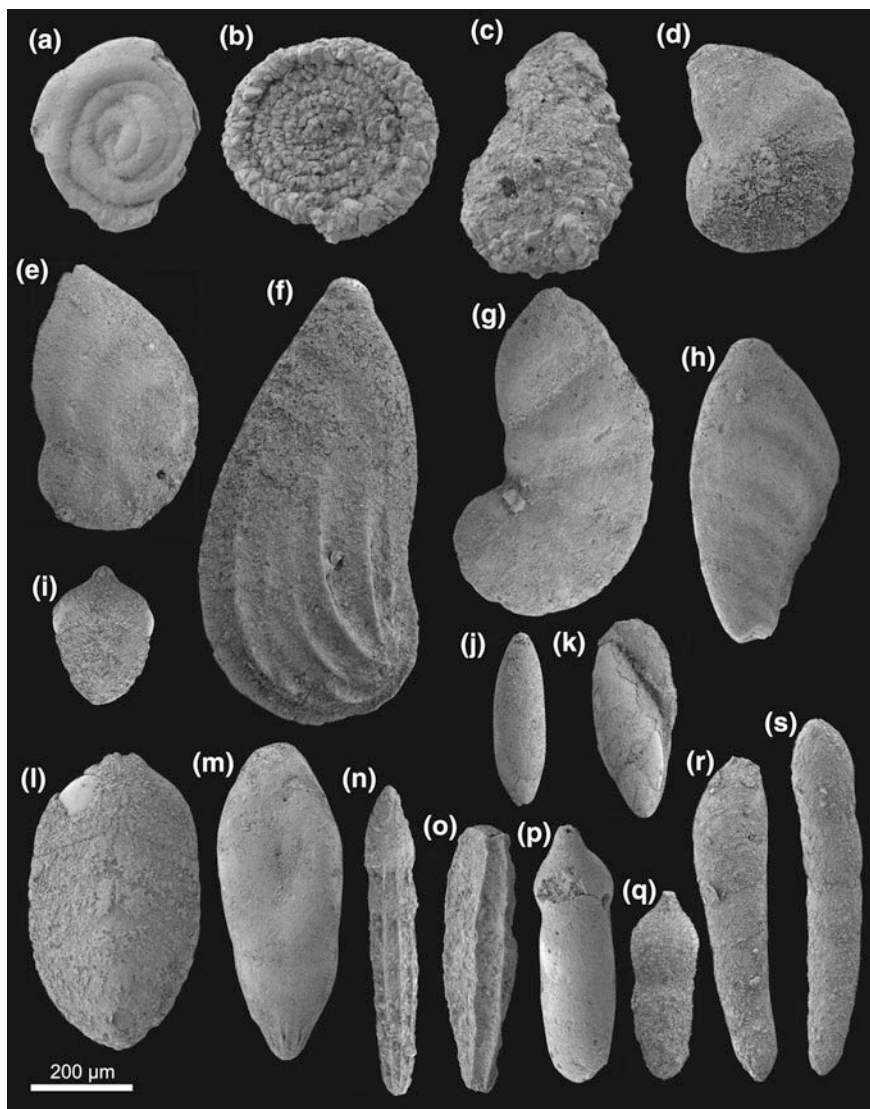


Fig. 3.17 Secondary electron images of foraminifera from Cueva del Agua section. **a** *Glomospira*. **b** *Ammodiscus*. **c** *Ammobaculites*. **d** *Lenticulina*. **e** *Astacolus*. **f** *Planularia*. **g** *Marginulinopsis*. **h** *Vaginulinopsis*. **i** *Pseudonodosaria*. **j** and **k** *Eoguttulina*. **l** *Titrix*. **m** *Pseudonodosaria*. **n** *Nodosaria*. **o** *Lingulina*. **p** and **q** *Pseudonodosaria*. **r** and **s** *Dentalina*

constituted by irregular layers of 7–15 cm thick characterised by the presence of parallel lamination to wavy lamination of the type HCS. The base of these beds is bioturbated. The microfacies are constituted by laminated bands of radiolariids and less common micritic bands, separated by thin surfaces rich in iron oxides. In this

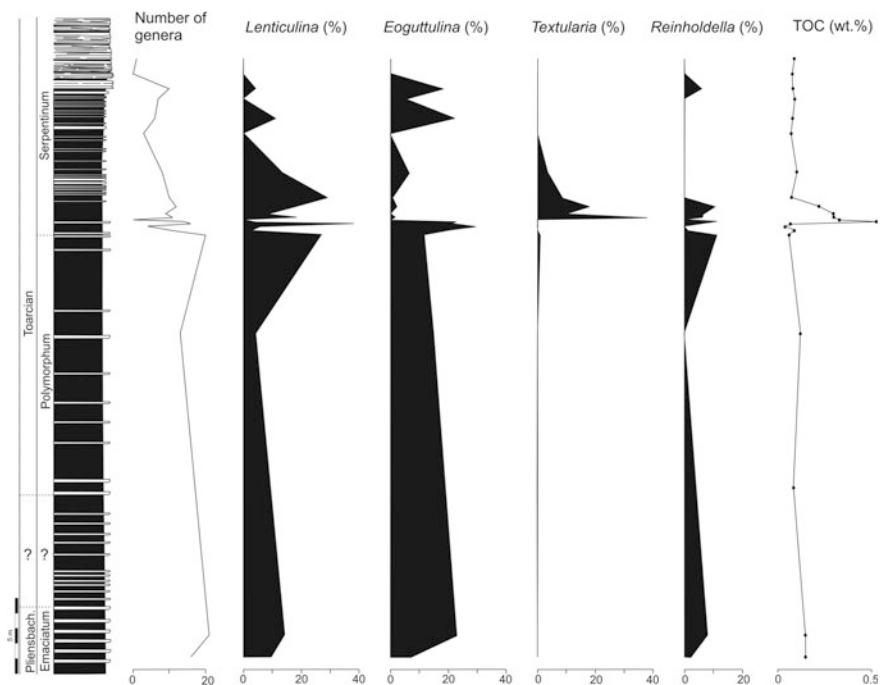


Fig. 3.18 Stratigraphic distribution of the diversity of foraminifera (number of genera) and proportion of selected opportunist genera, compared with TOC distribution

lithofacies the ammonoids are absent and the age assigned is Serpentinum Zone according to Jiménez (1986).

3.2.2 *Microfossil Assemblages*

Foraminiferal assemblages are composed mainly by components of the Suborder Lagenina (mainly *Lenticulina*, *Dentalina*, *Lingulina*, *Nodosaria* and *Eoguttulina*) (Fig. 3.17). Less common suborders represented are Textulariina (mainly *Reophax* and *Ammobaculites*), Spirillinina (mainly *Spirillina*), Robertinina and Milionina. The abundance of foraminifera and ostracods (specimens/100 g) as well as the mean size decrease from the top of Pliensbachian to the base of Serpentinum Zone. Just before the Serpentinum Zone opportunist forms such as *Lenticulina* (38%) and *Eoguttulina* (29%) are dominant (Fig. 3.18). The number of genera also decreases in this sense (Fig. 3.18). The base of the Serpentinum Zone is characterised by a barren interval where foraminifera and ostracods are not recorded. This interval is located in the lower part of the thin laminated dark marls.

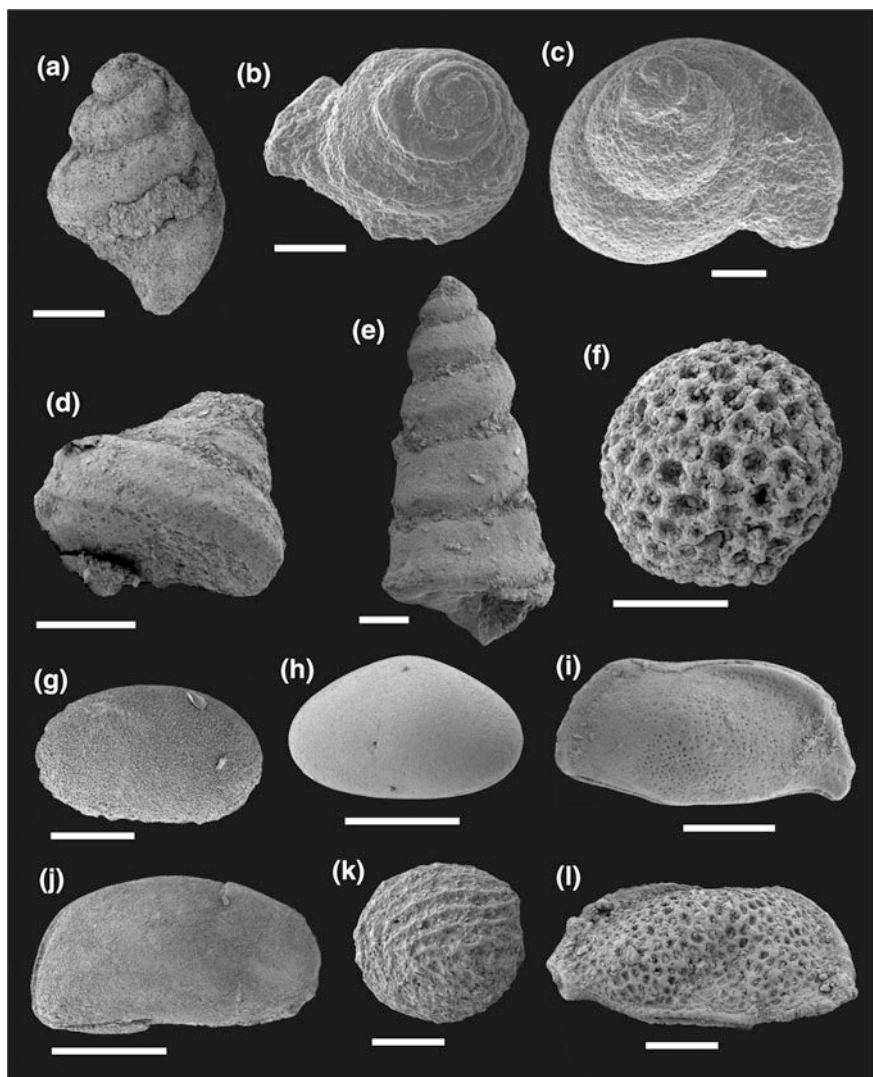


Fig. 3.19 Secondary electron images of different microfossils not foraminifera from Cueva del Agua section. **a–e** Small ferruginous moulds of gastropods. **f** Radiolarid preserved as calcitic mould. **g** *Bairdiacypris*. **h** *Ogmococonchella*. **i** *Ptychobairdia*. **j** *Pontocyprrella*. **k** *Polycope*. **l** *Ptychobairdia*. Scale bar 0.1 mm

The foraminiferal assemblages are subsequently recovered with high values of *Textularia* (38%) and *Lenticulina* (28%). The ferruginous moulds of small gastropods (<1 mm) are abundant just over the thin laminated dark marls (Fig. 3.19). Other foraminifera proliferate 1.5 m above the barren interval with common *Lingulina*, *Nodosaria* and *Dentalina*. On top of the barren interval the abundance of

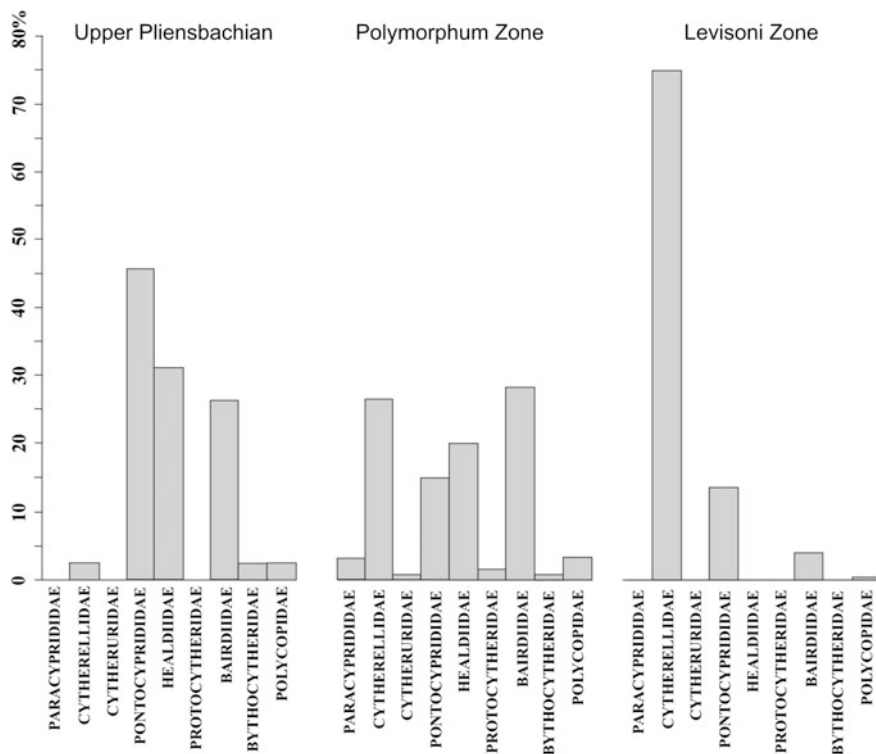


Fig. 3.20 Composition of the ostracod assemblages from the Cueva del Agua section

foraminifera in the <math><100\ \mu\text{m}</math> fraction abruptly increases. The number of genera increases upsection from the dark laminated marls but diversity levels of the top of the Pliensbachian are not reached. The abundance of foraminifera in the thin bedded limestones is very low.

The ostracods (Fig. 3.19) in the upper part of the Pliensbachian are dominated by Family Pontocypridae (mainly *Liasina lanceolata*) and secondarily Family Healdiidae (mainly *Ogmoconcha amalthei* and *O. contractula*) and Bairdiidae (Fig. 3.20). The Toarcian begins with high values of Family Bairdiidae (28%) and Family Cytherellidae (mainly *Cytherella toarcensis*) and secondarily by families Healdiidae and Pontocypridae (Fig. 3.20). The ostracod assemblage of the lower part of the Serpentinum Zone is dominated by Family Cytherellidae, and secondarily Pontocypridae and Bairdiidae. In the Cueva del Agua section *Cytherella toarcensis*, presents very high values (86%), just after a microfossil barren interval of the dark laminated marls.

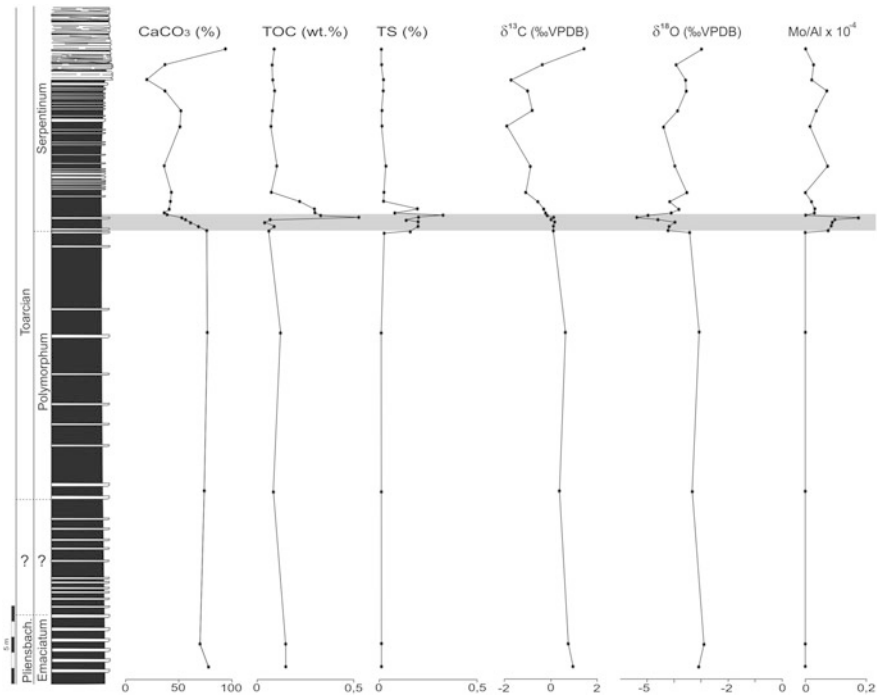


Fig. 3.21 Stratigraphic distribution of selected geochemical parameters in the Cueva del Agua section with the main changes in the base of the Serpentinum Zone

3.2.3 Geochemistry

The main changes in the geochemistry occur at the base of the Serpentinum Zone (Fig. 3.21). The CaCO_3 content abruptly decreases in the dark marl interval of the Serpentinum Zone where values are usually $<42\%$. Respect to the TOC, values are very low in the Cueva del Agua section, commonly <0.2 wt%. At the base of the Serpentinum Zone the TOC abruptly increases to 0.53% in the clay rich interval of the dark marls where thin lamination is developed and the trace fossils are absent. Over this interval the TOC newly decreases to values <0.1 wt%.

A similar trend describes the sulphur content (total sulphur, TS) with very low values in the section ($<0.02\%$) except at the base of the Serpentinum Zone where it reaches 0.32% (Fig. 3.21).

The $\delta^{13}\text{C}$ values range between -1.87 and 1.83‰ with the lowest values in dark marls of the Serpentinum Zone (Fig. 3.21). The $\delta^{13}\text{C}$ of the Polymorphum Zone ranges between 0.96 and 0.63‰ , and experiment an accentuated decrease in the lower part of the Serpentinum Zone in coincidence with the thin laminated marly interval and the lowest values of TOC and TS. However, the values of $\delta^{13}\text{C}$ are not

recovered rapidly as occur with the TOC and TS, and $\delta^{13}\text{C}$ decreases to reach the lowest values (-1.87 and -1.70%) just below the thin bedded limestones (upper part of the Serpentinum Zone sensu Jiménez 1986). In the thin bedded limestones $\delta^{13}\text{C}$ is recovered to pre-Toarcian values.

Respect to $\delta^{18}\text{O}$ values, they are around -3% in the Polymorphum Zone, showing a strong decrease to values ranging between -5.36 and -4.95% in the dark laminated marls of the base of the Serpentinum Zone (Fig. 3.21). Above this isotopic excursion, $\delta^{18}\text{O}$ increases but values similar to Polymorphum Zone are recovered in the thin bedded limestones.

The Mo content in the Cueva del Agua section describes a trend similar to those of TOC and TS (Fig. 3.21). The highest values (0.84 ppm) are recorded in the dark laminated marls. The Mo/Al ratio shows a peak in the dark laminated interval, and in general, higher values in the dark marls of the Serpentinum Zone than in the marl-limestone rhythmite of the Polymorphum Zone or the thin bedded limestones of the upper part of the Serpentinum Zone.

3.2.4 Interpretation

Signification of facies and microfacies

The Zegrí Formation is integrated within the sedimentary sequence II of García-Hernández et al. (1989) limited at the base by the Carixian-Domerian discontinuity (Lower-Upper Pliensbachian boundary) and limited to the top by the finibathonian discontinuity (Fig. 3.3). This sedimentary cycle coincides with the main phase of intracontinental fragmentation (rifting) developed from the Late Pliensbachian-Bathonian (Fig. 3.4). The bottom topography of the basin was irregular with different semigrabens and variable subsidence (Nieto et al. 2004; Molina et al. 2007), as occurred in other Tethyan Alpine Domains (e.g., Jenkyns 1988; de Graciansky et al. 1998; Marok and Reolid 2012).

The alternance of grey marls and marly limestones of the Zegrí Formation represents a pelagic environment with scarce continental influence according to the scarce terrigenous content, as interpreted by the Fuente Vidriera section. According to Reolid et al. (2013b) the bathymetry was <200 m in depth taking into account the record of HCS type structures. Cheel and Leckie (1993) proposed that the HCS are formed when storm waves reach the sea bottom at maximum depths ranging between 125 and 200 m. The presence of these beds indicates a context where water column is recycled and oxygenated during the Pliensbachian, as confirmed by the presence of cephalopods, brachiopods, foraminifera, ostracods and ophiuroids.

The beginning of the Toarcian is characterised by decreasing carbonate content and the absence of HCS structures. This is related to topographic changes of the sea bottom with the development of troughs and swells in addition to the transgressive regional and global context (Jenkyns 1988; Jiménez et al. 1996; de Graciansky et al. 1998; Vera 2001).

The CaCO_3 content abruptly decreases when dark laminated marls are recorded together with the negative fall of $\delta^{13}\text{C}$ (around 0.84‰; Fig. 3.21). These fluctuations are well-correlated to the T-OAE and the perturbation of the carbon cycle and the carbonate production located in the lower part of the Serpentinum Zone (Erba 2004; Mattioli et al. 2004, 2008; Tremolada et al. 2005; Wignall et al. 2005; Hermoso et al. 2009; Suan et al. 2010). Values equivalent to those of the Pliensbachian are not recovered until the thin bedded limestones (Fig. 3.21). The perturbation in the carbon cycle coincides with the decrease on abundance (included the barren interval) of ostracods and foraminifera (Figs. 3.18 and 3.21).

Above the thin laminated marls the first limestone beds that constitute an upwards carbonate increase are recorded. This upward increase of the carbonates finishes in the thin bedded limestones. This first limestone beds show, again, HCS structures that indicate the presence of currents reaching the sea bottom and accordingly an increasing oxygenation. As a consequence, over the dark marls the foraminifera, ostracods and trace fossils are progressively more abundant. Respect to the foraminiferal assemblages, the first colonisers of the sea-bottom were opportunist *Lenticulina* and agglutinated foraminifera such as *Textularia*. The decreasing size of the foraminifera is interpreted as the Lilliput Effect (Urbanek 1993; Twitchett 2007). This strategy consists in a temporary size decrease within the surviving species under unfavourable conditions that enables them to be successful in more or less confined environments (Urbanek 1993).

The main change in the environmental conditions is related to the deposition of the calcilimolites that constitute the thin bedded limestones. The abundance of HCS structures (Fig. 3.16c) indicates higher energy conditions in the sea bottom and the input of pelagic sediment coming from neighbour areas. Taking into account the extensional tectonic context of the Subbetic (Vera 2001) and the instability of the bottom, evidenced in other sections by the record of tempestites, slumps and breccia in the Zegrí Formation (e.g., Nieto 1997; Nieto et al. 2004; Reolid et al. 2015b), the thin bedded limestones could be related to the reactivation of the tectonic activity as well as a global sea-level fall. Different volcanic events occurred in the South Iberian Palaeomargin at the same time of the deposition of the Zegrí Formation. Those events are recorded as volcanic edifices constituted by pillowlava (Comas et al. 1986; Reolid and Abad 2014). The record of the thin bedded limestone interval could be also related to the intensification of tropical cyclones during the Lower Toarcian proposed for Krencker et al. (2015).

A similar distribution of facies here described has been reported in the North of Lusitanian Basin, in the Coimbra-Rabaçal Region (Duarte 1998). The Lower Toarcian in this region corresponds to the S. Gião Formation. The lower interval is constituted by the marly limestones with *Leptaena* followed by the thin bedded limestones with *Hildaites* characterised by parallel lamination and cross lamination. Related to these limestones a negative carbon isotopic excursion was recorded. Duarte (1997) interpreted the thin bedded limestones as tempestitic-turbiditic deposits, also related to tectonic reactivation (Duarte and Soares 1993; Duarte 1997). This interpretation is similar to that of the Cueva del Agua section.

Organic matter and sea-bottom oxygenation

The integrated analysis of facies, microfacies and geochemistry evidences the main environmental changes occurred in the dark laminated limestones (middle part of the dark marls). In this interval the values of TOC, TS and Mo/Al ratio increase whereas the $\delta^{18}\text{O}$ and $\delta^{13}\text{C}$ data show an accentuated decrease. In this stratigraphic interval diversity of foraminifera decreases together with the abundance. The maximum values of TOC, TS and Mo/Al coincides with a benthic microfossil barren sample.

The Mo/Al peak indicates depleted oxygen conditions in the sea-bottom. The mechanism that explain the fixation of the Mo in the sediment implies reducing conditions, with the Mo being trapped from the water column where is located as MoO_4^{2-} (Broecker and Peng 1982), through the mineralisation of organic thiomolibdates and complex groups of Fe-Mo-S probably forming a solid solution with iron sulphides (Helz et al. 1996). The organic matter traps Mo because: (a) the transport of Fe and other trace metals and, (b) the direct fixation of the MoO_4^{2-} by O-S groups of the organic matter. Therefore, in marine facies, the enrichment of organic matter together with the Mo content are proxies for interpreting reducing conditions (e.g., Meyers et al. 2005). An increase in the Mo/Al ratio has been identified in the T-OAE from the Saharian Atlas (Algeria, Reolid et al. 2012b) in a benthic barren interval similar to the dark laminated marls of Cueva del Agua, where trace fossils and microfossils are not recorded.

Depleted oxygen conditions can be interpreted in the dark marls and more concretely in the laminated interval due to the absence of trace fossils, but also the lack of fossil macroinvertebrates, as well as the abundance of pyrite framboids that indicate redox conditions, almost in the sediment pore-water. The decrease in the diversity of foraminifera as well as the increase in the proportions of opportunists such as *Lenticulina*, *Eoguttulina* and *Reinholdella* just before the negative carbon isotopic excursion indicate disturbance of the environmental conditions during the pre-biotic crisis.

The oxygen depleted conditions are congruent with the increase of TOC values (from 0.20 to 0.53%) in this interval, but always being low values if compared with Central and North Europe outcrops. Thus, for the Serpentinum Zone (Levisoni Zone for Mediterranean Biozonation and Falciferum Zone for the Sub-boreal Biozonation), the TOC values range from 5 to 15% in North Europe outcrops (Sælen et al. 2000; Röhl et al. 2001; Bucefalo-Palliani et al. 2002; Mailliot et al. 2006; McArthur et al. 2008, among others) whereas in the Tethys region (Southern Europe and North Africa) range from 0.5 to 3% (Jenkyns 1985, 1988; Jenkyns et al. 2002; Hesselbo et al. 2007; Bodin et al. 2010, 2011; Reolid et al. 2012b, among others). This is an evidence of the geographic variations of the T-OAE signal (see also Hermoso et al. 2009). The record of the thin laminated dark marls has been also reported in the T-OAE in other areas (Parisi et al. 1996; Hermoso et al. 2009; Izumi et al. 2012).

Above the dark laminated marls interval Mo/Al ratio and TOC decrease, at the same time that foraminifera are newly recorded with high proportions of the genera

Textularia and *Lenticulina*, and common ferruginised moulds of small gastropods. These data suggest an environmental improvement of oxygen availability in the sea bottom. *Lenticulina* is considered an opportunist during the Jurassic (Tyszka 1994; Reolid 2008; Reolid et al. 2008, 2012a; Rita et al. 2016) and it is described during the first phases of colonisation of the sea bottom after the T-OAE (Reolid et al. 2012a, b). The record of numerous small gastropods is congruent with the first phases of the sea bottom recolonisation as described in other context (Suan et al. 2013; Teichert and Nutzel 2014; Gatto et al. 2015). The proliferation of opportunist organisms with small sizes (such as *Lenticulina* and gastropods) is an adaptative strategy to unfavourable conditions, the Lilliput Effect (Urbanek 1993; Morten and Twitchett 2009), recently recognised in trace fossils associated to some bio-events, as the K/Pg boundary (Łaska et al. 2017), and in particular in *Thalassinoides* structures associated to the T-OAE in the Lusitanian basin (Miguez-Salas et al. 2017; Rodríguez-Tovar et al. 2017). The hematite composition of the gastropod moulds after the dark laminated marls is indicative of the presence of an oxidation front, also favouring the precipitation of Mn oxides and oxyhydroxides in the sediment-water interface due to the oxygen availability (Thomson et al. 1999; Powell et al. 2003).

The presence of hematite moulds must be related to oxygen availability in the sea bottom, but the diagenetic history of these moulds is complex. The microtextural features of the hematite forming the moulds evidence a pyritic original composition in the initial infilling of the gastropod shell. This pyrite was originated as sulphides that precipitated before the shell dissolution during the early diagenesis, while there were reducing conditions in the sediment-water interface. The advance within the sediment pore-water of the oxygenation favoured the precipitation of Fe and Mn oxides and oxyhydroxides, as well as the transformation of gastropod pyrite moulds.

In Recent marine environments there is a positive relation between the TOC and the S coming from the pyrite (Berner and Raiswell 1983). The pyrite is formed from reaction of H₂S generated by sulphate reducing bacteria (SRB) in anoxic environments with Fe. Such organisms are currently very abundant; thus they oxidise more than half of all the organic matter reaching the sediments (Rickard et al. 2017). This bacterial reduction is related to the organic matter oxidation under dysoxic to anoxic conditions ($2\text{CH}_2\text{O} + \text{SO}_4^{2-} \rightarrow \text{H}_2\text{S} + 2\text{HCO}_3^-$). Under oxygen depleted conditions (dysoxic or anoxic), the organic matter is not aerobically decayed at the sea-bottom or at the sediment-water interface; then the sulphate reduction rate increases and the subsequent concentration of H₂S in the sediment pore-water and the shallowing of the redox boundary within the sediment just to locates in the sediment-water interface. In this situation, great amount of H₂S is available for reacting with detritic Fe to forming pyrite. In this sense, the increase of TS in the dark laminated marl interval is congruent with the increase of TOC values and the depleted oxygen conditions indicated by the Mo/Al ratio. Caswell and Coe (2012) showed a parallel increase in TOC and TS in the Falciferum Zone from deposits of the East Midlands Shelf. However, the C_{org}/S ratio in this interval experiments a decrease related to the high decaying rate of the organic matter

during the sulphate reduction processes, and only residual organic matter is preserved in the geological record. That is, there is not a constant fraction of organic matter decayed respect to the initially accumulated. This is probably under euxinic conditions with BSR decaying the organic matter both in the sea-bottom and in the water column where H_2S is dissolved (Sweeney and Kaplan 1980), and then, the organic matter degradation is higher. However, the TS in the dark laminated marls interval presents relatively low values for interpreting euxinic conditions during the T-OAE in the Cueva del Agua section.

The return to oxic conditions and the potential advance within the sediment of the oxic front (evidenced by the ferruginous moulds of gastropods and small Mn nodules) could also favour the oxidation of organic matter and the remobilisation of sulphur.

Isotopic fluctuations and environmental changes

The $\delta^{13}\text{C}$ values show a strong decrease of 0.84‰ from the base of dark laminated marl interval at the same time of the decrease on CaCO_3 wt%. These fluctuations are driven by the global changes related to the T-OAE such as sea-level fluctuations, sea-water acidification, and the perturbation of the carbon cycle (see Dera and Donnadiou 2012; Reolid et al. 2014b; Casellato and Erba 2015) that affected to the marine biota and the carbonate productivity. As mentioned above, this event is located at the base of the Serpentinum Zone (Erba 2004; Mattioli et al. 2004, 2008; Wignall et al. 2005; Tremolada et al. 2005; Suan et al. 2010; Izumi et al. 2012; among others). Values similar to those of the Pliensbachian are not recovered until the thin bedded limestones (upper part of Serpentinum Zone, s. Jiménez 1986).

The magnitude and the global record of the negative CIE have been interpreted as the result of the massive input of ^{12}C to the atmosphere-ocean system as a consequence of: (a) the volcanic activity of the Karoo-Ferrar igneous province (see McElwain et al. 2005; Svensen et al. 2007), and (b) the massive injection of methane gas hydrates (Hesselbo et al. 2000; Kemp et al. 2005). At the scale of the Iberian palaeomargins, the fluctuations in the $\delta^{13}\text{C}$ may also be influenced by the volcanic activity recorded during the Toarcian in the Subbetic (Betic Cordillera; Comas et al. 1986; Portugal et al. 1995; Vera et al. 1997; Reolid and Abad 2014) and in the Iberian Range (Gautier and Odin 1985; Martínez et al. 1996a, b, 1997). The extensional tectonic peak along extensive faults is related to the opening of the Atlantic-Alpine-Tethys rift system, controlling highs and depocentres, as well as to alkaline volcanic activity in the Eastern and Southern Iberian palaeomargins (Gautier and Odin 1985; Comas et al. 1986; Martínez et al. 1996a).

The $\delta^{18}\text{O}$ values for the Lower Toarcian are within the range reported in previous works (Dera et al. 2009), around -3‰ in the Polymorphum Zone, showing a strong decrease at the base of the Serpentinum Zone, represented in the Cueva del Agua section by the dark laminated marls (-5.36 to -4.95‰). These data are similar to those reported by Gómez and Goy (2011) for $\delta^{18}\text{O}$ from bulk samples of the Rodiles Oeste (Asturias, North Spain) and Sierra Palomera (Iberian Range, eastern Spain) sections. These authors indicated a negative excursion at the base of Serpentinum Zone (from -3.0 to -5.5‰). Other European sections also show this

negative isotopic excursion with $\delta^{18}\text{O}$ values obtained from bulk sample, belemnites and brachiopods (Anderson and Arthur 1983; Jenkyns 2003; Rosales et al. 2004; Suan et al. 2008, 2010; Harazim et al. 2013).

According to $\delta^{18}\text{O}$ values Rosales et al. (2004) and Gómez and Goy (2011) interpreted a palaeotemperature of 24 °C during Late Pliensbachian and the Polymorphum Zone with an abrupt increase to 32 °C at the base of the Serpentinum Zone. Other authors have interpreted a global warming related to the T-OAE (e.g., McArthur et al. 2000; Bailey et al. 2003; Suan et al. 2010, 2011; García Joral et al. 2011; Gómez and Goy 2011; Korte and Hesselbo 2011), related to a sea-level rise (e.g., Hallam 1986, 1987; Elmi 1996; Hylton and Hart 2000; Ruban and Tyszka 2005; Wignall et al. 2005; Korte and Hesselbo 2011). A global warming increases the temperature of waters and decreases the oxygen solubility. The negative excursion of $\delta^{18}\text{O}$ could be related to the input of warm waters (isotopically light) depleted in oxygen, probably favouring the water stagnation. However, other proposals suggest that the decrease of $\delta^{18}\text{O}$ values is related to the increase of fresh continental waters (isotopically light) (Bailey et al. 2003; Dera et al. 2009) as a consequence of the global climatic change (Cohen et al. 2004).

3.3 La Cerradura Section

La Cerradura (CE) section is located in the trench of motorway A-44, km 57 (37° 41' 47.8" N; 3° 37' 57.6" W). The section is 15 km south of Jaén city (Jaén province, Fig. 3.1). Previous works analysed this section in a narrow ravine previously to the existence of the motorway A-44. The La Cerradura section was initially studied by Mouterde et al. (1971) and Busnardo (1979), with special emphasis on the Upper Pliensbachian marl-marly limestone rhythmite. Ruget and Martínez-Gallego (1979) and Mira (1987) studied the foraminiferal assemblages of the Upper Pliensbachian. The Pliensbachian ammonites were studied by Braga (1983) and the Toarcian ones by Jiménez (1986). Recently, Sandoval et al. (2012) included this section in a study of the Toarcian of the Subbetic focused on bioevents of ammonites and calcareous nannofossils. Reolid et al. (2014b) analysed the lithofacies, ichnology, calcareous nannoplankton and geochemistry of La Cerradura section and identified the T-OAE. Baeza-Carratalá et al. (2017) have studied the behaviour of the brachiopod assemblages in this section related to the T-OAE. The studied interval in La Cerradura section consists of a 27.5-m-thick marl-marly limestone rhythmite dated from the Algovianum Zone (Upper Pliensbachian) to the Polymorphum Zone (Lower Toarcian), and 12-m-thick dark marls of the Serpentinum Zone (Lower Toarcian) (Fig. 3.22).

The marly limestone beds correspond to mudstones and less common wackestones with sporadic bioclasts (fragments of mollusks, echinoderms, and foraminifera). The marly layers are rich in illite, smectite and chlorite (Palomo et al. 1985; Palomo 1987; Caniçó et al. 2015).

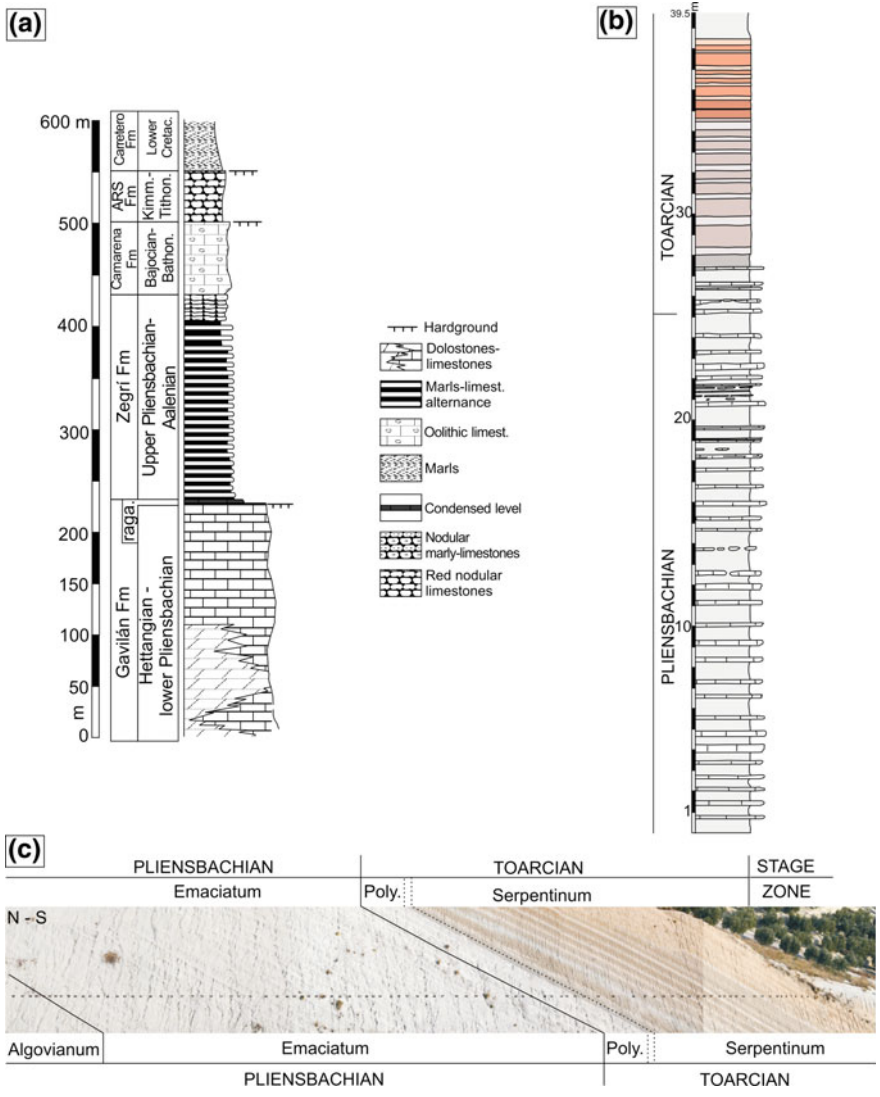


Fig. 3.22 La Cerradura section. **a** General column of the Mesozoic rocks in the External Subbetic in the central area of the Betic Cordillera. **b** Detailed studied interval of the La Cerradura section. **c** Field view of La Cerradura section

3.3.1 Macroinvertebrates

The marl-marly limestone rhythmite is very rich in ammonites and belemnites, favouring a fine biostratigraphy (Braga 1983; Jiménez 1986), with species of the genera *Canavaria*, *Emaciatoceras*, *Fontanelliceras*, *Lioceratoides*, *Neolioceratoides*,

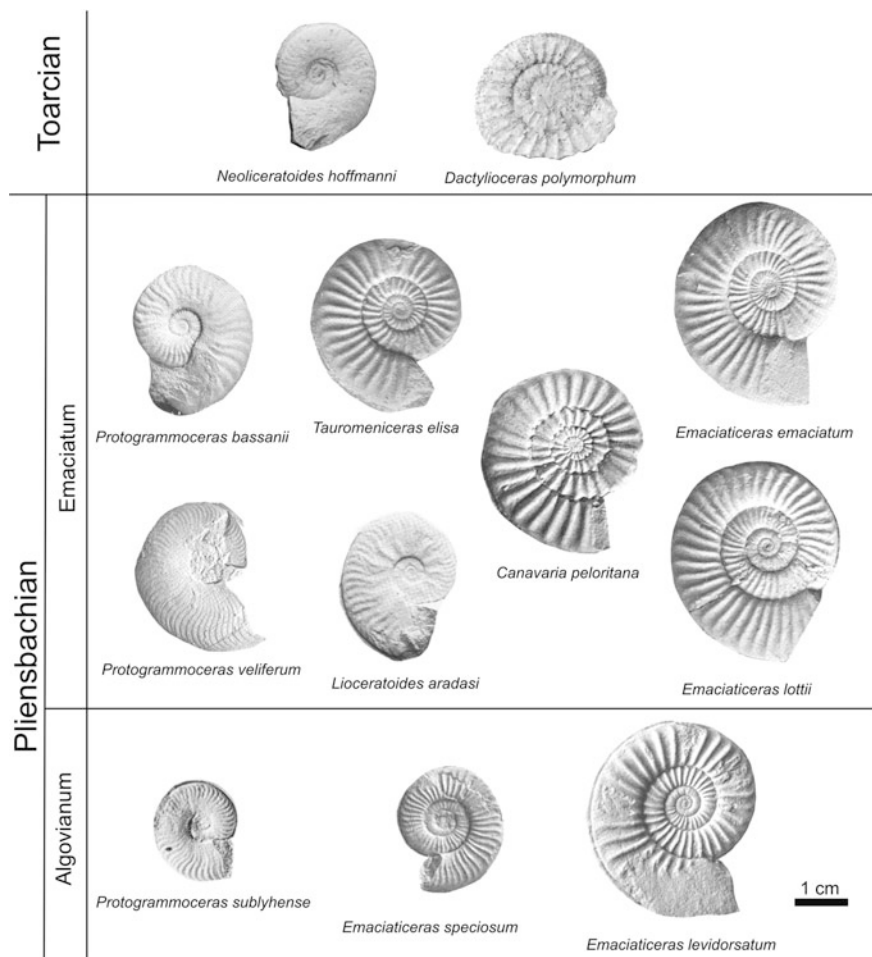


Fig. 3.23 Selected ammonites with biostratigraphic interest recorded in the La Cerradura section. Specimens from the Ph.D. Thesis of Prof. Juan Carlos Braga (Univ. of Granada)

Protogrammoceras and *Tauromeniceras* (Upper Pliensbachian) and the genus *Dactylioceras* (Polymorphum Zone; Lower Toarcian) (Figs. 3.23 and 3.24). The base of the Emaciatium Zone (Upper Pliensbachian) is characterised by the first occurrence of *Pleuroceras solare* (bed 93 at 2.2 m above the base), and the top is characterised by the first occurrence of *Dactylioceras pseudocommune* and *D. simplex* that indicate the beginning of the Polymorphum Zone (Lower Toarcian, bed 38 at 25 m above the base). The differentiation between the Solare and Elisa subzones (Emaciatium Zone) is recorded by the first occurrence of *Emaciaticerias imitator* at the base of the Elisa Subzone (bed 62, at 15 m above the base). The top of the marl-limestone rhythmite is a horizon with high contents of ammonites (*Dactylioceras pseudocommune*, *D.*

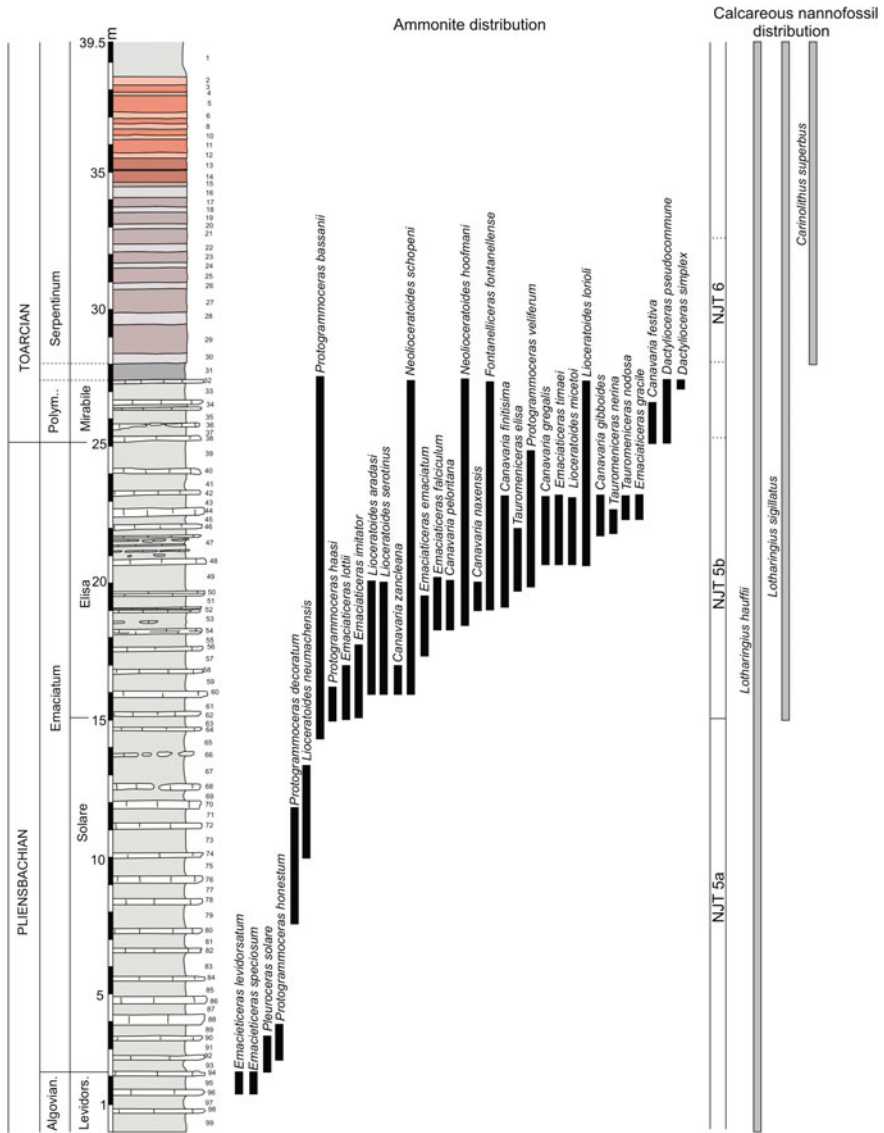


Fig. 3.24 Lithological column with ammonite and calcareous nannofossil zones and the stratigraphic distribution of the main biostratigraphic taxa. The distribution of ammonite is based on ammonites recorded in this work and data from Braga (1983) and Jiménez (1986). The calcareous nannofossil distribution is based on Reolid et al. (2014b)

polymorphum and *Neoliceratooides hoffmanni*), belemnites and small brachiopods. In addition, microfossils such as foraminifera (mainly Suborder Lagenina) and ostracods are common.

The beginning of the dark marly interval (at 27.5 m above the base) is characterised by the absence of macroinvertebrates as well as microfossils (benthic foraminifera and ostracods). At 40 cm above the base of the dark marly interval (CE-28, at 29.5 m above the base of the section), the first brachiopods (*Liospiriferina subquadrata*, *Orthotoma* aff. *globulina*, *Koninckodonta sumuntanensis* and *Atychorhynchia falsiorigo*; Baeza-Carratalá et al. 2017) are recorded. The first belemnites featuring serpulid encrustations (*Dorsoserpula*), attached foraminifera (*Bullopore tuberculata*) and microborings (including cirripedes borings) are recorded 2 m above the top of the rhythmite. In addition, a small stem and roots with cirra of crinoids (<10 ossicles, and <20 mm long) colonised by attached foraminifera (*B. tuberculata*) was found (Reolid et al. 2014b). Ammonites are very scarce and they correspond to small juvenile specimens (<10 mm), which makes their identification difficult.

3.3.2 Trace Fossils

Trace fossil content and ichnofabric features were examined in all marl and marly limestone beds of the section (Fig. 3.25). Trace fossils, identified mostly in cross sections, are relatively abundant in the marl-limestone rhythmite. The marly limestone beds show a moderately diverse trace-fossil assemblage consisting of abundant *Chondrites* (small and large), *Planolites*, *Thalassinoides* and *Teichichnus*, comparatively scarcer *Palaeophycus* and potential *Taenidium*, and rare *Trichichnus* (Reolid et al. 2014b). The filling of trace fossils is dark, well differentiated from the light-grey host sediment, usually rich in organic matter (small charcoal wood fragments) and pyrite framboids.

Some trace-fossils show a clear crosscutting relationship in the La Cerradura section. *Planolites*, *Teichichnus* and *Thalassinoides* are crosscut by small *Chondrites*. Trace fossil diversity and abundance decrease just above the top of the marl-limestone rhythmite, with the only local record of small *Chondrites* in the first 1.5 m of the marly interval. Trace fossils are completely absent in bed CE-31 (first 40 cm above the rhythmite). The subsequent gradual recovery shows a relative increase in diversity and abundance of trace fossils (mainly small size *Chondrites*, *Planolites* and *Thalassinoides*), but below the values of the marl-limestone rhythmite.

3.3.3 Calcareous Nannofossils

The nannofossil assemblage of La Cerradura is of Tethyan affinity with a dominance of *Mitrolithus jansae* and *Schizosphaerella* mainly in the Pliensbachian marl-limestone rhythmite, whilst *Crepidolithus crassus* having a N Tethyan affinity is very scarce (Figs. 3.26 and 3.27).

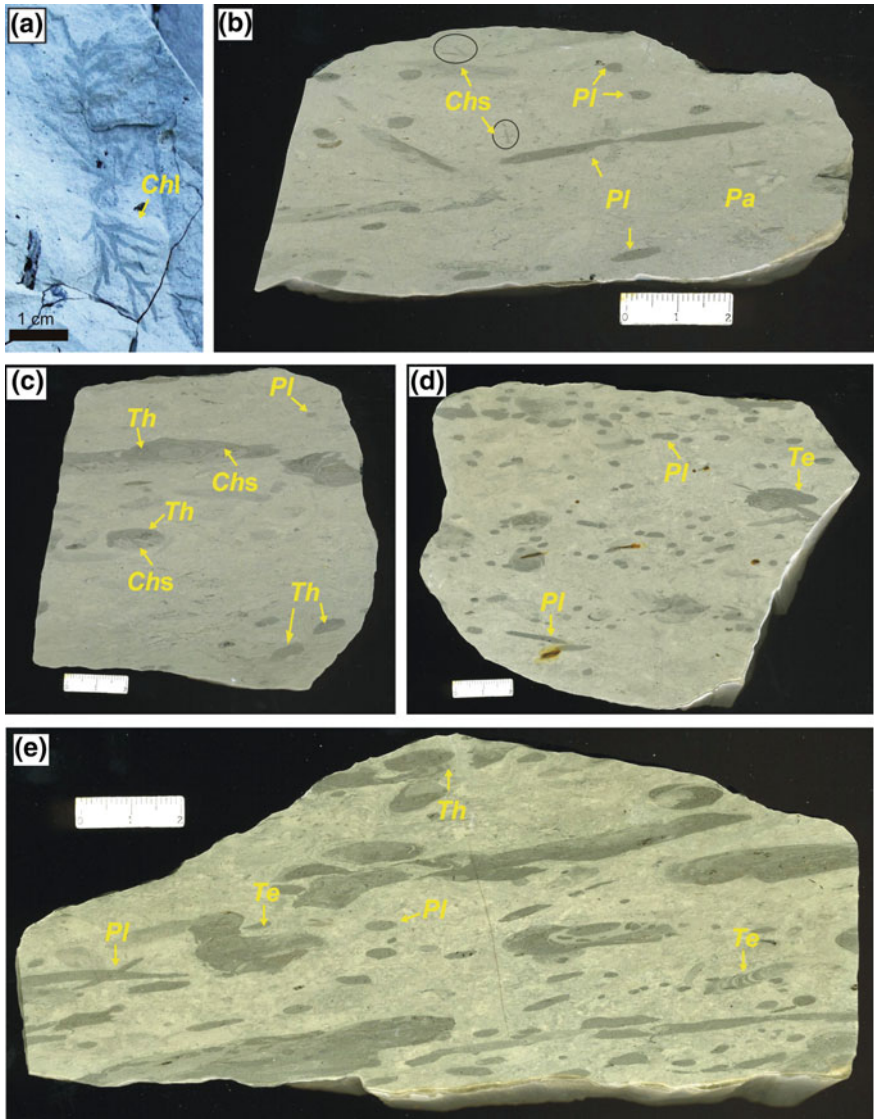


Fig. 3.25 Trace fossils from the marl-marly limestone rhythmite of La Cerradura section. Note *Pl* *Planolites* isp.; *Pa* *Palaeophycus* isp.; *Chs* *Chondrites* isp. (small); *Chl* *Chondrites* isp. (large); *Te* *Teichichnus* isp.; *Th* *Thalassinoides* isp. Modified from Reolid et al. (2014b)

The base of NJT 5b nannofossil Zone is marked by the first occurrence of *Lotharingius sigillatus* (Mattioli and Erba 1999) which is found in the bed CE-62 (at 15 m above the base; Fig. 3.24). The interval below is attributed to NJT 5a Zone because of the presence since the base of the section of *Lotharingius hauffii*, whose

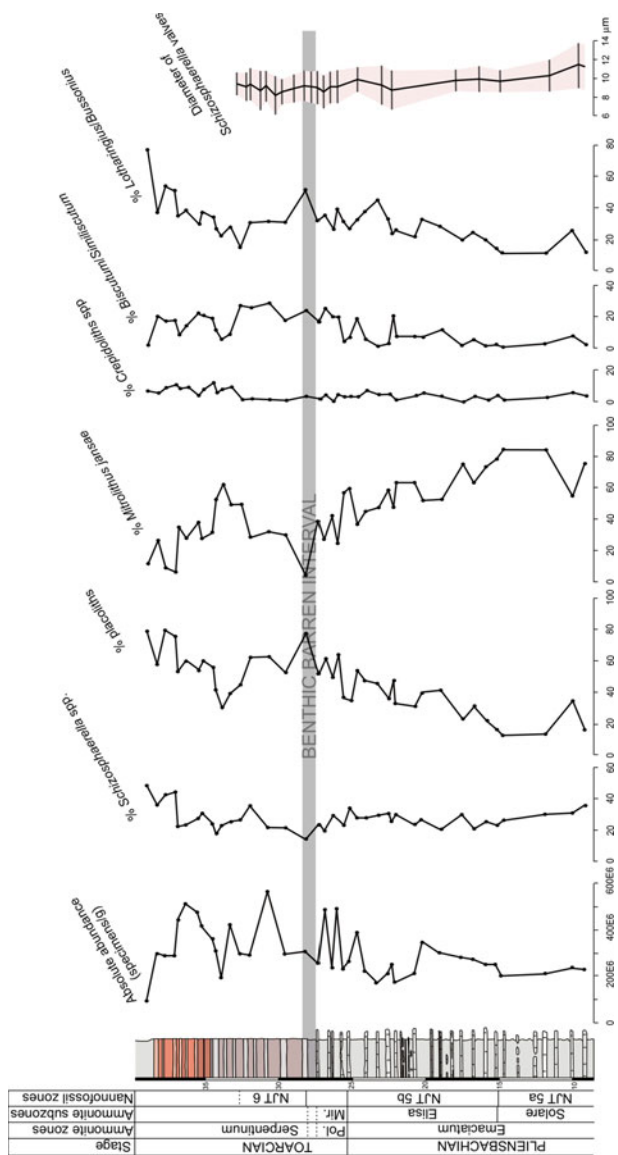


Fig. 3.26 Stratigraphic distribution of nanofossils, with absolute abundance (specimens/g), the relative abundance (%) of different components, and the range of diameter of *Schizosphaerella* valves and the mean values

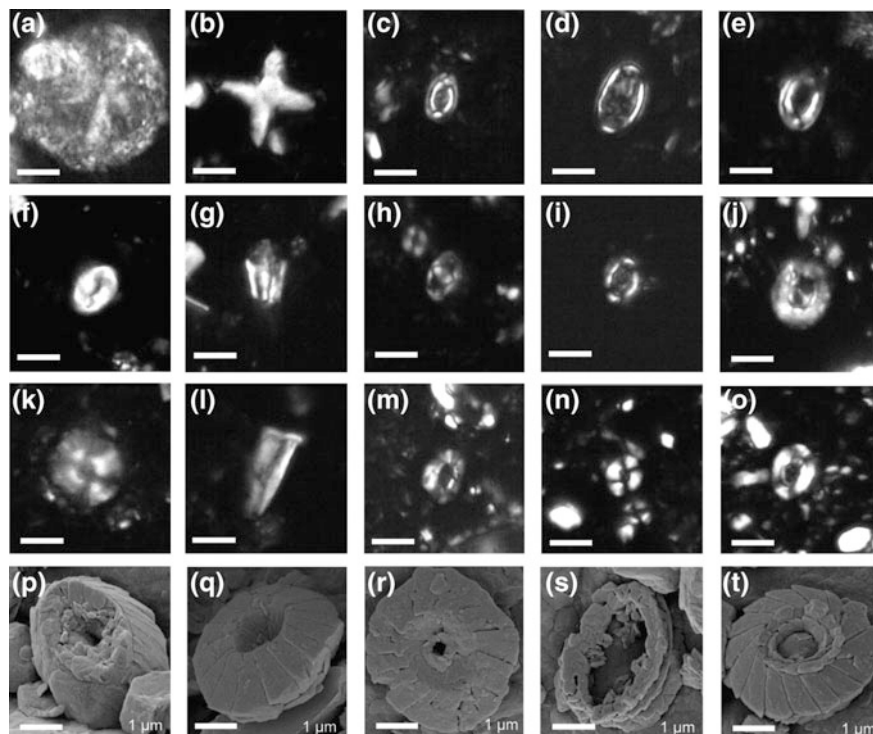


Fig. 3.27 Micrographs of common nanofossil taxa recorded in La Cerradura section. **a** *Schizosphaerella* sp. **b** *Orthogonoides hamiltoniae*. **c** *Tubirhabdus patulus*. **d** *Crepidolithus granulatus*. **e** *Crepidolithus cavus*. **f** *Crepidolithus crassus*. **g** *Mitrolithus jansae*. **h** *Zeugrhabdodus erectus*. **i** *Axopodorhabdus atavus*. **j** *Biscutum grande*. **k** *Similiscutum giganteum*. **l** *Carinolithus superbus*. **m** *Calyculus* sp. **n** *Lotharingius sigillatus*. **o** *Lotharingius crucicentralis*. **p** *Crepidolithus crassus*. **q** *Similiscutum novum*. **r** *Similiscutum cruciulus*. **s** *Mazaganella* sp. **t** *Lotharingius* sp. White bar is 5 μm , except for SEM pictures, 1 μm

first occurrence (lying below the studied interval) marks the base of NJT 5a Zone. The boundary between NJT 5B and NJT 6 zones is defined based on the first occurrence of *Carinolithus superbus* which is found in the bed CE-30 (28 m above the base of the studied interval; Fig. 3.24). This Zone has been defined according to Mattioli and Erba (1999). The first occurrence of *C. superbus* is noted 60 cm above the top of the marl-limestone rhythmite and defines the NJT 6 Zone that normally contains the record of T-OAE (Mattioli et al. 2004, 2008, 2009). Due to a lack of ammonites in the dark marly interval, the study of calcareous nanofossils represents a useful biostratigraphic tool in this section to identify the NJT6 nanofossil Zone (Fig. 3.24), which in other Tethyan sections spans the upper part of the Polymorphum and part of the Levisoni/Serpentinum ammonite zones.

Absolute abundances are very high, between 200 E6 and 600 E6 specimens per gram of rock (Fig. 3.26). However, the abundances dramatically drop down in the interval between beds 31 and 27 (first 2 m above the top of the rhythmite), where *Mitrolithus jansae* relative abundance also decreases (Fig. 3.26). A similar trend is observed in several western Tethyan sections (Mattioli et al. 2008, 2009). The dinoflagellates also decrease at the base of the dark marly interval. In general, throughout the section, the proportions of *M. jansae* are compensated mainly by the proportions of placoliths. The analysis of the diameter of *Schizosphaerella* valves shows a decrease just at the base of the dark marly interval with a diameter ranging from 7 to 10.5 μm . *Orthogonoides hamiltoniae*, an *incertae sedis* taxon that is normally recorded in levels enriched in organic matter (Mailliot et al. 2009), occurs very sporadically in the interval comprised between samples 21 and 31 (interval between 0 and 5.2 m above the top of the marl-limestone rhythmite). The proportions of *Biscutum* and *Similiscutum* in the Early Toarcian are generally higher than in the Upper Pliensbachian.

3.3.4 Geochemistry

Geochemistry indicates an abrupt change related to the beginning of the dark marly interval (Fig. 3.28). The CaCO_3 content (wt%), which ranges from 44.0 to 78.0% in the marly layers of the rhythmite, sharply decreases to its lowest values (19.3%) in the lower part of the dark marly interval (CE-29, 90–195 cm above the marl-limestone rhythmite) in coincidence with relatively higher values of TOC, nearly 0.4 wt%. Yet maximum TOC values are low compared with central and north European localities, they are in the range of Fuente Vidriera (Rodríguez-Tovar and Reolid 2013) and Cueva del Agua (Reolid et al. 2013b). Total sulphur (TS) presents the highest values (0.47%) just above the marl-limestone rhythmite (CE-31), though the increase of values takes place at the Pliensbachian-Toarcian boundary within the marl-limestone rhythmite.

The values of $\delta^{13}\text{C}$ from bulk-rock in the marl-limestone rhythmite (Upper Pliensbachian to Polymorphum Zone) are around 1.20‰, and a negative excursion of $\delta^{13}\text{C}$ (with amplitude of -0.8‰) occurs from 2 m above the rhythmite (0.41‰, Fig. 3.28). From there (CE-31 to CE-29), $\delta^{13}\text{C}$ increases to the top of the marls (reaching 2.47‰). The NJT 6 nannofossil Zone dates the base of the T-OAE negative excursion and demonstrates that the record of T-OAE in the External Subbetic is synchronous with many other Tethyan settings (Mattioli et al. 2004, 2008, 2009).

The $\delta^{18}\text{O}$ from bulk-rock mainly changes during Polymorphum Zone and the lower part of the dark marly interval (Serpentinum Zone). The $\delta^{18}\text{O}$ abruptly decreases in the Polymorphum Zone with minimum values (-2.50‰) at the contact between the marl-limestone rhythmite and the dark marly interval (with an isotopic excursion of -0.55‰). The first dark marly bed (CE-31) records the subsequent positive isotopic excursion (+1.0‰, reaching -1.50‰). After the first two metres of

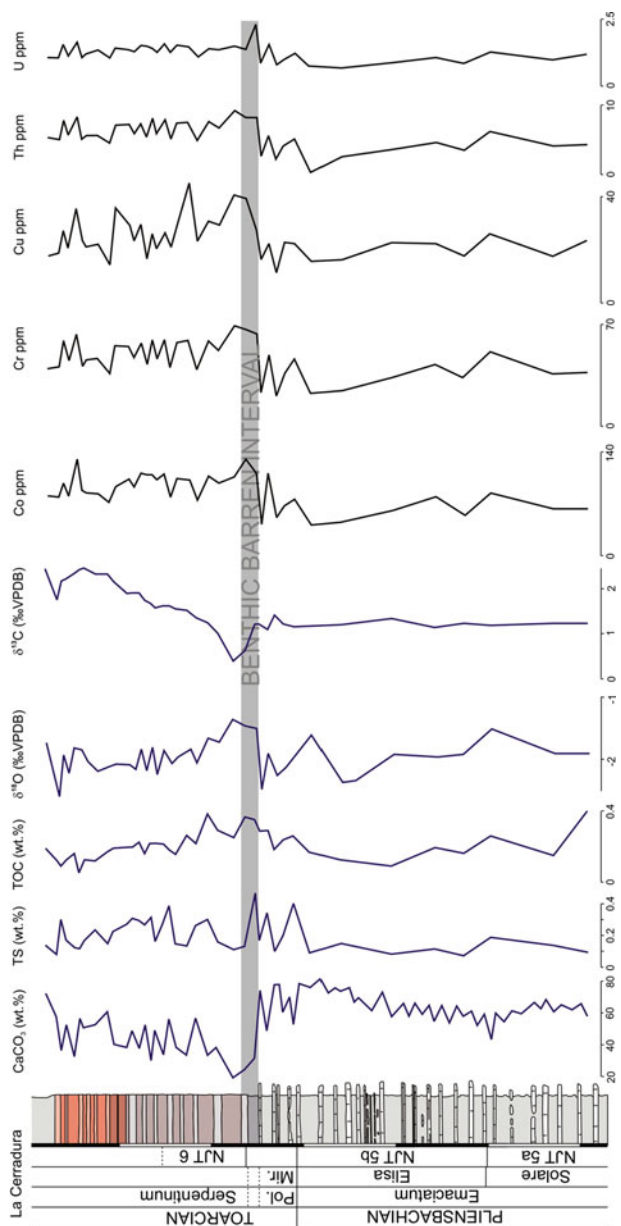


Fig. 3.28 Stratigraphic distribution of CaCO₃ content, total sulphur (TS), total organic carbon (TOC), and δ¹⁸O and δ¹³C from bulk sample, and content of redox sensitive elements (ppm)

dark marls, the $\delta^{18}\text{O}$ returns to values comparable to those of the Upper Pliensbachian.

The content, at ppm, of redox-sensitive elements Co, Cr, Cu, U and Th increases from the base of the Polymorphum Zone (Lower Toarcian), but the highest values occur in the first two metres of the dark marly interval (Fig. 3.28). The maximum value of U occurs in the first 60 cm (CE-31); the maximum value of Co occurs from 60 to 90 cm (CE-30); and maximum values of Cr, Cu and Th occur from 90 to 195 cm (CE-29) above the top of the rhythmite. The stratigraphic coincidence of maximum contents of redox sensitive elements and the negative carbon isotopic excursion (CIE) is intriguing. In SEM, small pyrite framboids ($\sim 4\ \mu\text{m}$) are also recorded in the lower part of the marl interval.

3.3.5 Interpretation

The carbon cycle perturbation related to the T-OAE is clearly recorded in the La Cerradura section by the increase of TOC and redox sensitive elements, the decrease of CaCO_3 and the negative excursion of $\delta^{13}\text{C}$ at the base of Serpentinum Zone, the NJT 6 nannofossil Zone (Fig. 3.29). Three different phases can be differentiated in this section mainly based on benthic assemblages and geochemistry: (a) Pre-biotic crisis, (b) T-OAE biotic crisis, and (c) recovery.

Pre-biotic crisis phase

This phase is represented by the marl-limestone rhythmite (Algovianum Zone, Upper Pliensbachian to Polymorphum Zone, Lower Toarcian). This is characterised by the record of necto-planktic and necto-benthic organisms (ammonites and belemnites) and minor benthic organisms (brachiopods and bivalves). Through the marl-limestone interval, deposits are totally bioturbated and reveal no evidence of primary lamination. In the marl-limestone rhythmite the trace-fossil assemblage is abundant and relatively diverse with *Chondrites*, *Palaeophycus*, *Planolites*, *Thalassinoides*, *Teichichnus* and *Trichichnus* (Reolid et al. 2014b). Despite the scarcity of fossils of benthic organisms, the abundance of trace fossils indicates a well-developed tiered macrobenthic tracemaker community, associated with favourable oxygen conditions (oxic to slightly dysoxic). The uppermost tier corresponds to a totally bioturbated background, related to an intense benthic activity on or just below the sea-bottom, in very soft sediments. The middle tier is mainly represented by a continuous record of *Planolites*, the tracemakers of which use oxygen from pore water, and *Thalassinoides*, *Teichichnus* and *Palaeophycus* recording the activity of mobile organisms, and indicating oxygen availability in the uppermost part of this tier. The deepest tier comprises small and large *Chondrites* and *Trichichnus*, all representing stationary or semistationary deposit feeders probably produced in a slightly firmer substrate, in comparatively low oxygen levels in pore-water (dysoxic) in the deeper tiers (McBride and Picard 1991; Rodríguez-Tovar and Uchman 2010). *Chondrites* is commonly attributed to

r-strategist tracemakers tolerant of very low-oxygen conditions (e.g., Ekdale and Bromley 1984; Savrda and Bottjer 1986; Wetzel 1994). The presence of foraminifera and ostracods from preliminary analyses confirms oxygen availability in the sea-floor.

Calcareous nannofossil assemblages are characterised by a progressive increase in placolith-coccoliths, mainly represented by species of the genera *Similiscutum*/*Biscutum* and *Lotharingius/Bussonius*, and a progressive decrease in *Mitrolithus jansae* (Fig. 3.26). These shifts in the assemblages can be interpreted as a response of the nannoplankton community to a progressive change of the water column structure. Namely, *M. jansae* has been interpreted as a deep-dweller species thriving in the lower photic zone (Bucefalo-Palliani and Mattioli 1995; Erba 2004; Mattioli and Pittet 2004; Mattioli et al. 2008), whilst placolith-coccoliths (*Similiscutum*/*Biscutum* and *Lotharingius/Bussonius*) were likely shallow-dwellers (Mattioli and Pittet 2004; Tremolada et al. 2005; Mattioli et al. 2008) (Fig. 3.29). This attests to an increase in productivity in the shallow euphotic zone between the end of Pliensbachian and the base of Toarcian. This would produce a comparative increase in proportions of meso-eutrophic shallow-dweller coccoliths and as a collateral consequence of increased production, less light in the deep photic zone, thus unfavourable conditions for photosynthetic deep-dwellers.

The size of *Schizosphaerella* decreased from the top of Algovianum Zone (Pliensbachian), with very low values in the uppermost Pliensbachian (Elisa Subzone, Emaciatum Zone). Size values of this rock-forming nannofossil are in the same range as in the central Italy and in Portugal (Mattioli and Pittet 2002; Suan et al. 2010), where this taxon also drastically decreased in size in the transition from the Pliensbachian to the Lower Toarcian.

The geochemical proxies and stable isotopes do not fluctuate strongly during the marl-limestone rhythmite and confirm the absence of relevant changes in the environmental conditions. The TOC presents a positive peak in the mid Solare Subzone (Emaciatum Zone, Upper Pliensbachian), but this is not correlated with any change in other geochemical indicators.

The top of this interval (CE-32) is characterised by an increase in abundance of fossil macroinvertebrates, mainly ammonites, belemnites and brachiopods. This top is also characterised by a negative oxygen isotopic excursion. Therefore, it is probably a condensed or omission surface related to the transgression of the Early Toarcian (e.g., Hallam 1986, 1987, 2001; Elmi 1996; Hylton and Hart 2000; Ruban and Tyszka 2005; Wignall et al. 2005; Korte and Hesselbo 2011; Pittet et al. 2014). The negative excursion of $\delta^{18}\text{O}$ could be correlated to the warming proposed by McArthur et al. (2000), Bailey et al. (2003), Suan et al. (2010, 2011), García Joral et al. (2011), Gómez and Goy (2011), and Korte and Hesselbo (2011) in other basins. In the Subbetic Basin this negative excursion of $\delta^{18}\text{O}$ is also recorded in the Cueva del Agua section (Reolid et al. 2013b) but not in Fuente Vidriera section (Reolid 2014a).

T-OAE biotic crisis phase

This phase is represented in the first two metres of the dark marly interval corresponding to the lower part of the NJT 6 nannofossil Zone (stratigraphically equivalent to the base of Serpentinum Zone). The main feature, in addition to the lithofacies change, is the absence of fossil macroinvertebrates and benthic microfossils at the beginning of the dark marl interval (around 40 cm). A drastic decrease in trace fossil diversity and abundance is registered, with only local records of small traces assignable to *Chondrites* (Fig. 3.29). This benthic barren interval reveals adverse conditions in the sea-floor, probably related to anoxic-dysoxic conditions, similar to the barren intervals recorded in Cueva del Agua and Fuente Vidriera sections in the Subbetic (see also Reolid et al. 2013b; Rodríguez-Tovar and Reolid 2013) and Ratnek El Kahla section from Saharan Atlas (Reolid et al. 2012a, b). The local presence of *Chondrites* may reflect a later colonisation from above when oxygen conditions started to improve, favourable for r-strategists tracemakers tolerant to very low-oxygen conditions such as *Chondrites* tracemakers, but not enough to maintain a diverse and abundant macrobenthic tracemaker community. *Chondrites* tracemaker can burrow from above into older anoxic sediments but to limited depth, probably no more than 20 cm. So, the record of *Chondrites* in this interval also implicates the incidental colonisation during the generally anoxic period. Benthic forms disappear in the first levels of Levisoni Zone or Serpentinum Zone at other Iberian margins, as reported by Duarte and Soares (2002), Gahr (2005), García Joral and Goy (2009), García Joral et al. (2011), and Comas-Rengifo et al. (2013), among others.

Two new taxa of brachiopods described in La Cerradura section, *Koninckodonta sumuntanensis* and *Atychorhynchia falsiorigo* (Baeza-Carratalá et al. 2017), supported pre-extinction dwarfing and resilience in La Cerradura section like a deep refugia linked to the Early Toarcian Mass Extinction Event, and an episode of speciation which is interpreted in terms of a pre-extinction radiation (Baeza-Carratalá et al. 2017).

All the brachiopods recorded in the La Cerradura section (*Liospiriferina*, *Koninckodonta*, *Orthotoma*, *Atychorhynchia*) are consistent with a very stable external morphotype consisting of a smooth ornament or very faint ribbing pattern, indicative of deep-water habitats (Vörös 2005; Baeza-Carratalá et al. 2017). The high evolutionary stability of this kind of deep and resilient environment enabled smooth latest Pliensbachian-Early Toarcian morphotypes to withstand several perturbation peaks within the extinction interval. The assemblage of the La Cerradura nowhere else throughout the Subbetic area. They not only survived the main mass extinction of the T-OAE, probably recorded in the lowermost Serpentinum Zone in the expanded La Cerradura section, but also underwent a radiation during the extinction interval (Baeza-Carratalá et al. 2017) as CE brachiopods diversified their lineages developing new taxa such as *Koninckodonta sumuntanensis* and *Atychorhynchia falsiorigo*. This speciation event occurred in deep areas which can serve as isolated evolutionary factories due to the trough and swell configuration of the South Iberian Palaeomargin. The first occurrence of these

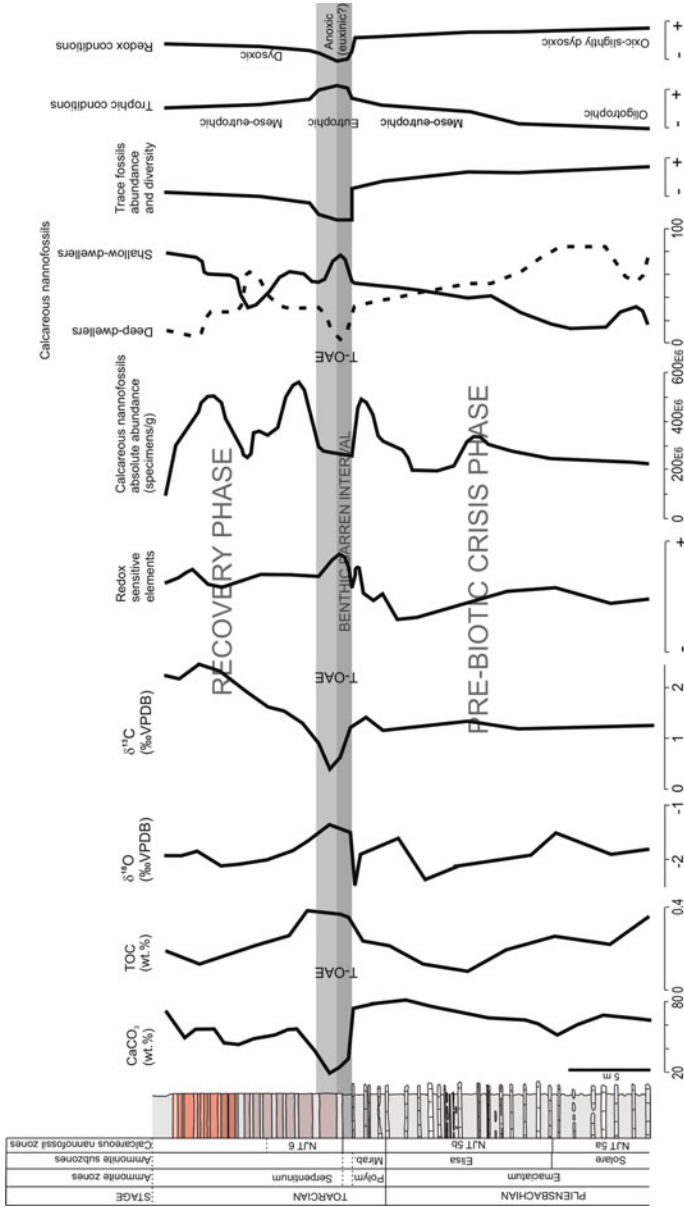


Fig. 3.29 Summary figure including the distribution of trace fossils, nanofossils and geochemical information (CaCO_3 , TOC, redox sensitive elements, $\delta^{18}\text{O}$ and $\delta^{13}\text{C}$), and interpreted redox and trophic conditions

taxa is recorded within the extinction interval and did not reach the repopulation interval as defined by the first occurrence of *S. bouchardi*. Thus, they can be regarded as failed crisis progenitors (cf. Kauffman and Harries 1996; Harries and Little 1999), as they could have played the role of pioneers that *S. bouchardi* achieved.

Environmental conditions were also unfavourable for the development of calcareous nannoplankton in the surface waters as well, as confirmed by the drop in absolute abundances of both coccoliths and *Schizosphaerella* and also by the decrease in size of *Schizosphaerella* (Fig. 3.26). Thus, the conditions were likewise hostile for calcareous dinoflagellates. Furthermore, the deep photic zone seems to have been particularly adverse for phytoplankton, as shown by the main decrease in relative abundance of the deep-dweller *M. jansae* (Figs. 3.26 and 3.29), probably related to shoaling of the oxygen minimum zone in the water column (Reolid et al. 2014b). Only the proportions of placoliths and *Lotharingius/Bussonius* relatively increased, but this could be related to a closed-sum effect. The proportion of *Similiscutum* keeps values higher than in Pliensbachian. This is a meso-eutrophic coccolith taxon (e.g., Bucefalo-Palliani et al. 2002; Mattioli and Pittet 2004) that may indicate relatively high trophic resources. The absence of ammonoids and belemnites in this interval indicates adverse conditions in the water column, probably related to poor oxygenation.

The base of the dark marly interval is characterised by the negative excursion of $\delta^{13}\text{C}$ (base of Serpentinum Zone, the NJT 6 nannofossil Zone) and increasing $\delta^{18}\text{O}$ values. The negative CIE occurring in this interval is widely known in the literature (e.g., Jenkyns and Clayton 1997; Mattioli et al. 2004, 2009; Hesselbo et al. 2007; Suan et al. 2008, 2010; Hermoso et al. 2009; Littler et al. 2010). However, the increase of $\delta^{18}\text{O}$ after the condensed surface, during the biotic crisis, is not correlated to the negative excursion of $\delta^{18}\text{O}$ identified by Bailey et al. (2003), Suan et al. (2010, 2011), García Joral et al. (2011), Gómez and Goy (2011), among others.

Increasing values of TOC, TS and redox sensitive elements (Co, Cr, Cu, Th and U) confirm the oxygen restricted conditions (Figs. 3.28 and 3.29). Similar trends have been recorded in the Cueva del Agua and Fuente Vidriera sections (e.g., Reolid et al. 2013b; Rodríguez-Tovar and Reolid 2013) and other southwestern Tethyan areas such as the Saharan Atlas (Reolid et al. 2012a, b, 2014a). Pyrite framboids <5 μm size confirm anoxia, probably widespread within the water column at any moment, as the small mean diameters (3–5 μm) with very limited size range are indicative of euxinic conditions (Wilkin et al. 1996; Bond and Wignall 2010; Dustira et al. 2013; Gallego-Torres et al. 2015). Van de Schootbrugge et al. (2013) propose that a phytoplankton shift occurred, with the establishment of photic-zone euxinia, driven by a salinity stratification and warming of surface waters. Studies from other outcrops in the External Subbetic propose water stagnation like in the Fuente Vidriera section (Rodríguez-Tovar and Reolid 2013; Reolid 2014a) and in the Cueva del Agua section (Reolid et al. 2013b), but anoxia is only proposed in the Cueva del Agua section in the dark laminated marl interval.

As indicated in the previous sections of the External Subbetic, the TOC values for this interval (0.4 wt%) would lie within the lower range of those registered in other Tethyan Toarcian sections. A potential explanation for the low TOC values in this setting could be a decline of calcareous nannoplankton and dinoflagellates due to the hostile conditions in the water column during the T-OAE. However, a drop in nannofossil abundance and the temporary disappearance of dinoflagellates is a common feature all around the Tethys (e.g., Bucefalo-Palliani et al. 2002; Mattioli et al. 2004; van de Schootbrugge et al. 2005a), also in sections where TOC is higher. Therefore, low productivity in the phytoplankton is not the reason why TOC is low in the La Cerradura section and in other sections of the Subbetic (Sandoval et al. 2012; Reolid et al. 2013b; Rodríguez-Tovar and Reolid 2013). Low TOC content of sections in the South margin of Tethys with respect to sections in North Tethys can be due to climatic differences (humidity vs. dryness, as discussed by van de Schootbrugge et al. 2005b) leading to more or less effective water stratification of the basin. Other studies relate the absence of anoxic conditions with low TOC, for example in the Cantabrian Basin, North Spain (Gómez and Goy 2011). However, the La Cerradura section shows evidence of temporal anoxia, even if TOC is low. Suan et al. (2013) has discussed the preservation of the TOC signal in Beaujolais (Central France), drawing comparisons with outcrops from the Lusitanian Basin (Portugal) and SW Germany, and the influence of recent weathering in TOC loss due to the infiltration of O₂-rich meteoric water. For this reason, extreme caution should be applied when interpreting the palaeoenvironmental significance of low TOC sediments, and it is necessary to support the interpretations with redox proxies, nannofossils, microfossils and/or ichnofossil assemblages.

Recovery phase

This phase is recorded as starting 2 m above the base of the dark marly interval. It is a fossil-poor interval containing belemnites, very small brachiopods, juvenile ammonites, foraminifera and ostracods. A repopulation phase with opportunistic strategy occurs typified by *Soaresirhynchia bouchardi* (Baeza-Carratalá et al. 2017).

The trace fossils show a gradual recovery with increasing diversity and abundance (mainly small *Planolites* and *Thalassinoides*), but still below the levels of the marl-limestone rhythmite during the pre-biotic crisis. These features indicate improved oxygen conditions in the sea-floor. Reolid et al. (2014b) reveal the presence of serpulids and foraminifera encrusting belemnite rostra and microborings, including those produced by cirripedes, pointing to an improved oxygenation level at the sea-floor. The record of root fragments of crinoid encrusted by *Bullopore tuberculata* also indicates oxygenation of the sea-floor. Toarcian crinoids have been interpreted as floating at the sea surface attached to driftwood fragments (e.g., Simms 1986; Seilacher and Hauff 2004). The remains in the dark marly interval of the La Cerradura section include coated roots of crinoids, however, indicating anchorage to a soft bottom (*s.* Seilacher and MacClintock 2005). Whole cirral and columnar complexes with a cortical stereom in continuity with core ossicles is coated, resulting in a loss of flexibility in such roots. Seilacher and

MacClintock (2005) propose that this kind of root was coated by a tough, tight-fitting cuticular sock that protected the living epidermis against toxic pore water in reduced zones of the sediment. This is congruent with the record in bed CE-28, directly over the benthic barren interval where the sediment pore-water would be very deficient in oxygen.

The amelioration in environmental conditions is also indicated by a greater absolute abundance of calcareous nannofossils and the greater diameter of *Schizosphaerella* valves. The relative abundance of the deep-dweller *Mitrolithus jansae* increases again, corroborating the improved oxygenation in the deep photic zone. The relative proportions of *Crepidolithus* increased in the upper part of the dark marly interval, although this is not a dominant species in the La Cerradura section. A similar rise in the abundance of *Crepidolithus* has been recorded in other Tethyan settings (Mattioli et al. 2008; Mailliot et al. 2009). Such an increase attests to the re-establishment of primary production in the entire photic zone, which most likely resulted in improved biomass production (Mailliot et al. 2009). This interpretation is further supported by relatively high proportions of *Similiscutum* (a meso-eutrophic taxon), higher than in Pliensbachian. These data indicate the persistence of high mesotrophic conditions after the T-OAE, or possibly higher values than during the Late Pliensbachian.

Geochemistry indicates the progressive recovery of carbonate production, some beds having 50% of CaCO₃. The TOC and the redox sensitive elements decrease throughout this interval as an evidence of oxygen availability in the sea-floor. However, some fluctuations reflect minor changes in oxygen conditions.

The values of $\delta^{13}\text{C}$ from bulk-rock also increase after the anoxic event to the top of the marls. The $\delta^{18}\text{O}$ shows minor fluctuations along this interval, returning to values of the Upper Pliensbachian.

References

- Anderson TF, Arthur MA (1983) Stable isotopes of oxygen and carbon and their application to sedimentologic and paleoenvironmental problems. In: Arthur MA (ed) Stable isotopes in sedimentary geology. SEPM Short Course, 10:1–151
- Baeza-Carratalá JF, Reolid M, García Joral F (2017) New deep-water brachiopod resilient assemblage from the South-Iberian Palaeomargin (Western Tethys) and its significance for the brachiopod adaptive strategies around the Early Toarcian Mass Extinction Event. Bull Geosci (in press)
- Bailey TR, Rosenthal Y, McArthur JM, van de Schootbrugge B, Thirlwall MF (2003) Paleooceanographic changes of the Late Pliensbachian-Early Toarcian interval: a possible link to the genesis of an anoxic event. Earth Planet Sci Lett 212:307–320
- Baturin GN (2002) Uranium and phosphorous in deep-sea clay from the Pacific Ocean. Oceanology 42:723–730
- Berner RA, Raiswell R (1983) Burial of organic carbon and pyrite sulfur in sediments over Phanerozoic time: a new theory. Geochim Cosmochim Acta 47:855–862
- Bodin S, Mattioli E, Frölich S, Marshall JD, Boutib L, Lahsini S, Redfern J (2010) Toarcian carbon isotope shifts and nutrient changes from the Northern margin of Gondwana (High Atlas,

- Morocco, Jurassic): palaeoenvironmental implications. *Palaeogeogr Palaeoclimatol Palaeoecol* 297:377–390
- Bond DPG, Wignall PB (2010) Pyrite framboid study of marine Permian-Triassic boundary sections: a complex anoxic event and its relationship to contemporaneous mass extinction. *GSA Bull* 122:1265–1279
- Braga JC (1983) Ammonites del Domerense de la Zona Subbética (Cordilleras Béticas, Sur de España). Ph.D. Thesis, Universidad de Granada
- Broecker WS, Peng T-H (1982) *Tracers in the sea*. Eldigio Press, Columbia University, Palisades, New York
- Bucefalo-Palliani R, Mattioli E (1995) Ecology of dinoflagellate cyst and calcareous nannofossils from bituminous facies of the Early Toarcian, central Italy. 3rd Workshop: Black Shales Models, European Palaeontological Association, Dotternhausen, Germany
- Bucefalo-Palliani R, Mattioli E, Riding JB (2002) The response of marine phytoplankton and sedimentary organic matter to the Early Toarcian (Lower Jurassic) oceanic anoxic event in northern England. *Mar Micropaleontol* 46:223–245
- Busnardo R (1979) Prebétique et Subbétique de Jaén à Lucena (Andalusie). *Lias. Documents Laboratoires Geologie Faculté Sciences Lyon* 74, p 140
- Calvert SE, Pedersen TF (1993) Geochemistry of recent oxic and anoxic marine sediments: implications for the geological record. *Mar Geol* 113:67–88
- Caníçó A, Duarte LV, Rocha F, Reolid M, Terroso D (2015) Palaeoenvironmental meaning of clay minerals assemblages across the Late Pliensbachian-Early Toarcian (Early Jurassic) of Iberian Peninsula: Lusitanian, Algarve and Subbetic basins. *Euroclay Programme and Abstracts*, p 115
- Casellato CE, Erba E (2015) Calcareous nannofossil biostratigraphy and paleoceanography of the Toarcian Oceanic Anoxic Event at Colle di Sogno (Southern Alps, Northern Italy). *Riv Ital Paleontol Stratigr* 121:297–327
- Caswell BA, Coe AL (2012) A high-resolution shallow marine record of the Toarcian (Early Jurassic) Oceanic Anoxic Event from the East Midlands Shelf, UK. *Palaeogeogr Palaeoclimatol Palaeoecol* 365–366:124–135
- Cheel RJ, Leckie DA (1993) Hummocky cross-stratification. In: Wright PW (ed) *Sedimentology review/1*. Blackwell Scientific Publication, London, pp 103–122
- Chester R, Baxter GB, Behairy AKA, Connor K, Cross D, Elderfield H, Padgham RC (1977) Soil-sized eolian dusts from the lower troposphere of the eastern Mediterranean Sea. *Mar Geol* 24:201–217
- Cohen AS, Coe AL, Harding SM, Scwark L (2004) Osmium isotope evidence for the regulation of atmospheric CO₂ by continental weathering. *Geology* 32:157–160
- Comas MC, Puga E, Bargossi GM, Morten L, Rossi PL (1986) Paleogeography, sedimentation and volcanism of the central Subbetic Zone, Betic Cordilleras, Southeastern Spain. *Neues Jb Geol Paläontol Monat* 7:385–404
- Comas-Rengifo MJ, Duarte LV, García-Joral F, Goy A (2013) Los braquiópodos del Toarciense Inferior (Jurásico) en el área de Rabaçal-Condeixa (Portugal): distribución estratigráfica y paleobiogeografía. *Comun Geol* 100(Especial I):37–42
- de Graciansky PC, Jacquin T, Hesselbo SP (1998) The Ligurian cycle: an overview of Lower Jurassic 2nd-order transgressive/regressive facies cycles in western Europe. In: *Mesozoic and Cenozoic sequence stratigraphy of European Basins*. SEPM Special Publication, 60, pp 467–479
- Dera G, Donnadiou Y (2012) Modeling evidences for global warming, Arctic seawater freshening, and sluggish oceanic circulation during the Early Toarcian anoxic event. *Paleoceanography* 27: PA2211
- Dera G, Pucéat E, Pellenard P, Neige P, Delsate D, Joachimski MM, Reisberg L, Martínez M (2009) Water mass exchange and variations in seawater temperature in the NW Tethys during the Early Jurassic: evidence from neodymium and oxygen isotopes of fish teeth and belemnites. *Earth Planet Sci Lett* 286:198–207
- Duarte LV (1997) Facies analysis and sequential evolution of the Toarcian-Lower Aalenian series in the Lusitanian Basin (Portugal). *Comun Inst Geol Min* 83:65–94

- Duarte LV (1998) Clay minerals and geochemical evolution in the Toarcian-Lower Aalenian of the Lusitanian Basin. *Cuad Geol Ibérica* 24:69–98
- Duarte LV, Soares AF (1993) Eventos de natureza tempestítica e turbidítica no Toarciano inferior da Bacia Lusitânica (Sector Norte). *Cad Geogr Fac Let Univ Coimbra* 12:89–95
- Duarte LV, Soares AF (2002) Litostratigrafia das series margo-calcárias do Jurásico inferior da Bacia Lusitânica (Portugal). *Commun Inst Geol Min* 89:135–154
- Dustira AM, Wignall PB, Joachimski M, Blomeier D, Hartkopf-Fröder C, Bond DPG (2013) Gradual onset of anoxia across the Permian-Triassic boundary in Svalbard, Norway. *Palaeogeogr Palaeoclimatol Palaeoecol* 374:303–313
- Ekdale AA, Bromley RG (1984) Sedimentology and ichnology of the Cretaceous-Tertiary boundary in Denmark: implications for the causes of the terminal Cretaceous extinction. *J Sediment Petrol* 54:681–703
- Elmi S (1996) Stratigraphic correlations of the main Jurassic events in the Western Mediterranean Tethys (western Algeria and eastern Morocco). *Geores Forum* 1–2:343–357
- Ennyu A, Arthur MA, Pagani M (2002) Fine-fraction carbonate stable isotopes as indicators of seasonal shallow mixed-layer paleohydrography. *Mar Micropaleontol* 46:317–342
- Erba E (2004) Calcareous nannofossils and Mesozoic oceanic anoxic events. *Mar Micropaleontol* 52:85–106
- Fohrer B, Samankassou E (2005) Paleocological control of ostracod distribution in a Pennsylvanian Auernigg cyclothem of the Carnic Alps, Austria. *Palaeogeogr Palaeoclimatol Palaeoecol* 225:317–330
- Gahr ME (2005) Response of Lower Toarcian (Lower Jurassic) macrobenthos of the Iberian Peninsula to sea level changes and mass extinction. *J Iberian Geol* 31:197–215
- Gallego-Torres D, Martínez-Ruiz F, Paytan A, Jiménez-Espejo FJ, Ortega-Huertas M (2007) Pliocene-Holocene evolution of depositional conditions in the eastern Mediterranean: role of anoxia vs. productivity at time of sapropel deposition. *Palaeogeogr Palaeoclimatol Palaeoecol* 246:424–439
- Gallego-Torres D, Martínez-Ruiz F, De Lange GJ, Jiménez-Espejo FJ, Ortega-Huertas M (2010) Trace-elemental derived paleoceanographic and paleoclimatic conditions for Pleistocene Eastern Mediterranean sapropels. *Palaeogeogr Palaeoclimatol Palaeoecol* 293:78–89
- Gallego-Torres D, Reolid M, Nieto-Moreno V, Martínez-Casado FJ (2015) Pyrite framboids size distribution as a record for relative variations in sedimentation rate: an example on the Toarcian Oceanic Anoxic Event in Southiberian Palaeomargin. *Sed Geol* 330:59–73
- García Joral F, Goy A (2009) Toarcian (Lower Jurassic) brachiopods in Asturias (Northern Spain): stratigraphic distribution, critical events and palaeobiogeography. *Geobios* 42:255–264
- García Joral F, Gómez JJ, Goy A (2011) Mass extinction and recovery of the early Toarcian (early Jurassic) brachiopods linked to climate change in northern and central Spain. *Palaeogeogr Palaeoclimatol Palaeoecol* 302:367–380
- García-Hernández M, López-Garrido AC, Martín-Algarra A, Molina JM, Ruiz-Ortiz PA, Vera JA (1989) Las discontinuidades mayores del Jurásico de las Zonas Externas de las Cordilleras Béticas: Análisis e interpretación de los ciclos sedimentarios. *Cuad Geol Ibérica* 13:35–52
- Gatto R, Monari S, Neige P, Pinard JD, Weis R (2015) Gastropods from upper Pliensbachian-Toarcian (Lower Jurassic) sediments of Causses basin, southern France and their recovery after the early Toarcian anoxic event. *Geol Mag* 152:871–901
- Gautier F, Odin GS (1985) Volcanisme Jurassique du sud de l'Aragon (Espagne). *Bulletin de Liaison et Information, I.G.C.P. Project 196, offset Paris*, 5:34–38
- Gómez JJ, Goy A (2000) Definition and organization of limestone-marls cycles in the Toarcian of the Northern and East-Central part of the Iberian Subplate (Spain). *Geores Forum* 6:301–310
- Gómez JJ, Goy A (2005) Late Triassic and Early Jurassic palaeogeographic evolution and depositional cycles of the Western Tethys Iberian platform system (Eastern Spain). *Palaeogeogr Palaeoclimatol Palaeoecol* 222:77–94
- Gómez JJ, Goy A (2011) Warming-driven mass extinction in the Early Toarcian (Early Jurassic) of northern and central Spain. Correlation with other time-equivalent European sections. *Palaeogeogr Palaeoclimatol Palaeoecol* 306:176–195

- Hallam A (1986) The Pliensbachian and Tithonian extinction events. *Nature* 319:765–768
- Hallam A (1987) Radiations and extinctions in relation to environmental change in the marine Lower Jurassic of northwest Europe. *Paleobiology* 13:152–168
- Hallam A (2001) A review of the broad pattern of Jurassic sea-level changes and their possible causes in the light of current knowledge. *Palaeogeogr Palaeoclimatol Palaeoecol* 167:23–37
- Haq BU, Hardenbol J, Vail PR (1987) Chronology of fluctuating sea level since the Triassic. *Science* 235:1156–1167
- Harazim D, van de Schootbrugge B, Sorichter K, Fiebig J, Weug A, Suan G, Oschmann W (2013) Spatial variability of watermass conditions within the European Epicontinental Seaway during the Early Jurassic (Pliensbachian–Toarcian). *Sedimentology* 60:359–390
- Harries PJ, Little CTS (1999) The Early Toarcian (Early Jurassic) and the Cenomanian–Turonian (Late Cretaceous) mass extinctions: similarities and contrasts. *Palaeogeogr Palaeoclimatol Palaeoecol* 154:39–66
- Helz GR, Miller CV, Charnock JM, Mosselmans JLW, Patrick RAD, Garner CD, Vaughan DJ (1996) Mechanisms of molybdenum removal from the sea and its concentration in black shales: EXAFS evidences. *Geochim Cosmochim Acta* 60:3631–3642
- Hermoso M, Minoletti F, Le Callonnec L, Jenkyns HC, Hesselbo SP, Rickaby REM, Renard M, de Rafaeli M, Emmanuel L (2009) Global and local forcing of Early Toarcian seawater chemistry: a comparative study of different paleoceanographic settings (Paris and Lusitanian basins). *Paleoceanography* 24:PA4208
- Hesselbo SP, Gröcke DR, Jenkyns HC, Bjerrum CJ, Farrimond P, Morgans-Bell HS, Green OR (2000) Massive dissociation of gas hydrate during a Jurassic oceanic anoxic event. *Nature* 406:392–395
- Hesselbo SP, Jenkyns HC, Duarte LV, Oliveira LCV (2007) Carbon-isotope record of the Early Jurassic (Toarcian) Oceanic Anoxic Event from fossil wood and marine carbonate (Lusitanian Basin, Portugal). *Earth Planet Sci Lett* 253:455–470
- Hylton MD, Hart MB (2000) Benthic foraminiferal response to Pliensbachian–Toarcian (Lower Jurassic) sea-level change and oceanic anoxia in NW Europe. *Geores Forum* 6:455–462
- Izumi K, Miyaji T, Tanabe K (2012) Early Toarcian (Early Jurassic) oceanic anoxic event recorded in the shelf deposits in the northwestern Panthalassa: evidence from the Nishinakayama Formation in the Toyora area, west Japan. *Palaeogeogr Palaeoclimatol Palaeoecol* 315–316:100–108
- Jenkyns HC (1985) The Early Toarcian and Cenomanian–Turonian anoxic events in Europe: comparisons and contrasts. *Geol Rundsch* 74:505–518
- Jenkyns HC (1988) The Early Toarcian (Jurassic) anoxic event: stratigraphic, sedimentary, and geochemical evidence. *Am J Sci* 288:101–151
- Jenkyns HC (2003) Evidence for rapid climate change in the Mesozoic–Palaeogene greenhouse world. *Philos Trans R Soc Lond A361:1885–1916*
- Jenkyns HC, Clayton CK (1997) Lower Jurassic epicontinental carbonates and mudstones from England and Wales: chemostratigraphic signals and the early Toarcian anoxic event. *Sedimentology* 44:687–706
- Jenkyns HC, Géczy B, Marshall JD (1991) Jurassic manganese carbonates of central Europe and the early Toarcian anoxic event. *J Geol* 99:137–149
- Jenkyns HC, Jones CE, Gröcke DR, Hesselbo SP, Parkinson DN (2002) Chemostratigraphy of the Jurassic System: applications, limitations and implications for paleoceanography. *J Geol Soc London* 159:351–378
- Jiménez AP (1986) Estudio paleontológico de los ammonites del Toarciense inferior y medio de las Cordilleras Béticas (Dactylioceratidae e Hildoceratidae). Ph.D. Thesis, Universidad de Granada
- Jiménez AP, Rivas P (2007) El OAE toarciense en la secuencia de la Fuente de la Vidriera, Zona Subbética, región de Caravaca (Murcia). In Aguirre J, Company M, Rodríguez-Tovar FJ (eds) XXIII Jornadas de la Sociedad Española de Paleontología, Caravaca, Field Trip Guidebook. Universidad de Granada, pp 3–16

- Jiménez AP, Jiménez de Cisneros C, Rivas P, Vera JA (1996) The early Toarcian anoxic event in the westernmost Tethys (Subbetic): paleogeographic and paleobiogeographic significance. *J Geol* 104:399–416
- Jiménez-Espejo FJ, Martínez-Ruiz F, Sakamoto T, Iijima K, Gallego-Torres D, Harada N (2007) Paleoenvironmental changes in western Mediterranean since the last glacial maximum: high resolution multiproxy record from the Algero-Balearic basin. *Palaeogeogr Palaeoclimatol Palaeoecol* 246:292–306
- Kauffman EG, Harries PJ (1996) The importance of crisis progenitors in recovery from mass extinction. In: Hart MB (ed) *Biotic recovery from mass extinction events*. Geological Society, London, Special Publications 102, pp 15–39
- Kemp DB, Coe AL, Cohen AS, Schwark L (2005) Astronomical pacing of methane release in the Early Jurassic period. *Nature* 437:396–400
- Korte C, Hesselbo SP (2011) Shallow marine carbon and oxygen isotope and elemental records indicate icehouse-greenhouse cycles during the Early Jurassic. *Paleoceanography* 26:PA4219
- Krencker FN, Bodin S, Suan G, Heimhofer U, Kabiri L, Immenhauser A (2015) Toarcian extreme warmth led to tropical cyclone intensification. *Earth Planet Sci Lett* 425:120–130
- Laska W, Rodríguez-Tovar FJ, Uchman A (2017) Evaluating macrobenthic response to the Cretaceous-Palaeogene event: a high-resolution ichnological approach at the Agost section (SE Spain). *Cretac Res* 70:96–110
- Latimer JC, Filippelli GM (2001) Terrigenous input and paleoproductivity in the Southern Ocean. *Paleoceanography* 16:627–643
- Littler K, Hesselbo SP, Jenkyns HC (2010) A carbon-isotope perturbation at the Pliensbachian-Toarcian boundary: evidence from the Lias Group, NE England. *Geol Mag* 147:181–192
- Mailliot S, Mattioli E, Guex J, Pittet B (2006) The Early Toarcian anoxia, a synchronous event in the Western Tethys? An approach by quantitative biochronology (Unitary Associations), applied on calcareous nannofossils. *Palaeogeogr Palaeoclimatol Palaeoecol* 240:562–586
- Mailliot S, Mattioli E, Bartolini A, Baudin F, Pittet B, Guex J (2009) Pliensbachian-Toarcian (Early Jurassic) environmental changes in an epicontinental basin of NW Europe (Causse area, central France): the evidence from an integrated study of microfossils and geochemistry. *Palaeogeogr Palaeoclimatol Palaeoecol* 273:346–364
- Marok A, Reolid M (2012) Lower Jurassic sediments from the Rhar Roubane Mountains (Western Algeria): stratigraphic precisions and synsedimentary block-faulting. *J Afr Earth Sc* 76:50–65
- Martínez RM, Lago M, Valenzuela JI, Vaquer R, Salas R (1996a) El magmatismo alcalino jurásico del sector SE de la Cadena Ibérica: Composición y estructura. *Geogaceta* 20:1687–1690
- Martínez RM, Lago M, Vaquer R, Valenzuela JI, Arranz E (1996b) Composición mineral del volcanismo jurásico (pre-Bajociense medio) en la Sierra de Javalambre (Cordillera Ibérica, Teruel): Datos preliminares. *Geogaceta* 19:41–44
- Martínez RM, Lago M, Valenzuela JI, Vaquer R, Salas R, Dumitrescu R (1997) El volcanismo Triásico y Jurásico del sector SE de la Cadena Ibérica y su relación con los estadios de rift mesozoicos. *Bol Geol Min* 108-4 y 5(367–376):39–48
- Martínez-Ruiz F, Kastner M, Paytan A, Ortega-Huertas M, Bernasconi SM (2000) Geochemical evidence for enhanced productivity during S1 sapropel deposition in the eastern Mediterranean. *Paleoceanography* 15:200–209
- Martínez-Ruiz F, Paytan A, Kastner M, González-Donoso JM, Linares D, Bernasconi SM, Jiménez-Espejo FJ (2003) A comparative study of the geochemical and mineralogical characteristics of the S1 sapropel in the western and eastern Mediterranean. *Palaeogeogr Palaeoclimatol Palaeoecol* 190:23–37
- Mattioli E, Erba E (1999) Synthesis of calcareous nannofossil events in tethyan Lower and Middle Jurassic successions. *Riv Ital Paleontol Stratigr* 105:343–376
- Mattioli E, Pittet B (2002) Contribution of calcareous nannoplankton to carbonate deposition: a new approach applied to the Lower Jurassic of central Italy. *Mar Micropaleontol* 45:175–190

- Mattioli E, Pittet B (2004) Spatial and temporal distribution of calcareous nannofossils along a proximal-distal transect in the Lower Jurassic of the Umbria-Marche Basin (central Italy). *Palaeogeogr Palaeoclimatol Palaeoecol* 205:295–316
- Mattioli E, Pittet B, Bucefalo-Palliani R, Röhl HJ, Schmid-Röhl A, Moretini E (2004) Phytoplankton evidence for the timing and correlation of palaeoceanographical changes during the early Toarcian oceanic anoxic event (Early Jurassic). *J Geol Soc London* 161:685–693
- Mattioli E, Pittet B, Suan G, Mailliot S (2008) Calcareous nannoplankton across the Early Toarcian anoxic event: implications for paleoceanography within the western Tethys. *Paleoceanography* 23:PA3208
- Mattioli E, Pittet B, Petitpierre L, Mailliot S (2009) Dramatic decrease of the pelagic carbonate production by nannoplankton across the Early Toarcian Anoxic Event (T-OAE). *Glob Planet Changes* 65:134–145
- McArthur JM, Donovan DT, Thirlwall MF, Fouke BW, Matthey D (2000) Strontium isotope profile of the Early Toarcian (Jurassic) oceanic anoxic event, the duration of ammonite biozones, and belemnite palaeotemperatures. *Earth Planet Sci Lett* 179:269–285
- McArthur JM, Algeo TJ, van de Schootbrugge B, Li Q, Howarth RJ (2008) Basinal restriction, black shales, Re-Os dating, and Early Toarcian (Jurassic) oceanic anoxic event. *Paleoceanography* 23:PA4217
- McBride EF, Picard DM (1991) Facies implications of *Trichichnus* and *Chondrites* in turbidites and hemipelagites, Marnoso-arenacea formation (Miocene), Northern Apennines, Italy. *Palaios* 6:281–290
- McElwain JC, Wade-Murphy J, Hesselbo SP (2005) Changes in carbon dioxide during an anoxic event linked to intrusion of Gondwana coals. *Nature* 435:479–482
- Meyers SR, Sageman BB, Lyons TW (2005) Organic carbon burial rate and the molybdenum proxy: theoretical framework and application to Cenomanian–Turonian oceanic event 2. *Paleoceanography* 20:PA2002
- Míguez-Salas O, Rodríguez-Tovar FJ, Duarte LV (2017) Selective incidence of the Toarcian Oceanic Anoxic Event (T-OAE) on macroinvertebrate marine communities: a case from the Lusitanian basin (Portugal). *Lethaia*. doi:[10.1111/let.12212](https://doi.org/10.1111/let.12212)
- Mira F (1987) Foraminíferos del Lías margoso de las Cordilleras Béticas. Zona Subbética. Ph.D. Thesis, Universidad de Granada (unpublished)
- Molina JM, Nieto LM, Ruiz-Ortiz PA, Vera JA (2007) The Zegrí Formation: a record of Lower Jurassic syn-rift sedimentation in the Betic Cordillera. In: 25th IAS Meeting of Sedimentology, Patras (Grecia). Book of Abstracts, p 278
- Morard A, Guex J, Bartolini A, Moretini E, De Weyer P (2003) A new scenario for the Domesian-Toarcian transition. *Bull Soc Géol Fr* 174:351–376
- Morten SD, Twitchett RJ (2009) Fluctuations in the body size of marine invertebrates through the Pliensbachian-Toarcian extinction event. *Palaeogeogr Palaeoclimatol Palaeoecol* 284:29–38
- Mouterde R, Busnardo R, Linares A (1971) Le Domérien dans le Subbétique Central (Andalousie). Données préliminaires. *Cuad Geol Ibérica* 2:237–254
- Nagao S, Nakashima S (1992) Possible complexation of uranium with dissolved humic substances in pore water of marine-sediments. *Sci Total Environ* 118:439–447
- Nieto LM (1997) La Cuenca subbética mesozoica en el sector oriental de las Cordilleras Béticas. Ph.D. Thesis, Universidad de Granada
- Nieto LM, Molina JM, Ruiz-Ortiz PA (2004) La Formación Zegrí: registro de los primeros estadios de una etapa sin-rift en el Jurásico de las Zonas Externas Béticas. *Geotemas* 6: 157–160
- Nikitenko BL, Reolid M, Gliinskikh L (2013) Ecostratigraphy of benthic foraminifera for interpreting Arctic record of Early Toarcian biotic crisis (Northern Siberia, Russia). *Palaeogeogr Palaeoclimatol Palaeoecol* 376:200–212
- Palomo I (1987) Mineralogía y geoquímica de sedimentos pelágicos del Jurásico inferior de las Cordilleras Béticas (SE de España). Ph.D. Thesis, Universidad de Granada
- Palomo I, Ortega-Huertas M, Fenoll P (1985) The significance of clay minerals in studies of the evolution of the Jurassic deposits of the Betic Cordilleras, SE Spain. *Clay Miner* 20:39–52

- Parisi G, Ortega-Huertas M, Nocchi M, Palomo I, Monaco P, Ruiz F (1996) Stratigraphy and geochemical anomalies of the Early Toarcian oxygen-poor interval in the Umbria-Marche Apennines (Italy). *Geobios* 29:469–484
- Pingfang W, Yongjian H, Chengshan W, Zihui F, Qunghua H (2012) Pyrite morphology in the first member of the Late cretaceous Qingshankou Formation, Songliao Basin, northeast China. *Palaeogeogr Palaeoclimatol Palaeoecol* 385:125–136
- Pittet B, Suan G, Lenoir F, Duarte LV, Mattioli E (2014) Carbon isotope evidence for sedimentary discontinuities in the lower Toarcian of the Lusitanian Basin (Portugal): sea-level change at the onset of the Oceanic Anoxic Event. *Sed Geol* 303:1–14
- Portugal M, Morata DA, Puga E, Demant A, Aguirre L (1995) Evolución geoquímica y temporal del magmatismo básico mesozoico en las Zonas Externas de las Cordilleras Béticas. *Estud Geol* 51:109–118
- Powell WG, Johnston PA, Collom CJ (2003) Geochemical evidence for oxygenated bottom waters during deposition of fossiliferous strata of the Burgess Shale Formation. *Palaeogeogr Palaeoclimatol Palaeoecol* 201:249–268
- Pye K (1987) Aeolian dust and dust deposits. Academic Press, San Diego
- Reolid M (2008) Taphonomic features of *Lenticulina* as a tool for palaeoenvironmental interpretation of mid-shelf deposits of Upper Jurassic (Prebetic Zone, southern Spain). *Palaios* 23:482–494
- Reolid M (2014a) Stable isotopes on foraminifera and ostracods for interpreting incidence of the Toarcian Oceanic Anoxic Event in Westernmost Tethys: role of water stagnation and productivity. *Palaeogeogr Palaeoclimatol Palaeoecol* 395:77–91
- Reolid M (2014b) Pyritized radiolarians and siliceous sponges from oxygen restricted deposits (Lower Toarcian, Jurassic). *Facies* 60:789–799
- Reolid M, Abad I (2014) Glauconitic laminated crusts as a consequence of hydrothermal alteration of Jurassic pillow-lavas from Median Subbetic (Betic Cordillera, S Spain): a microbial influence case. *J Iberian Geol* 40:389–408
- Reolid M, Martínez-Ruiz F (2012) Comparison of benthic foraminifera and geochemical proxies in shelf deposits from the Upper Jurassic of the Prebetic (southern Spain). *J Iberian Geol* 38:449–465
- Reolid M, Rodríguez-Tovar FJ, Nagy J, Olóriz F (2008) Benthic foraminiferal morphogroups of mid to outer shelf environments of the Late Jurassic (Prebetic Zone, southern Spain): characterisation of biofacies and environmental significance. *Palaeogeogr Palaeoclimatol Palaeoecol* 261:280–299
- Reolid M, Rodríguez-Tovar FJ, Marok A, Sebane A (2012a) The Toarcian Oceanic Anoxic Event in the Western Saharan Atlas, Algeria (North African paleomargin): role of anoxia and productivity. *Geol Soc Am Bull* 124:1646–1664
- Reolid M, Sebane A, Rodríguez-Tovar FJ, Marok A (2012b) Foraminiferal morphogroups as a tool to approach the Toarcian Anoxic Event in the Western Saharan Atlas (Algeria). *Palaeogeogr Palaeoclimatol Palaeoecol* 323–325:87–99
- Reolid M, Chakiri S, Bejjaji Z (2013a) Adaptive strategies of the Toarcian benthic foraminiferal assemblages from the Middle Atlas (Morocco): palaeoecological implications. *J Afr Earth Sc* 84:1–12
- Reolid M, Nieto LM, Sánchez-Almazo IM (2013b) Caracterización geoquímica de facies pobremente oxigenadas en el Toarciense inferior (Jurásico inferior) del Subbético Externo. *Rev Soc Geol Esp* 26:69–84
- Reolid M, Marok A, Sebane A (2014a) Foraminiferal assemblages and geochemistry for interpreting the incidence of Early Toarcian environmental changes in North Gondwana paleomargin (Traras Mountains, Algeria). *J Afr Earth Sc* 95:105–122
- Reolid M, Mattioli E, Nieto LM, Rodríguez-Tovar FJ (2014b) The Early Toarcian Oceanic Anoxic Event in the External Subbetic (Southiberian Paleomargin, Westernmost Tethys): geochemistry, nannofossils and ichnology. *Palaeogeogr Palaeoclimatol Palaeoecol* 411:79–94

- Reolid M, Sánchez-Quiñónez CA, Alegret L, Molina E (2015a) Palaeoenvironmental turnover across the Cenomanian-Turonian transition in Oued Bahloul, Tunisia: foraminifera and geochemical proxies. *Palaeogeogr Palaeoclimatol Palaeoecol* 417:491–510
- Reolid M, Rivas P, Rodríguez-Tovar FJ (2015b) Toarcian ammonitico rosso facies from the South Iberian Paleomargin (Betic Cordillera, southern Spain): paleoenvironmental reconstruction. *Facies* 61:22. doi:10.1007/s10347-015-0447-3
- Rey J, Delgado A (2002) Carbon and oxygen isotopes: a tool for Jurassic and early Cretaceous pelagic correlation (southern Spain). *Geol J* 37:337–345
- Rey J, Bonnet L, Cubaynes R, Qajoun A, Ruget C (1994) Sequence stratigraphy and biological signals: statistical studies of benthic foraminifera from Liassic series. *Palaeogeogr Palaeoclimatol Palaeoecol* 111:149–171
- Rickard D, Mussmann M, Steadman JA (2017) Sedimentary sulfides. *Elements* 13:117–122
- Rita P, Reolid M, Duarte LV (2016) Benthic foraminiferal assemblages record major environmental perturbations during the Late Pliensbachian—Early Toarcian interval in the Peniche GSSP, Portugal. *Palaeogeogr Palaeoclimatol Palaeoecol* 454:267–281
- Robertson AK, Filippelli GM (2008) Paleoproductivity variations in the eastern equatorial Pacific over glacial timescales. American Geophysical Union Fall Meeting 2008, Abstract PP33C-1576
- Rodríguez-Tovar FJ, Reolid M (2013) Environmental conditions during the Toarcian Oceanic Anoxic Event (T-OAE) in the westernmost Tethys: influence of the regional context on a global phenomenon. *Bull Geosci* 88:697–712
- Rodríguez-Tovar FJ, Uchman A (2010) Ichnofabric evidence for the lack of bottom anoxia during the Lower Toarcian Oceanic Anoxic Event (T-OAE) in the Fuente de la Vidriera section, Betic Cordillera, Spain. *Palaios* 25:576–587
- Rodríguez-Tovar FJ, Miguez-Salas O, Duarte LV (2017) Toarcian Oceanic Anoxic Event induced unusual behaviour and palaeobiological changes in *Thalassinoides* tracemakers. *Palaeogeogr Palaeoclimatol Palaeoecol* (in press)
- Röhl HJ, Schmid-Röhl A, Oschmann W, Frimmel A, Swark L (2001) The Posidonian Shale (Lower Toarcian) of SW-Germany: an oxygen-depleted ecosystem controlled by sea level and paleoclimate. *Palaeogeogr Palaeoclimatol Palaeoecol* 165:27–52
- Rosales I, Quesada S, Robles S (2004) Paleotemperature variations of Early Jurassic seawater recorded in geochemical trends of belemnites from the Basque-Cantabrian basin, northern Spain. *Palaeogeogr Palaeoclimatol Palaeoecol* 203:253–275
- Rubán DA, Tyszká J (2005) Diversity dynamics and mass extinctions of the Early-Middle Jurassic foraminifers: a record from the Northwestern Caucasus. *Palaeogeogr Palaeoclimatol Palaeoecol* 222:329–343
- Ruget C, Martínez-Gallego J (1979) Foraminifères du Lias moyen et supérieur. *Cuad Geol Univ Granada* 10:311–316
- Sabatino N, Neri R, Bellanca A, Jenkyns HC, Baudin F, Parisi G, Masetti D (2009) Carbon-isotope records of the Early Jurassic (Toarcian) oceanic anoxic event from the Valdorbia (Umbria-Marche Apennines) and Monte Mangart (Julian Alps) sections: palaeoceanographic and stratigraphic implications. *Sedimentology* 56:1307–1328
- Sælen G, Tyson RV, Telnæs N, Talbot MR (2000) Contrasting watermass conditions during deposition of the Whitby Mudstone (Lower Jurassic) and Kimmeridge Clay (Upper Jurassic) formations, UK. *Palaeogeogr Palaeoclimatol Palaeoecol* 163:163–196
- Sandoval J, Bill M, Aguado R, O'Dogherty L, Rivas P, Morard A, Guex J (2012) The Toarcian in the Subbetic basin (southern Spain): bio-events (ammonite and calcareous nannofossils) and carbon-isotope stratigraphy. *Palaeogeogr Palaeoclimatol Palaeoecol* 342–343:40–63
- Savrda CE, Bottjer DJ (1986) Trace-fossil model for reconstruction of paleo-oxygenation in bottom waters. *Geology* 14:3–6
- Sebane A, Marok A, Elmi S (2007) Évolution des peuplements de foraminifères pendant la crise toarcienne à l'exemple des données des Monts des Ksour (Atlas Saharien Occidental, Algérie). *C R Palevol* 6:189–196
- Seilacher A, Hauff RB (2004) Constructional morphology of pelagic crinoids. *Palaios* 19:3–16

- Seilacher A, MacClintock C (2005) Crinoid anchoring strategies for soft-bottom dwelling. *Palaios* 20:224–240
- Siebert C, Nagler TF, von Blanckenburg F, Kramers JD (2003) Molybdenum isotope records as a potential new proxy for paleoceanography. *Earth Planet Sci Lett* 211:159–171
- Simms MJ (1986) Contrasting lifestyles in Lower Jurassic crinoids: a comparison of benthic and pseudopelagic Isocrinida. *Palaeontology* 29:475–493
- Sohn IG (1960) Paleozoic species of *Bairdia* and related genera –revision of some Paleozoic ostracod genera. *US Geol Surv Prof Pap* 330-B:107–160
- Suan G, Pittet B, Bour I, Mattioli E, Duarte LV, Mailliot S (2008) Duration of the Early Toarcian carbon isotope excursion deduced from spectral analysis: consequence for its possible causes. *Earth Planet Sci Lett* 267:666–679
- Suan G, Mattioli E, Pittet B, Lécuyer C, Suchéras-Marx B, Duarte LV, Philippe M, Reggiani L, Martineau F (2010) Secular environmental precursors to Early Toarcian (Jurassic) extreme climate changes. *Earth Planet Sci Lett* 290:448–458
- Suan G, Nikitenko BL, Rogov MA, Baudin F, Spangenberg JE, Knyazev VG, Glinskikh LA, Goryacheva AA, Adatte T, Riding JB, Föllmi KB, Pittet B, Mattioli E, Lécuyer C (2011) Polar record of Early Jurassic massive carbon injection. *Earth Planet Sci Lett* 312:102–113
- Suan G, Rulleau L, Mattioli E, Suchéras-Marx B, Rousselle B, Pittet B, Vincent P, Martin JE, Lena A, Spangenberg JE, Föllmi KB (2013) Palaeoenvironmental significance of Toarcian black shales and event deposits from southern Beaujolais, France. *Geol Mag* 150:728–742
- Sun YB, Wu F, Clemens SC, Oppo DW (2008) Processes controlling the geochemical composition of the South China Sea sediments during the last climatic cycle. *Chem Geol* 257:234–249
- Svensen H, Planke S, Chevallier L, Malthe-Sørensen A, Corfu F, Jamtveit B (2007) Hydrothermal venting of greenhouse gases triggering Early Jurassic global warming. *Earth Planet Sci Lett* 256:554–566
- Sweeney RE, Kaplan LR (1980) Stable isotope composition of dissolved sulfate and hydrogen sulfide in the Black Sea. *Mar Chem* 9:145–152
- Teichert S, Nutzelt A (2014) Early Jurassic anoxia triggered the evolution of the oldest holoplanktonic gastropod *Coelodiscus minutus* by means of heterochrony. *Acta Palaeontol Pol* 60:269–276
- Thomson J, Mercione D, de Lange GJ, Van Santvoort PJM (1999) Review of recent advances in the interpretation of eastern Mediterranean sapropel S1 from geochemical evidence. *Mar Geol* 153:77–89
- Tremolada F, van de Schootbrugge B, Erba E (2005) Early Jurassic schizosphaerellid crisis in Cantabria, Spain: implications for calcification rates and phytoplankton evolution across the Toarcian oceanic anoxic event. *Paleoceanography* 20:PA2011
- Tribouillard N, Algeo T, Lyons T, Riboulleau A (2006) Trace metals as palaeoredox and palaeoproductivity proxies: an update. *Chem Geol* 232:12–32
- Twitchett RJ (2007) The Lilliput effect in the aftermath of the end-Permian extinction event. *Palaeogeogr Palaeoclimatol Palaeoecol* 252:132–144
- Tyson RV, Pearson TH (1991) Modern and ancient continental shelf anoxia: an overview. In: Tyson RV, Pearson TH (eds) *Modern and ancient continental shelf anoxia*. Geological Society Special Publication 58, pp 1–24
- Tyszká J (1994) Response of Middle Jurassic benthic foraminiferal morphogroups to dysoxic/anoxic conditions in the Pieniny Klippen Basin, Polish Carpathians. *Palaeogeogr Palaeoclimatol Palaeoecol* 110:55–81
- Tyszká J, Jach R, Bubik M (2010) A new vent-related foraminifer from the lower Toarcian black claystone of the Tatra Mountains, Poland. *Acta Palaeontol Pol* 55:333–342
- Urbanek A (1993) Biotic crisis in the history of upper Silurian graptoloids: a palaeobiological model. *Hist Biol* 7:29–50
- van de Schootbrugge B, Bailey TR, Rosenthal Y, Katz ME, Wright JD, Miller KG, Feist-Burkhardt S, Falkowski PG (2005a) Early Jurassic climate change and the radiation of organic walled phytoplankton in the Tethys Ocean. *Paleobiology* 31:73–97

- van de Schootbrugge B, McArthur JM, Bailey TR, Rosenthal Y, Wright JD, Miller KG (2005b) Toarcian oceanic anoxic event: an assessment of global causes using belemnite C isotope records. *Paleoceanography* 20:3008. doi:[10.1029/2004PA001102](https://doi.org/10.1029/2004PA001102)
- van de Schootbrugge B, Bachan A, Suan G, Richoz S, Payne JL (2013) Microbes, mud and methane: cause and consequence of recurrent Early Jurassic anoxia following the End-Triassic mass extinction. *Palaeontology* 56:685–709
- Vera JA (2001) Evolution of the Iberian continental margin. *Mém Mus Natl d’Hist Nat Paris* 186:109–143
- Vera JA, Molina JM, Montero P, Bea F (1997) Jurassic guyots on the Southern Iberian Continental Margin: a model of isolated carbonate platforms on volcanic submarine edifices. *Terra Nova* 9:163–166
- Vörös A (2005) The smooth brachiopods of the Mediterranean Jurassic: refugees or invaders? *Palaeogeogr Palaeoclimatol Palaeoecol* 223:222–242
- Wang P, Huang Y, Wang C, Feng Z, Huang Q (2012) Pyrite morphology in the first member of the Late Cretaceous Qingshankou Formation, Songliao Basin, northeast China. *Palaeogeogr Palaeoclimatol Palaeoecol* 385:125–136
- Wei H, Algeo TJ, Yu H, Wang J, Guo C, Shi G (2015) Episodic euxinia in the Changhsingian (late Permian) of South China: evidence from framboidal pyrite and geochemical data. *Sed Geol* 319:78–97
- Wendler I, Huber BT, MacLeod KG, Wendler JE (2013) Stable oxygen and carbon isotope systematics of exquisitely preserved Turonian foraminifera from Tanzania—understanding isotopic signatures in fossils. *Mar Micropaleontol* 102:1–33
- Wetzel A (1994) The environmental significance of “opportunistic” and “equilibrium” strategies of the Chondrites and Phycosiphon producers. In: 14th International Sedimentological Congress, Recife, Brazil, pp 17–18
- Wignall PB, Myers KJ (1988) Interpreting the benthic oxygen levels in mudrocks: a new approach. *Geology* 16:452–455
- Wignall PB, Newton RJ, Little CTS (2005) The timing of paleoenvironmental change and cause-and-effect relationships during the Early Jurassic mass extinction in Europe. *Am J Sci* 305:1014–1032
- Wilkin RT, Barnes HL, Brantley SL (1996) The size distribution of framboidal pyrite in modern sediments: an indicator of redox conditions. *Geochim Cosmochim Acta* 60:3897–3912
- Yilmaz IO, Altiner D, Tekin UK, Tuysuz O, Ocakoglu F, Acikalın S (2010) Cenomanian-Turonian Oceanic Anoxic Event (OAE2) in the Sakarya zone, northwestern Turkey: sedimentological, cyclostratigraphic, and geochemical records. *Cretac Res* 31:207–226
- Ziveri P, Stoll H, Probert I, Klaas C, Geisen M, Ganssen G, Young J (2012) Stable isotope “vital effects” in coccolith calcite. *Earth Planet Sci Lett* 210:137–149

Chapter 4

Median Subbetic Outcrops

4.1 Iznalloz Section

The Iznalloz (IZ) section is located in the km 13 of the Granada-Moreda railway scarpment (N 37° 23' 24.4"; E 03° 29' 19.5"), 3 km east of the village of Iznalloz (Granada Province, Figs. 3.1 and 4.1). The study section pertains to the Toarcian of the Zegrí Formation, and contains alternating marls and marly limestones in the lower part with nodular marly limestones (ammonitico rosso facies) in the upper part (Braga et al. 1981; Reolid et al. 2015).

The studied interval in the Iznalloz section is 18.5 m-thick. It comprises 3.2 m of yellow limestones, marls and marly limestones (Polymorphum and Serpentinum zones), 6.8 m of red marls and marly limestones having a nodular appearance, with intercalations of white laminated limestones (Bifrons and lower part of Gradata zones), and 8.5 m of nodular limestones and marly limestones (from upper part of Gradata Zone to Aalensis Zone) (Figs. 4.1 and 4.2).

The Iznalloz section was initially studied by Mouterde and Linares (1960), Rivas (1972), Braga et al. (1981) and Jiménez (1986), with special emphasis on the ammonite biostratigraphy, whereas Palomo (1987) focused on clay minerals. Recently, Reolid et al. (2015) studied the lithofacies and trace fossils. In this section the T-OAE is not well represented due to the thickness of the Polymorphum and Serpentinum zones, the presence of stratigraphic gaps as well as the environmental conditions of this setting favouring the oxygenation. However, this section presents a very different set of lithofacies during the Toarcian that help in the understanding of the evolution of the South Iberian Palaeomargin.

4.1.1 Ammonite Biostratigraphy

The Iznalloz section is very rich in ammonites and belemnites, favouring a fine biostratigraphy both in the marly interval and in the red nodular limestones (Rivas

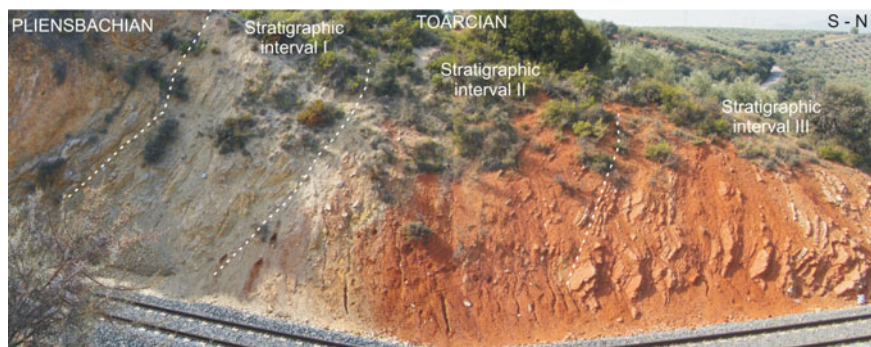


Fig. 4.1 Field view of Iznalloz section and differentiates stratigraphic intervals for the Toarcian. Note the inverted disposition of the stratigraphic succession

1972; Jiménez 1986). Above the micritic limestones of the upper Pliensbachian, three stratigraphic intervals have been differentiated in the Toarcian of the Iznalloz section (Reolid et al. 2015; Figs. 4.1 and 4.2).

- First stratigraphic interval (3.2 m): is formed by grey to yellow limestones, marls and marly limestones with *Dactyloceras polymorphum*, *D. simplex*, *Hildaites serpentinus* and *Murleyiceras evagriori*, among others (Rivas 1972; Jiménez 1986). This assemblage characterises the Polymorphum and Serpentinum zones (Lower Toarcian).
- Second stratigraphic interval (6.1 m): is composed of grey and red marls and marly limestones with a nodular appearance, featuring intercalations of white laminated limestone beds at a decimetric scale. In this interval, the ammonites *Catacoeloceras* sp., *Hildoceras bifrons*, *H. sublevisoni*, *H. semipolatum*, *Mercaticeras mercati* and *Nodicoeloceras* sp., determine the Bifrons Zone (Rivas 1972; Jiménez 1986). The record of *Brodieia gradata* and *B. bayani* at the top of this stratigraphic interval indicates the base of the Gradata Zone (middle Toarcian).
- Third stratigraphic interval (8.5 m-thick): is constituted by nodular limestones and secondarily nodular marly limestones, marls and white laminated limestones. The record of *Brodieia gradata*, *Chartronia elegans*, *Ch. iserensis* and *Phymatoceras* sp. indicates the Gradata Zone (Middle Toarcian) at the beginning of this stratigraphic interval. The presence of *Pseudogrammoceras fallaciosum* indicates the beginning of the Upper Toarcian (Fallaciosum Zone) from the base of bed IZ-18. The record of *Dumortieria latumbilicata* and *Catulloceras meneghinii* characterise the Reynesi Zone, and the occurrence of *Erycites* sp., *Pleydellia subcompta* and *P. aalensis* from upper part of the IZ-23 confirms the beginning of the Aalensis Zone.

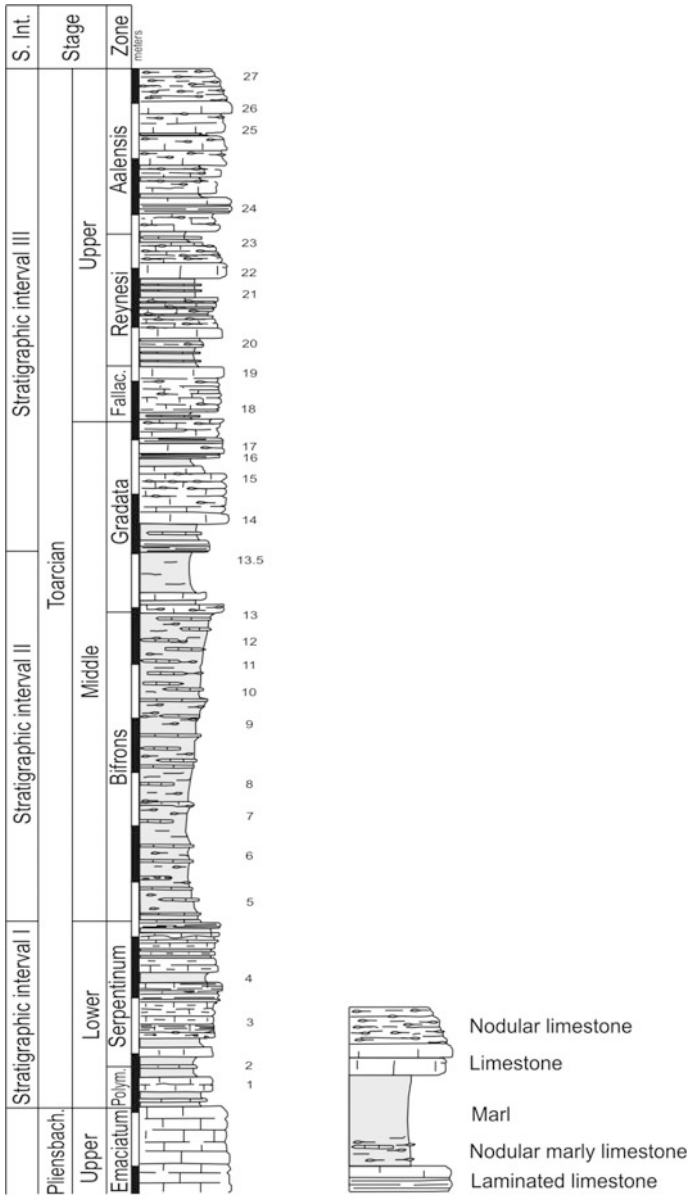


Fig. 4.2 Lithological column of the Iznalloz section. Biostratigraphic intervals according to Rivas (1972) and Jiménez (1986)

4.1.2 Lithofacies and Microfacies

Four main types of lithofacies were differentiated according to macroscopic and microscopic features (Figs. 4.2, 4.3, 4.4 and 4.5):

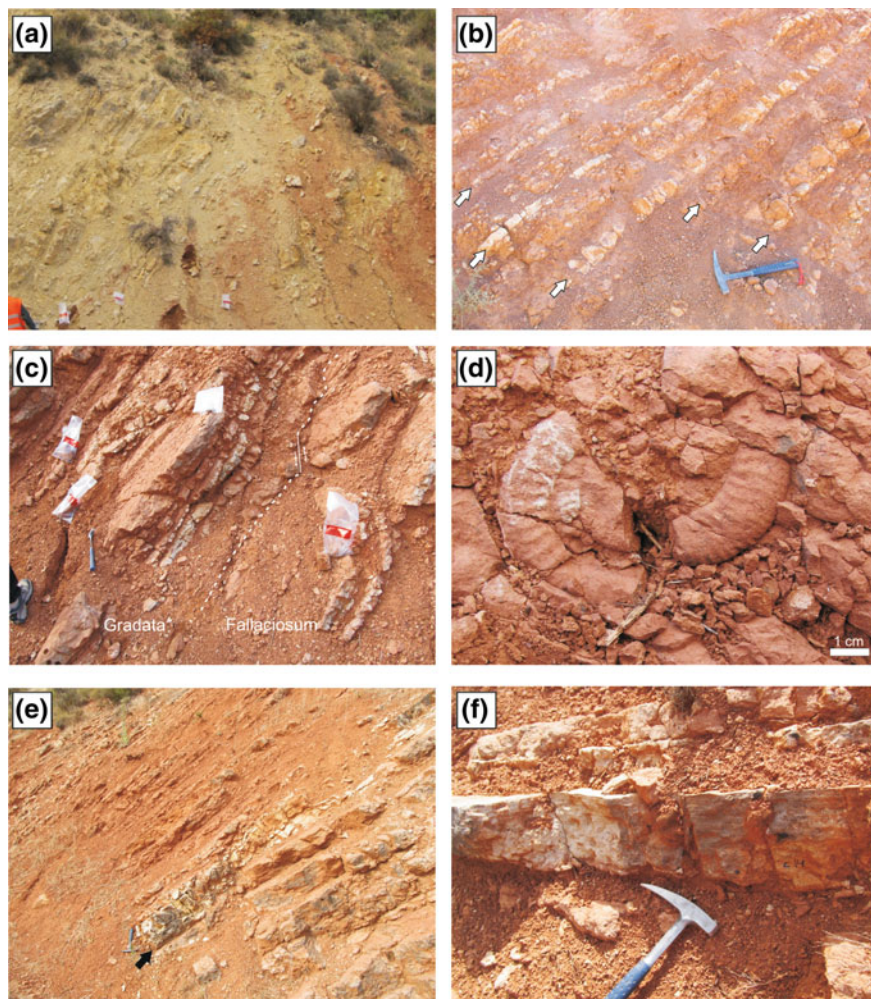


Fig. 4.3 Field view of lithofacies. **a** Grey-yellow limestones (Lower Toarcian, *left*) and grey marls (lower part of Bifrons Zone, Middle Toarcian, *right*). **b** Red marls from upper part of Bifrons Zone (Middle Toarcian) with thin white laminated limestones (*white arrows*). **c** Red nodular limestone (ammonitico rosso facies) from the boundary between Gradata Zone (Middle Toarcian) and Fallaciosum Zone (Upper Toarcian). **d** *Ericites* sp. close to Reynesi-Aalensis zone boundary. **e** White laminated limestone (*white arrow*) intercalated in ammonitico rosso facies of red nodular limestones from the base of Aalensis Zone (Upper Toarcian). **f** White laminated limestone from the upper part of Gradata Zone

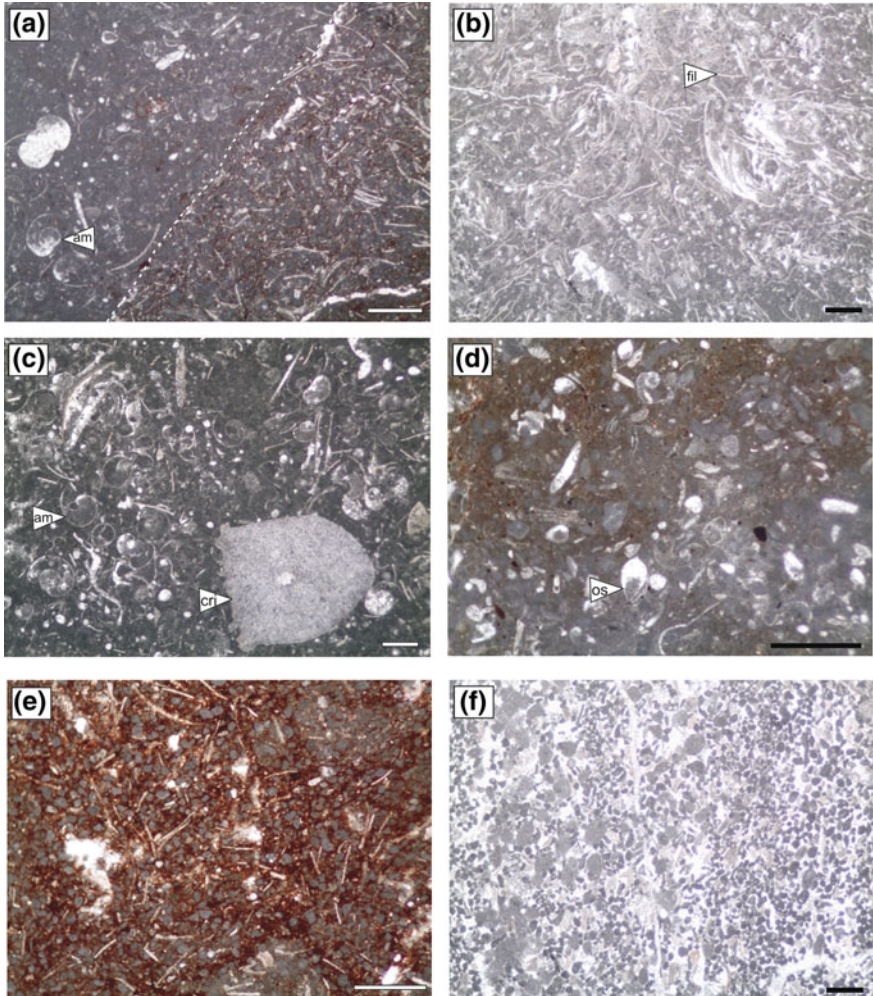


Fig. 4.4 Microfacies from Iznaloz section. **a** Contact between calcareous nodule (*left side*) rich in ammonitella and ostracods, and red clay rich matrix (*right side*) rich in fragments of filaments and iron oxides, indicated by a *dotted line* (Aalensis Zone). **b** Packstone of peloids and filaments from red nodular limestone (base of Gradata Zone). **c** Packstone of ammonitellas and echinoderm fragments from nodules (Aalensis Zone). **d** Packstone of bioclasts rich in ostracods and foraminifera from red pseudonodular marly limestone bed (Bifrons Zone). **e** Packstone of peloids and filaments from the clay rich matrix between nodules of the red nodular limestones (Reynesi Zone). **f** Laminated grainstone of peloids from white laminated limestone (Bifrons Zone). *Note* fil, filaments; am, ammonitella; cri, crinoid ossicle; os, ostracod. Scale bar 1 mm

- (a) Grey-yellow limestones (Fig. 4.3a): Mudstone-wackestone of bioclasts at the base of the section, and packstone of peloids and filaments (thin shelled bivalves in larval stages with planktotrophic lifestyle). The grain size is very

fine (<100 μm). The most abundant bioclasts are filaments and echinoderms. Trace fossils are scarce and undifferentiated. This lithofacies constitutes the first stratigraphic interval (Lower Toarcian, Fig. 4.5). Marly layers between limestones contain illite, smectite and chlorite, but no kaolinite (Palomo 1987).

- (b) Grey and red marls (Fig. 4.3b): They constitute most of the second stratigraphic interval (Middle Toarcian *p.p.*), with a predominance of grey marls in the lower part and red marls in the upper part. They present common microfossils such as foraminifera, ostracods and ophiuroids. Palomo (1987) indicated illite as the main component of clay minerals, with higher contents of smectites in the grey marls and higher contents of kaolinite in the red marls.
- (c) Red nodular limestones and marly limestones (Fig. 4.3c–e): These are red beds 10–45 cm-thick and pseudonodular to nodular appearance, with a continuous subfacies transition from limestones (calcareous ammonitico rosso) to marly limestones (marly ammonitico rosso). This lithofacies is dominant in the third stratigraphic interval. The base of these beds is commonly rich in subhorizontal trace fossils. These limestones correspond mainly to packstone of peloids and filaments, a minority being wackestone-packstones of bioclasts (Fig. 4.4a–e). The matrix among grains is reddish and iron-rich, while peloids and lumps are grey. Filaments and echinoderms are the most common bioclasts. Filaments are usually not-oriented or oriented according to nodule edges. Reolid et al. (2015) indicate that the reddish matrix shows fluidal appearance in some samples. In Gradata and Aalensis zones, ammonitella (embryonic shells of ammonoids) are common; while radiolarians are common mainly at the top of the Aalensis Zone. This lithofacies appears in the Bifrons Zone as decimetric beds among marly beds (marly ammonitico rosso), and is predominant in the upper part of the Gradata Zone, where there is an increase in carbonate content, thickness and nodularity (calcareous ammonitico rosso). In the beds of the Bifrons Zone and in the Gradata Zone to base of the Aalensis Zone, the nodules are diffuse, showing very irregular shape and lighter colour with respect to the red background. In Reynesi and Aalensis zones, the white-grey nodules (1.5–3.5 cm) are clearly differentiated from the red internodule matrix in short sequences of increasing nodularity in each bed. In some cases, the nodulous aspect is restricted to the top of the beds. They are irregular nodules distributed in the beds as nodule-rich horizons (floated), and the contact between nodules and internodes is well-marked by the colour. The topmost metre of the section presents large nodules (1.5–5 cm) with spheroidal shape, the sharp edges sometimes in contact (not floating in the internodule matrix) with stylolites. Examination at thin section of this lithofacies shows a compact packing of peloids (with microstylolites) resulting in a packstone of filaments and peloids and a fluidal texture in the internodule; in turn, the nodules are packstone-wackestones of peloids with high amounts of ammonitella, filaments and radiolarians. Clay analyses of marly interlayers and nodular marly limestones by Palomo (1987) indicate a dominance of illite, high contents in kaolinite and the absence of smectites.

- (d) White laminated limestones (Fig. 4.4e, f): This lithofacies is externally laminated and characterised by abundant trace fossils at the base. They are isolated beds 5–35 cm-thick (usually less than 15 cm), within the other lithofacies. They present parallel lamination that is well developed at the base of the bed, where fragmented remains of ammonites, brachiopods and bivalves are also recorded. Under the microscope they are seen to correspond to laminated grainstones of peloids (Fig. 4.4f). The laminated appearance is related to the alternating grain size of the peloids and to the sparitic amount. Echinoderm fragments and ooids are secondary grains in this microfacies, though locally abundant in some beds. This lithofacies is recorded, mainly recorded in the Serpentinum, Bifrons and Gradata zones; yet the thickest level (IZ-24) is located in the Aalensis Zone (Fig. 4.5). In general the record of this lithofacies decreases throughout the section. The contact between the white laminated limestones and the red nodular limestone lithofacies is irregular and sharp.

4.1.3 Microfossil Assemblages

The microfossil assemblage is dominated by filaments, foraminifera and ostracods, but radiolaria and ammonitella are very abundant in the nodular limestones of the Aalensis Zone (Figs. 4.4 and 4.5).

Filaments are the most common microfossil, with a size ranging from 5 to 3 mm for complete valves, but they appear frequently as smaller fragments (Fig. 4.4b). The filaments are common both in nodular limestones and locally in the white laminated limestones, where they are oriented according to lamination. In nodular limestones, filaments are short fragments and they are locally well preserved in intraclasts and in nodules.

Foraminifera (Figs. 4.6 and 4.7) are dominated by agglutinated forms of *Textulariina* (62%), followed by calcitic perforated shells of *Lagenina* (24%), and other orders (*Milionina*, *Spirillinina* and *Robertinina*). However, the composition of foraminiferal assemblages is clearly different in the grey-yellow limestones, the red nodular limestones and the white laminated limestones. The red nodular limestones and grey-yellow limestones are dominated by Suborder *Lagenina* (43%), mainly uniserial forms (*Dentalina* and *Nodosaria*) and coiled forms (*Lenticulina*). *Textulariina* (41%) are dominated by biserial and triserial shells (*Verneuilinoides*, *Pseudomarsonella* and *Gaudryina* among others). Agglutinated coiled forms are locally important, with local abundances of *Glomospira* and *Meandrospira*. The foraminiferal assemblage from these lithofacies is completed with *Spirillinina* (9%), *Milionina* (2.5%), undifferentiated encrusters and *Robertinina*.

The foraminiferal assemblage from the white laminated limestones is clearly different, characterised with the highest values of *Textulariina* (81%) and *Milionina* (15%), as well as low values of *Lagenina* (4%). *Spirillinina* and *Robertinina* are not recorded in this lithofacies. The most abundant foraminifera are *Verneuilinoides*,

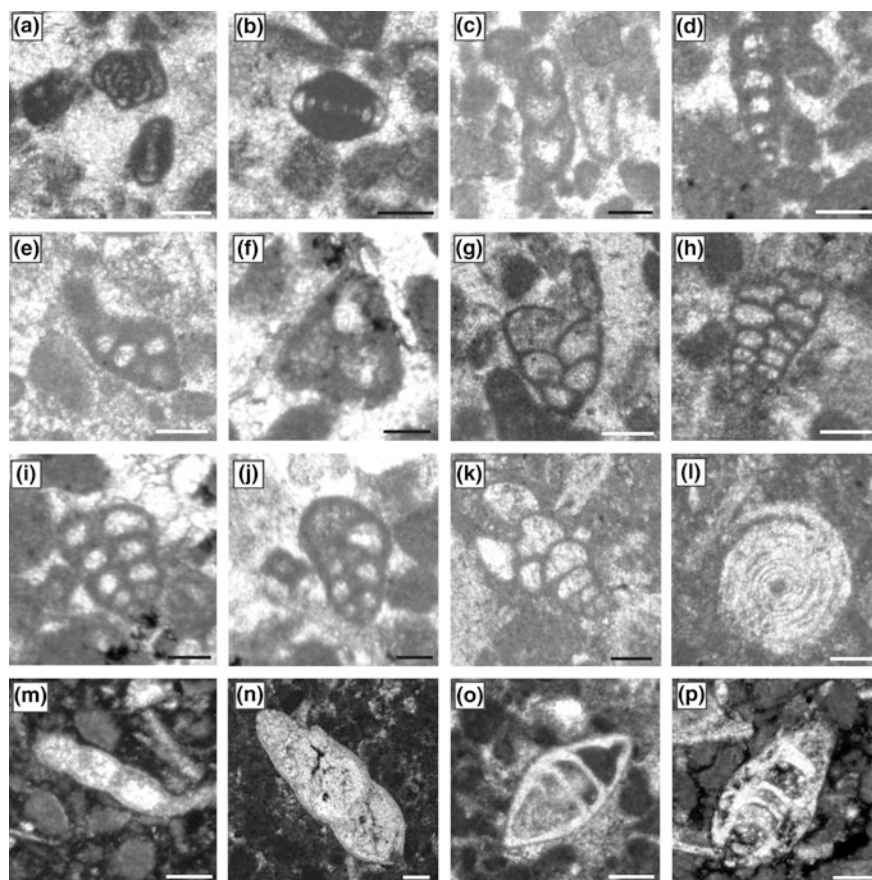


Fig. 4.6 Foraminifera from *thin* section. **a** *Glomospira* (upper specimen) and *Nautiloculina* (white laminated limestone, Serpentinum Zone). **b** *Nautiloculina* (white laminated limestone, Serpentinum Zone). **c** *Ammobaculites* (white laminated limestone, Bifrons Zone). **d** *Ammobaculites* (white laminated limestone, Aalensis Zone). **e** *Gaudryina heersumensis* (white laminated limestone, Bifrons Zone). **f** *Gaudryina heersumensis* (white laminated limestone, Aalensis Zone). **g** Biseriate agglutinated foraminifera (white laminated limestone, Serpentinum Zone). **h** *Textularia* (white laminated limestone, Serpentinum Zone). **i** *Textularia* (white laminated limestone, Aalensis Zone). **j** *Verneulinoides* (white laminated limestone, Aalensis Zone). **k** Verneulinoid (white laminated limestone, base of Gradata Zone). **l** *Spirillina* (red nodular limestone, Gradata Zone). **m** *Nodosaria* (red nodular limestone, Reynesi Zone). **n** *Dentalina* like (red nodular limestone, Aalensis Zone). **o** *Lenticulina* (white laminated limestone, Bifrons Zone). **p** *Lenticulina* (red pseudonodular limestone, Reynesi Zone). Scale bar 100 μ m

Gaudryina, *Glomospira*, *Pfenderina*, *Pseudomarsonella* and *Ophthalmidium*. Some of the genera recorded in the white laminated limestones are exclusively from shallow environments (e.g., *Paleopfenderina*, *Pseudomarsonella*, *Quinqueloculina* and *Nautiloculina*; see Helm 2005; Reolid et al. 2009; among others).

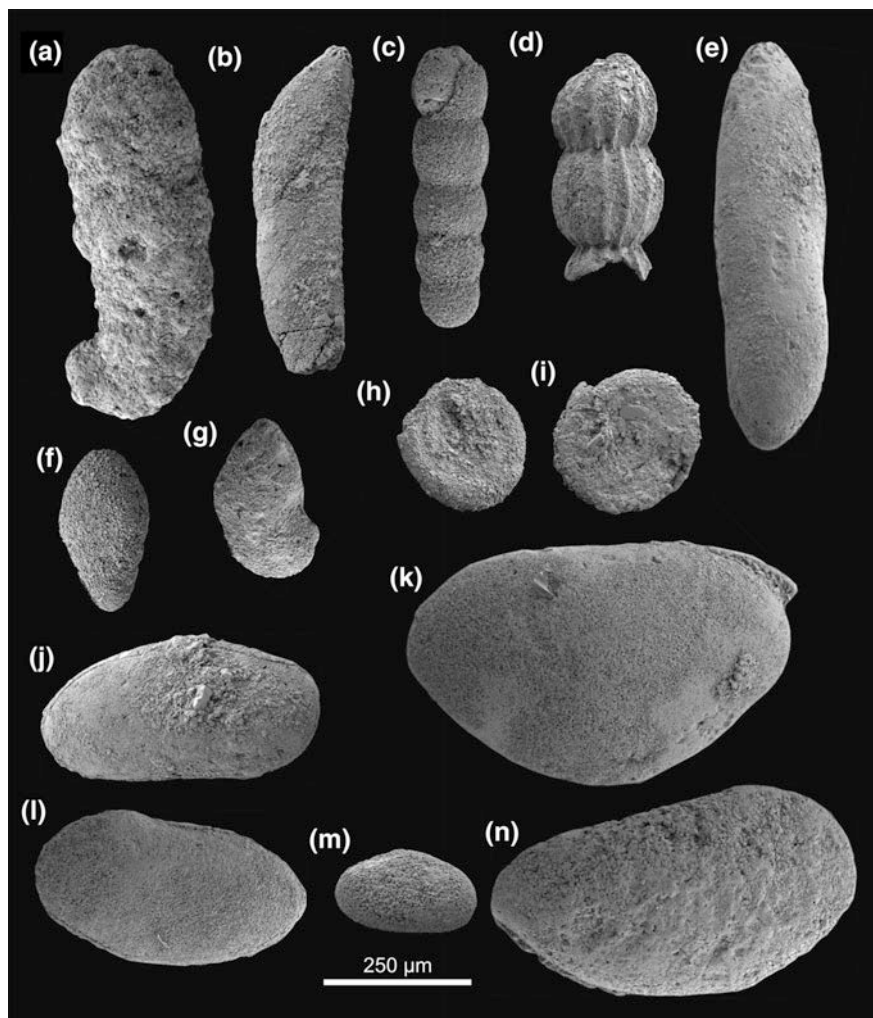


Fig. 4.7 Foraminifera and ostracods from sieved samples from Bifrons and Reysensi zones. **a** *Ammobaculites agglutinans* (Bifrons Zone). **b** *Dentalina* sp. (Bifrons Zone). **c** *Nodosaria* sp. (Reynesi Zone). **d** *Nodosaria fontinensis* (Bifrons Zone). **e** *Eoguttulina bilocularis* (?) (Reynesi Zone). **f** *Pseudonodosaria vulgata* (Reynesi Zone). **g** *Planularia* sp. (Bifrons Zone). **h** *Ammodiscus asper* (Reynesi Zone). **i** *Spirillina infima* (Reynesi Zone). **j** *Bairdiacypris rectangularis* (Bifrons Zone). **k** *Bairdia eirensis* (Bifrons Zone). **l** *Bairdiacypris triangularis* (Bifrons Zone). **m** *Pseudohealdia bispinosa* (Bifrons Zone). **n** *Bairdia molesta* (Bifrons Zone)

The stratigraphic distribution of foraminifera presents two maximum values of diversity represented by the number of genera, the first one in Bifrons Zone—after an increasing diversity trend from the base of the Toarcian—and the second one located in the Aalensis Zone, related to the input of shallow water foraminifera in a

white laminated limestone bed. The lowest values occur at the base of the section (Polymorphum Zone) and in the uppermost part of the Bifrons Zone. The highest proportions of foraminifera typical of shallow water environments are recorded in the lower part of the section, where white laminated limestones are more frequent, as well as in the bed IZ-24, which is a thick white laminated limestone within the ammonitico rosso facies of the Aalensis Zone.

Ostracods (Fig. 4.7) are common in the marls and marly limestones of the Bifrons Zone (second stratigraphic interval) and in the red nodular limestones of the Gradata Zone at the beginning of the third stratigraphic interval, and they are scarce in the white laminated limestones. Ostracods mainly correspond to Order Podocypina (superfamilies Bairdioidea and Pontocypridoidea)—with an abundance of *Bairdia*, *Bairdiacypris* and *Isobithocypris*; and secondarily *Liasina*, *Pontocyprilla* and *Pseudomacrocypris*. Bairdioids dominate the ostracod assemblage.

Radiolarids are preserved as recrystallised moulds. They appear in the upper part of the Bifrons Zone and they are more frequent in the top of the section (Aalensis Zone) inside nodules. This situation has been also reported in Upper Jurassic red nodular limestones of the Subbetic (Comas et al. 1981).

Ammonitella are recorded from the lower part of the Bifrons Zone (second stratigraphic interval) and they are very common in the Aalensis Zone (Figs. 4.4c and 4.5). The mean size of the ammonitellas is 0.9 mm. These embryonic shells are preserved exclusively in nodules.

4.1.4 Trace Fossils

Trace fossil assemblages vary according to the studied lithofacies (Fig. 4.8). In grey-yellow limestones the trace fossils are hardly observed and they correspond to *Chondrites*, *Planolites* and *Thalassinoides*.

In the red nodular limestones (calcareous ammonitico rosso) and nodular marly limestones (marly ammonitico rosso), trace fossils are very abundant and densely distributed, with a record of *Chondrites*, *Phycodes*, *Planolites* and *Thalassinoides* (Fig. 4.8c, d). Subhorizontal trace fossils are dominant. *Chondrites* appear in all of the beds. In the case of the most nodular limestones with nodules with sharp edges, small *Chondrites* (1.5 mm in diameter) are restricted to clay-rich intranodules and are not found inside the calcareous-rich nodules. The largest trace fossils are mostly located at the base of the beds. In the case of *Phycodes* and *Planolites* they reach a maximum diameter of 7.3 mm, and *Thalassinoides* reaches 15.5 mm. Colour infilling of the trace fossils allows for discernment between red and white trace fossils in each surface; red infilling is recorded in *Phycodes*, *Chondrites* and *Thalassinoides*, whereas white infilling is observed mostly in *Planolites* and *Phycodes*. White infilling traces cross-cut red infilling structures.

In the white laminated limestones trace fossils (Fig. 4.8e, f) are located in the base of the beds. *Chondrites* are absent. *Planolites* and *Phycodes* are recorded, as well as *Ophiomorpha*, characterised by a well-developed pelleted mud lining. The

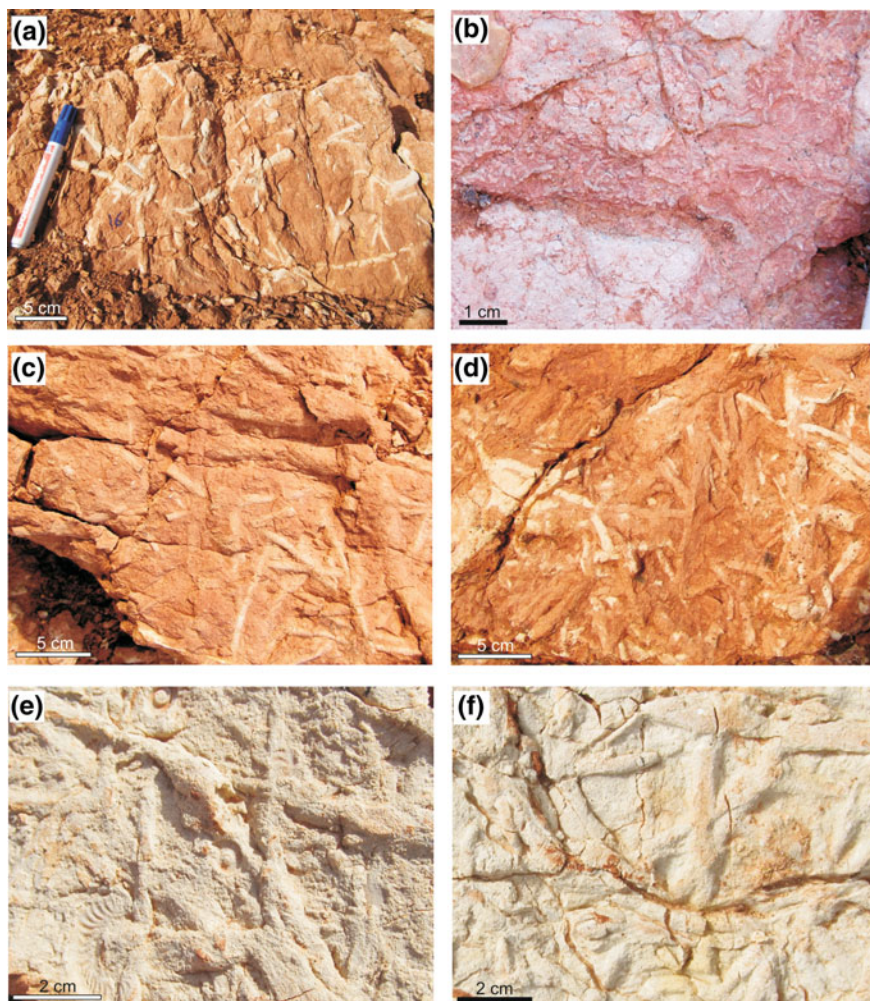


Fig. 4.8 Trace fossils. **a** *Planolites* from red nodular limestone (Gradata Zone, Middle Toarcian). **b** *Chondrites* mainly located in the matrix between nodules (Aalensis Zone, Upper Toarcian). **c** *Planolites* (white traces) and *Thalassinoides* (large red traces) from red nodular limestones (Gradata Zone, Middle Toarcian). **d** Dense burrowed base of red nodular limestone by *Phycodes* (Reynesi Zone, Upper Toarcian). **e** and **f** *Phycodes* and *Ophiomorpha* from white laminated limestone (Serpentinum Zone, Lower Toarcian)

maximum size is reached by *Ophiomorpha*, 6–8 cm in diameter. Different indeterminate trace fossils, in some cases showing a probable spreiten infilling, are common at the base of these beds. In some cases, external moulds of ammonoids have been recorded overprinting previously formed trace fossils.

4.1.5 Interpretation

Origin of sediment and lithofacies

The ammonitico rosso facies were associated with epi-oceanic slopes of a sedimentary swell-trough system related to the extensional phase of continental rifting. The Iznalloz section shows the progressive installation of ammonitico rosso facies during the Toarcian with an evolution to hemipelagic swells after the fragmentation of the carbonate platform. The hemipelagic swells are topographically high sea bottoms located in epi-oceanic environments, limited by faults (horst-graben systems or tilted blocks related to listric faults) and developed on continental crust containing condensed deposits (Santantonio 1993, 1994).

The record of well laminated limestones related to distal deposits of tempestites or turbidites within the marly interval and the ammonitico rosso facies would point to slope or foot-slope sedimentary environments. The presence of these beds could be related to the intensified storm events proposed by Krencker et al. (2015). These authors interpret an intensification of tropical cyclones during the Toarcian Oceanic Anoxic Event based on sections from West Europe and Morocco with inner to outer neritic settings represented. However, in the case of the Iznalloz section, and the Subbetic in general, this intensification of storm events during the Early Toarcian is not evident. The white laminated limestones are not restricted to or more abundant in Lower Toarcian, and they are recorded from Serpentinun to Aalensis zones. Other Subbetic sections such as Fuente Vidriera, La Cerradura and Colomera have not tempestite beds (e.g., Rodríguez-Tovar and Uchman 2010; Sandoval et al. 2012; Reolid et al. 2014b).

Carbonates and clay minerals are the main components of the studied lithofacies (Braga et al. 1981; Palomo 1987; Reolid et al. 2015). The pelagic character of the swells resulted in isolation or a poor connection with the emerged areas and the shallow platform. Hence, the input of sediment coming from these areas, including the carbonate factory, is severely reduced. The sedimentation is limited to the accumulation of planktic and nektonic organisms (calcareous nannoplankton, radiolarians, ammonites, nautiloids and belemnites) but probably affected by sediment winnowing by currents (Reolid et al. 2015).

Clay minerals (illite, smectite, chlorite and kaolinite; Palomo 1987) constitute the other important component, in this case allochthonous. The content of kaolinite is particularly interesting as a marker of continental runoff, indicative of palaeoclimatic conditions as well as of some incidence of pedogenesis and physico-chemical weathering in neighbouring emerged areas (e.g., Parisi et al. 1996; Dera et al. 2009; Hermoso and Pellenard 2014).

In terms of the benthic calcareous productivity, it is worth noting that the depth of this lithofacies was probably below the euphotic zone, due to the scarcity of benthic macroinvertebrates (crinoids and brachiopods recorded only locally). A depth within the euphotic zone could trigger carbonate production by primary photosynthetic organisms. However, the record of the white laminated limestones

with common oolites and foraminifera, typical of shallow water environments, suggests that the shallowest areas of the pelagic swell were within the shallow euphotic zone (s. Vogel et al. 1995). The white laminated limestones are distal deposits related to turbidites or tempestites with lamination in the base of the beds. Ichnological features support the turbiditic character of these lithofacies. *Phycodes* has been described as associated to turbiditic facies, usually preserved as convex hyporelief expressions of endorelief burrow systems on the soles (i.e., Han and Pickerill 1994; Gong 2001; Uchman and Tchoumatchenco 2003; Savrda 2012; Monaco and Trecci 2014). Thus, an abundance of *Phycodes* in the base of the white laminated limestone beds is compatible with the turbiditic deposition of these sediments; colonisation by *Phycodes* tracemaker was relatively immediate after deposition of the sandy interval, in a loose, unconsolidated substrate, as reflected by the deformation of *Phycodes* structures by deposition of ammonite carcasses.

Therefore, the white laminated limestones constitute allochthonous deposits but within this block of the Median Subbetic. The abundance of lumps and intraclasts in the other lithofacies—such as grey-yellow limestones, mainly in red nodular limestones and marly limestones—is also congruent with the transport according to the slope of a tilted block. The thin-shelled bivalves are common in the studied lithofacies, and they present different fragmentation degrees; but well-preserved shells of these delicate organisms are commonly recorded, probably being autochthonous or para-autochthonous.

In the Gradata Zone (Middle Toarcian), the ammonitico rosso facies debut (red nodular limestones and marly-limestones rich in trace fossils *Phycodes*, *Planolites*, *Thalassinoides* and *Chondrites*). Progressively more pelagic conditions and a restricted connection with emerged lands and carbonate platforms are reflected by the decrease in sedimentation rate, lesser input of turbidite-tempestite sediments (white laminated limestones) and increase of ammonitellas and radiolarids. The combined action of burrowing, compaction and dissolution controlled nodulation, which ranges from diffuse nodules to sharp edge nodules (Reolid et al. 2015). The sedimentation rate conditioned the time available for nodule growth, the migration of the Ca^{2+} and HCO_3^- precipitation horizon, and the nodulation degree (from horizons with diffuse edge nodules or semicontinuous to continuous layers formed by the coalescence of sharp edge nodules) (Fig. 4.9). Nodules are mainly composed by calcite whereas internodule areas are enriched in clay minerals as evidenced by X-ray microfluorescence mapping of elements (Fig. 4.9).

The differentiation between clay- and carbonate-rich areas within the sediment, in association with nodulation, is also favoured by burrowing (e.g., Fürsich 1973, 1979; Eller 1981; Reolid et al. 2015). Given the abundance of burrows in the nodular limestones of the Iznalloz section, it is evident that the activity of burrowers enhanced sediment permeability and porewater circulation, and thus the dissolution-reprecipitation processes.

The composition and richness of trace fossils from the calcareous ammonitico rosso and nodular marly limestones agree with the influence of bioturbation on nodular appearance. *Thalassinoides* has been frequently associated with ammonitico rosso facies and nodularity, reflecting greater substrate consistency during

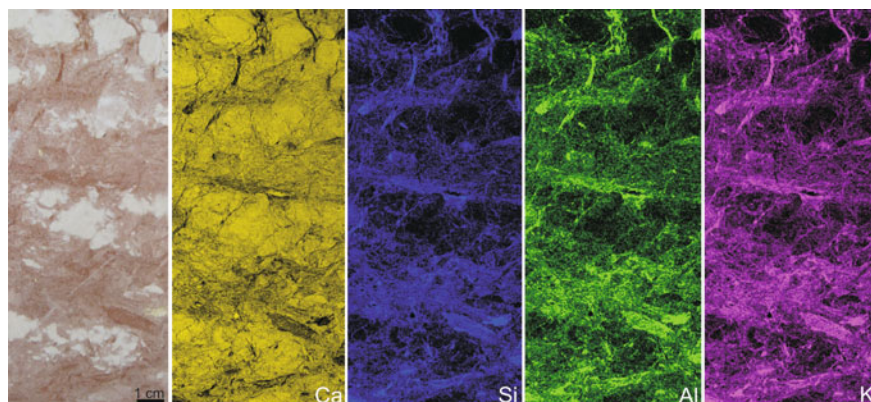


Fig. 4.9 Polished slab of red nodular limestone of the Upper Toarcian from Iznalloz section and X-ray microfluorescence compositional maps for Ca, Si, Al and K. See the white nodules correspond to Ca-rich areas (calcite), and red internodules correspond to areas comparatively rich in Si, Al and K (higher concentration of clays)

colonisation; for this reason it is used as a tool to evaluate sedimentation rates, minor erosions, discontinuities, or stratigraphic completeness, including examples from the Betic Cordillera (i.e., Caracuel et al. 1997, 2000; Monaco et al. 2007; Rodríguez-Tovar and Nieto 2013; Nieto et al. 2014). The abundance of burrows at the base of some calcareous beds from Gradata to Aalensis zones indicates pauses in deposition with minor or no erosion (omission surfaces, e.g., IZ-14, IZ-15, IZ-22, IZ-25, IZ-26), which is normal in a context of low sedimentation rate (e.g., Kennedy and Garrison 1975; Fürsich 1979; Braga et al. 1981; Reolid et al. 2010). In the Iznalloz section, differences in trace fossil composition and fossil infilling colour observed in the red nodular limestones—red infilling mainly in *Phycodes*, *Chondrites* and *Thalassinoides* and white infilling mostly in *Planolites* and *Phycodes*—could be related to two episodes of colonisation, reflecting the activity of two different communities, with minor erosion in between. During deposition of the red nodular limestone, a coetaneous red infilling trace fossil assemblage is emplaced. *Chondrites*, mostly associated to internodule sediment, reveal a less cohesive substrate, richer in organic matter than the one corresponding to the nodules. Later, during the deposition of white sediments, a white infilling trace fossil assemblage cross-cuts the previous one. These two successive communities must have been replaced in a short time, without significant environmental changes. The white laminated limestones are, in general, poorly developed in the nodular facies and support the interpretation of a short time deposition and/or minor erosion of the white sediments.

In comparison with ammonitico rosso facies, the trace fossils from the white laminated limestones indicate that these peloidal deposits constituted a loose-ground. This is also in agreement with the record of *Ophiomorpha*.

Oxygenation

In general terms, ichnofossil and microfossil assemblages (foraminifera, ostracoda and echinoderm fragments) recorded in the Iznalloz section indicate good oxygenation in the sea-bottom. The abundance of ammonoids, as well as the record of belemnites, also indicates good oxygen conditions in the water column.

Trace fossil composition and abundance are indicative of the good oxygenation degree, both in white laminated limestones and in ammonitico rosso facies. Trace fossils (*Chondrites*, *Planolites* and *Thalassinoides*) are less common and poorly observed in grey-yellow limestones of the Lower Toarcian.

In the ammonitico rosso facies, the *Phycodes* dominated assemblage reveals a predominance of deposit-feeders, probable tracemakers being vermiform annelids and crustaceans. In this context of oxygen availability, the diversity of behaviours (*Phycodes fodinichnia*, *Chondrites chemichnia*, *Thalassinoides domichnia-fodinichnia*, and *Planolites pascichnia*) reveals food content availability at the sea-bottom.

The foraminiferal assemblage of the white laminated limestone also indicates good oxygen availability in the source area, surely in shallower environments, due to the allochthonous character of these turbidites or tempestites.

In autochthonous lithofacies (grey-yellow limestones, grey-red marls and red nodular limestones and marly limestones) the foraminifera are well represented from potential deep infaunal forms (e.g., *Eoguttulina*, *Lenticulina*, *Verneuilinoides* and *Reophax*) to shallow infaunal (e.g., *Ammobaculites*, *Astacolus*, *Dentalina*, *Marginulina*, *Nodosaria*) and epifaunal forms (e.g., *Glomospira*, *Ophthalmidium*, *Spirillina*, *Trochammina*). This is clearly related to a high degree of oxygenation (e.g., Reolid et al. 2008; Olóriz et al. 2012). The dense burrowing favoured the oxygenation of the infaunal microhabitats of foraminifera.

The absence of the dark interval that typically characterises oxygen restricted biofacies with preservation of organic matter related to the Toarcian Oceanic Anoxic Event (as evidenced in External Subbetic sections such as La Cerradura, Cueva del Agua and Fuente Vidriera), would confirm the oxygen availability in the sea-bottom. These deposits, mainly the ammonitico rosso facies, are reddish due to the slow sedimentation under fully oxidizing conditions (e.g., Jenkyns 1971). According to Hallam (1967) and Berner (1969), the red colour is related to diagenetic alteration of goethite to hematite.

The physiography of the bottom in this setting during the Toarcian—evolving to pelagic swell affected by currents—was unfavourable to water stagnation and oxygen depleted conditions. However, these adverse conditions for benthic assemblages were recorded in comparatively deeper parts (subsident troughs) of the Subbetic dominated by expanded successions with marl-limestone rhythmites and dark marls (Reolid et al. 2013b, 2014b; Rodríguez-Tovar and Reolid 2013; Reolid 2014). In addition, oxygenation was favoured by the tempestite-turbidite inputs to the bottom waters during the Early Toarcian. In the Polymorphum and Serpentinum zones, the foraminiferal assemblages confirm good oxygenation with no dominance of opportunists such as *Lenticulina*, *Reinholdella* and *Eoguttulina* (Reolid et al. 2012a, b, 2014a; Reolid 2014; Rita et al. 2016).

Nutrient content

In the context of oxygen availability, a diversity of feeding behaviours reveals food content availability at the substrate. *Phycodes* has been related to a variety of behavioural activities, usually linked to the means of exploiting nutrient-rich sediments (Han and Pickerill 1994; Mángano et al. 2005). Complex *Thalassinoides-Phycodes* compound burrows have been related to dwelling-deposit feeding structures operating for relatively long intervals; reburrowing by *Chondrites* is associated with storage of organic material or feces and cultivating bacteria, as a behaviour that supplements deposit feeding (Miller 2001). As previously commented, the presence of *Chondrites* mostly associated to internodule sediment could reflect a comparatively higher abundance of organic material in the internodule substrate.

The diversity of benthic foraminifera confirms nutrient availability throughout the section, but not high values, probably owing to the hemipelagic context. The highest diversity values are related to allochthonous deposits, represented by the white laminated limestones, where foraminifera with epifaunal/epiphytal behaviour (*Ammodiscus*, *Glomospira*, *Meandrospira*, *Nautiloculina*, *Trochammina*, *Ophthalmidium*, *Quinqueloculina*, *Spirillina* and *Conicospirillina*) reach maximum values. These fauna come from a shallow environment with high productivity and water energy, where bacterial scavengers, phytodetrivores, grazing herbivores and primary weed fauna proliferate (e.g., Reolid et al. 2013a).

In the grey-yellow limestones, grey and red marls and red nodular limestones, the Suborder Lagenina dominates the foraminiferal assemblage, with shallow to deep infaunal forms being active deposit feeders, bacterial scavengers and grazing omnivores (mainly *Astacolus*, *Dentalina*, *Lenticulina*, *Nodosaria* and *Marginulina*); epifaunal grazing herbivores are represented by scarce *Spirillina*, *Epistomina* and *Trochammina* (Reolid et al. 2013a, 2014a). In these lithofacies, foraminiferal assemblages indicate that nutrients were exploited mainly in the infaunal microhabitat for foraminifera, perhaps related to the byproducts (fecal matter and mucous excretions for burrow stabilisation *s.* Petrash et al. 2010) of macroinvertebrate burrowers.

Palaeoenvironmental reconstruction

The evolution of the Central Median Subbetic in this area is mainly controlled by the rapture of the Lower Jurassic shelf during the late Pliensbachian (Vera 1988), in a scenario resembling other Tethyan Domains recorded in the Western Alps (Dercourt et al. 1985; Funk et al. 1987), Southern Alps (Bosellini 1973; Winterer and Bosellini 1981), Apennines (D'Argenio 1974; Cecca et al. 1992; Parisi et al. 1996), western Slovenia (Rožic and Smuc 2011), Rif Cordillera (El Kadiri 2002), Traras Mountains (Marok and Reolid 2012), Saharian Atlas (Elmi and Almeras 1984; Yelles-Chaouche et al. 2001), High Atlas of Morocco (Ettaki et al. 2000; Ettaki and Chellai 2005), and the Central Atlas of Tunisia (Soussi and Ben Ismail 2000; Soussi et al. 2000). The diversified physiography of the Subbetic basin during the Toarcian, related to synsedimentary tectonic activity and circulation patterns,

probably determined different intensities of ventilation conditions on the sea-floor. As happens in other areas of the southern Tethys, such as Apulia and the North African Margin, the Toarcian deposits overlie basinal pelagic limestones containing cherts as well as thick hemipelagic marly-limestone sequences (e.g., Marok and Reolid 2012). The Early Toarcian transgression (Haq et al. 1987; Hallam 1988, 2001) does not indicate the drowning of carbonate platforms because it usually overlies hemipelagic deposits of the upper Pliensbachian. Progressive fragmentation of the Lower Jurassic platform is even reflected by the input of turbidites or tempestites in the first and second stratigraphic intervals (mainly Serpentinum and Bifrons zones), represented by the white laminated limestones consisting almost exclusively of peloids, thin-shelled bivalves and shallow foraminifera. These turbidites were originated from fragmented drowned platform margins and subsequently redeposited along slopes of the tilted blocks. Therefore, the intercalations of white laminated limestones reflect regionally recognised events that characterised the sedimentary evolution of the Median Subbetic at the end of the Early Jurassic. The record of slumps in nearby areas of the Median Subbetic (e.g., Colomera section, 15 km west) reflects uneven sea-bottom palaeotopography that originated during an early to middle Toarcian phase of accelerated subsidence. The Lower Toarcian clay mineral association (illite, smectite, chlorite, *s.* Palomo 1987) is characteristic of a hemipelagic environment with a low influence of emerged reliefs. Given the transgressive context of the Early Toarcian (Haq et al. 1987; Hallam 2001) the source area of the clays (emerged land) was comparatively far away.

During the Middle and Late Toarcian the pelagic swell became fully installed in epi-oceanic conditions. The progressively more reddish facies show increasing contents in kaolinite and nodularity, and a less common record of white laminated limestones. The second stratigraphic interval is a marly ammonitico rosso, while the third stratigraphic interval increases in carbonate content and in the record of omission surfaces, resulting in calcareous ammonitico rosso (increasing nodulation toward the top of the section). A progressively higher condensation degree in the section can be deduced from these facies changes. However, this higher condensation for ammonitico rosso facies is not justified in this section. Stratigraphic condensation (as well as the presence of expanded sections) should be measured on the basis of thickness for a given (the same) time interval (i.e., Gómez and Fernández-López 1994) reflecting on this way the sedimentation rate. Within the Iznalloz section, the Polymorphum Zone is much thinner than any other biozone of the section but this is affected by the hiatuses located in the Pliensbachian-Toarcian boundary and in the Polymorphum-Serpentinum zone boundary also recorded in other sections of the Subbetic (e.g., Nieto et al. 2008; Reolid et al. 2014b). The Serpentinum Zone has duration of 1.08 Ma for Ogg and Hinnov (2012), 1.5–1.62 Ma for Boulila et al. (2014) and 1.31 Ma for Ruebsam et al. (2014) and is 2.62 m-thick, but is not represented by ammonitico rosso facies (sedimentation rate ranging from 0.24–0.16 cm/kyr). The Aalensis Zone, represented by ammonitico rosso facies is 3.00 m-thick for a duration of 1 Ma in Gradstein et al. (2004), 0.13 Ma for Ogg and Hinnov (2012) and 0.44–0.51 Ma in Boulila et al. (2014) (2.3–0.59 cm/kyr), so it can be said that is relatively expanded respect to the

Serpentinum Zone, but represented by the supposed condensed ammonitico rosso facies. There is not necessarily a univocal relationship between condensation and ammonitico rosso facies.

Estimations of sedimentation rate are of limited value because much of the time involved in the deposition of the red nodular limestones is represented by ubiquitous omission surfaces (Reolid et al. 2015) and the alluded disagreement of the proposals of duration for the different zones of the Toarcian Stage. However, it seems that sedimentation rate is not the main controlling factor for developing ammonitico rosso facies. The installation of pelagic swell in this area of the Subbetic, entailing isolation from sediment sources (emerged areas and carbonate factory represented by the Prebetic shelf) as well as the sea-level fall during the Middle-Late Toarcian (e.g., Hallam 1988, 2001), came to favour the sediment-winnowing by currents and seawater circulation in the uppermost sediment column, triggering early marine lithification and the subsequent nodulation. An increasing pelagic influence is signalled by the abundance of radiolarids and ammonitellas in the most calcareous ammonitico rosso.

The increase of kaolinite just in the third stratigraphic interval does not fit the trends described by Dera et al. (2009). These authors point to a kaolinite enrichment during Falciferum and Bifrons zones, and a decrease in kaolinite content during the Late Toarcian. These trends are held to be related to a warm climate with efficient runoff during the Falciferum and Bifrons zones, with cooler and drier climate during the Late Toarcian, mainly in northern parts of the Peritethyan Realm (Dera et al. 2009, 2011). In contrast, Reolid et al. (2015) interpret the absence of kaolinite during the Early Toarcian in the Median Subbetic as being related to high sea-level and relatively great distances to emerged lands; meanwhile, increasing values of kaolinite related to ammonitico rosso facies resulted from a low sea-level, favouring emersion of Subbetic islands. A latitudinal climatic zonation is envisaged, and the weathering and hydrolysis of emerged lands during Late Toarcian was possible in southern Tethys margins, despite the cooler conditions interpreted by other authors (e.g., Dera et al. 2009, 2011). According to Cecca et al. (1992), the Toarcian ammonitico rosso facies occurred between 15° and 30° N latitude, and it is widespread in the Mediterranean Tethys of the North Gondwana Palaeomargin (Apulian promontory and North African Margin) and the southern Iberian Palaeomargin (Betic Cordillera). The kaolinite-rich association of the Middle and Upper Toarcian must have been deposited under the influence of nearby emerged areas (perhaps Subbetic islands), as shown by the greater abundance of kaolinite and the decrease of smectite.

4.2 Arroyo Mingarrón Section

The Arroyo Mingarrón section is located in the Granada Province, 1 km northeast to the Colomera village, in front of the village, in the Mingarrón ravine (37° 22' 54.33" N; 3° 42' 27.18" W; Figs. 3.1 and 4.10). An additional section is observed in

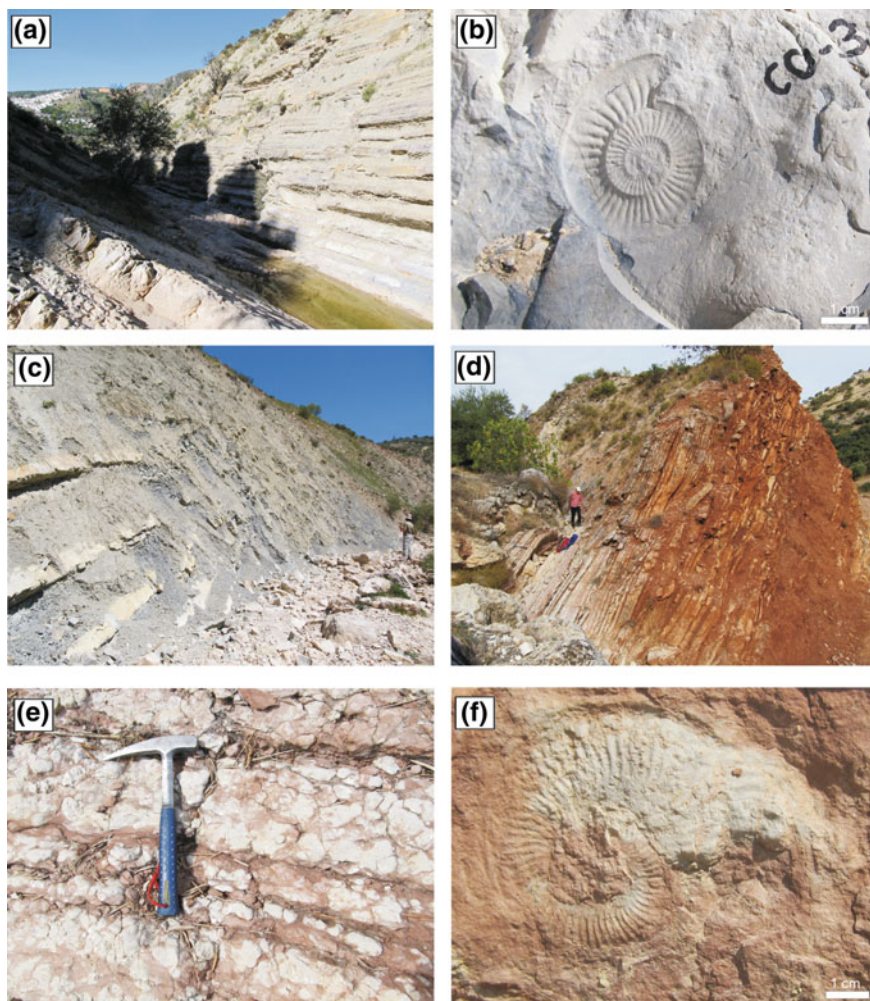


Fig. 4.10 Field view of the Arroyo Mingarrón section. **a** Yellowish marl and limestone alternance of the Uppermost Pliensbachian-Lower Toarcian (Polymorphum Zone). **b** Ammonite mould (*Canavaria*) in the uppermost Pliensbachian. **c** marls of the Lower Toarcian (Serpentinum Zone) to Middle Toarcian (Bifrons Zone). **d** Marly to calcareous ammonitico rosso facies of the Upper Toarcian. **e** Detail of the calcareous ammonitico rosso with sharp edge nodules. **f** Ammonite mould (*Pseudogrammoceras*) from the ammonitico rosso facies (Upper Toarcian)

the Colomera Village, from threshing floors to the Roman Bridge over the Colomera River (Fig. 4.11).

The Arroyo Mingarrón section, as well as the Colomera section, shows the progressive development of the ammonitico rosso facies during the Toarcian with

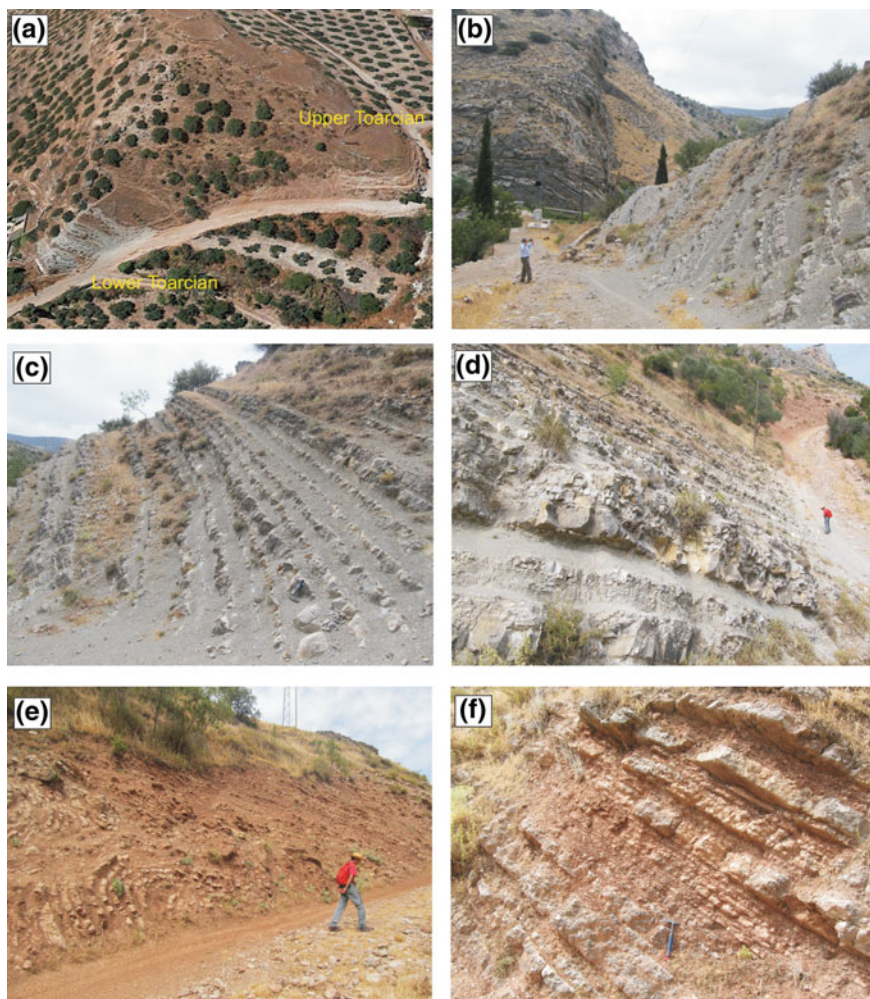


Fig. 4.11 Field view of the Colomera section. **a** Perspective from the blue-greyish marl-limestone rhythmite of the uppermost Pliensbachian-Lower Toarcian to red ammonitoco rosso facies of the Upper Toarcian (view from Google Earth). **b** Blue-greyish marl-limestone rhythmite of the uppermost Pliensbachian-Lower Toarcian, the relief in the bottom corresponds to the Pliensbachian cherty limestones. **c** Blue-greyish marls and limestones rhythmite of the Lower Toarcian. **d** Blue-greyish marls and limestones rhythmite of the Lower Toarcian and red ammonitoco rosso marls and nodular limestones in the upper part. **e** Slumps affecting the red marls and limestones of the Middle Toarcian. **f** The upper part of the Colomera sections is more calcareous and nodular (Upper Toarcian)

the onset of a hemipelagic swell. The analysis of the Arroyo Mingarrón section focused on the analysis of lithofacies and microfacies with a biostratigraphic control provided by calcareous nannofossils.

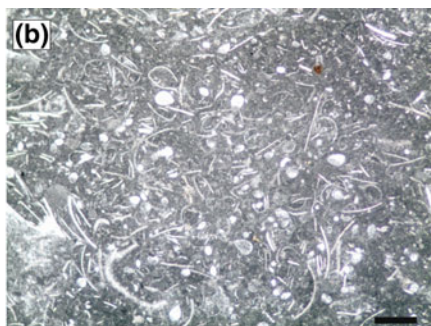
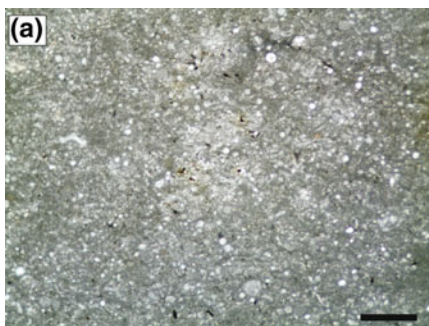
4.2.1 *Lithofacies and Microfacies*

The study section starts with a lower stratigraphic interval composed by yellowish marl-limestone alternances (11.3 m thick, Fig. 4.10a, b) developed over the cherty limestones of the Pliensbachian (Gavilán Fm). The lower part of this interval is characterised by ammonites of the genera *Emaciaticerias* and *Canavaria* (beds CO-1 to CO-30; Fig. 4.10b), while the upper part presents *Protogrammoceras* and *Dactylioceras*. The microfacies is characterised by peloidal mudstones to wackestones (Fig. 4.12a).

The second stratigraphic interval (42.8 m thick) consists of blue-greyish marls with scarce marly-limestone interlayers (Fig. 4.10c). Ammonites are scarce and poorly preserved. Trace fossils are close to those described in La Cerradura section, with dominance of *Planolites*. Clay content is high with dominance of illite and smectite, and chlorite.

The third stratigraphic interval (10.1 m thick) is constituted of reddish pseudo-nodular marls and marly-limestones (Fig. 4.10d). They are marly ammonitico rosso facies like those described in the Iznalloz section, but trace fossils are less common and poorly preserved compared to those of the Iznalloz section. These facies progressively change to red nodular limestones, the calcareous ammonitico rosso facies (Fig. 4.10e). The boundary between nodules and internodules is well-marked by the colour change, white nodules and red internodules. The largest nodules (3–5 cm) are located in the upper part of the section and they present spheroidal shape with the sharp edges usually in contact with stylolites forming more or less continuous nodular horizons. Trace fossils are scarcer than in the ammonitico rosso facies from Iznalloz section and they are represented mainly by *Thalassinoides*. *Phycodes* and *Chondrites* were not recorded whereas they are highly abundant in the Iznalloz section. The microfacies are packstones of peloids, filaments and ammonitella (Fig. 4.12b–d). Kaolinite content increases in this stratigraphic interval as occurs in the Iznalloz section.

The complementary Colomera section (Fig. 4.11) differs respect to the Arroyo Mingarrón section in the second stratigraphic interval here represented by a blue-greyish marls with abundant marly-limestone interlayers (24 m thick). This is thinner and with more carbonate than in the Arroyo Mingarrón section. The third stratigraphic interval in the Colomera section is represented by marly ammonitico rosso facies with *Thalassinoides* and *Zoophycos*, affected by slumps (39 m thick). The top of the section consists of 10 m of calcareous ammonitico rosso facies similar to those described in the Iznalloz and Arroyo Mingarrón sections, but locally with high amount of *Zoophycos*.



◀**Fig. 4.12** Most significant microfacies from Arroyo Mingarrón section. **a** Wackestone of radiolarians (yellowish marl-limestone alternance, NJT 5b nannofossil Subzone, uppermost Pliensbachian). **b** Wackestone-packstone of filaments and ostracods (calcareous ammonitico rosso facies, NJT 7b nannofossil Subzone, Upper Toarcian). **c** Wackestone of ammonitella (marl-limestone rhythmite, NJT 7a nannofossil Subzone, Middle Toarcian). **d** Packstone of filaments and peloids (calcareous ammonitico rosso facies, NJT 7b nannofossil Subzone, Upper Toarcian). **e** Packstone of lumps and peloids with thinning upward trend (blue greish marls, NJT 6 nannofossil Zone, Lower Toarcian) and incipient lamination. **f** Packstone of lumps and peloids with thinning upward trend and small trace fossils of *Chondrites* (blue greish marls, NJT 6 nannofossil Zone, Lower Toarcian). Scale bar 1 mm

4.2.2 Calcareous Nannofossil

Both coccoliths and the *incertae sedis* nannolith *Schizosphaerella* are in general poorly to very poorly preserved in the Arroyo Mingarrón section, with exception of a few samples (Figs. 4.13 and 4.14). Severely overgrown specimens of *Schizosphaerella*, with development of secondary fringes, and of *Mitrolithus jansae* are commonly recorded. In spite of this poor preservation, almost all the samples are productive, although nannofossil abundance is low. Assemblages are largely dominated by *Schizosphaerella* and *M. jansae* in the Upper Pliensbachian and Lower Toarcian, by *Schizosphaerella* and *Lotharingius* species (mainly *L. hauffii* and *L. frodoii*) in the upper part of Lower Toarcian and Middle Toarcian, and by *Carinolithus superbus* and *Discorhabdus* (*D. ignotus* and *D. striatus*) in the Middle Toarcian and at the base of the Upper Toarcian. This assemblage indicates a south-Tethyan affinity for the Arroyo Mingarrón section.

Some first occurrences (FO) and one last occurrence (LO) of coccolith species allow dating the section according to the biozonation scheme of Mattioli and Erba (1999) created for the south-Tethyan region. The assemblage at the base of the section is latest Pliensbachian in age and belongs to the NJT 5a nannofossil subzone (Mattioli and Erba 1999). In sample CO-11, the FO of *Lotharingius sigillatus* is recorded, marking the base of the NJT 5b subzone. Although Mattioli and Erba (1999) reported this subzone at the base of the Toarcian, a recent study (Mattioli et al. 2013) shows that it encapsulates the Pliensbachian/Toarcian boundary as *L. sigillatus* first occurs in the latest Pliensbachian Emaciatum ammonite Zone in the Peniche GSSP section. Because in this last reference section the FOs of *Biscutum intermedium* and *Lotharingius* aff. *L. velatus* did occur at the very end of Pliensbachian (Oliveira et al. 2007; Mattioli et al. 2013), we tentatively place the Pliensbachian/Toarcian boundary slightly above these FOs, between samples CO-30 and CO-31.

The contemporaneous FOs of *Carinolithus superbus* and *C. poulabronei* allow placing the base of the NJT 6 in the sample CO-48. This is the first sample of the blue-greyish marls that compound the second stratigraphic interval. This datum is very significant because the Early Toarcian Anoxic Event (T-OAE) is consistently recorded within the NJT 6 (Mattioli et al. 2004). Another relevant event is the LO of *Mitrolithus jansae* in the sample CO-78, that is usually recorded at the end of the

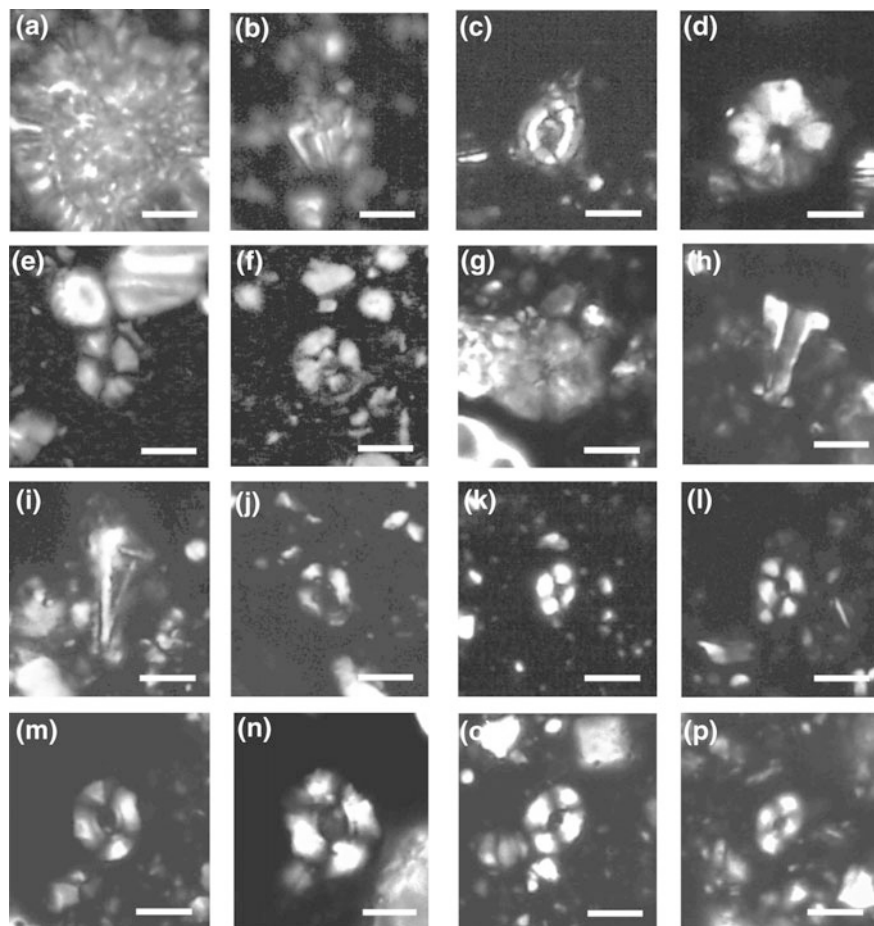


Fig. 4.14 Most significant calcareous nannofossils recorded in Arroyo Mingarrón section. Pictures by Prof. Emanuela Mattioli (Univ. Lyon). **a** *Schizosphaerella* spp. **b** *Mitrolithus jansae*. **c** *Tubirahbdus patulus*. **d** *Calyculus* spp. **e** *Similiscutum finchii*. **f** *Discorhabdus striatus*. **g** *Discorhabdus criotus*. **h** *Carinolithus poul nabronei*. **i** *Carinolithus superbus*. **j** *Bussonius leufuensis*. **k** *Lotharingius frodoi*. **l** *Lotharingius sigillatus*. **m** *Lotharingius crucicentralis*. **n** *Lotharingius velatus*. **o** *Watznaueria colacicchii*. **p** *Watznaueria fossacincta*. Scale bar 5 μm

4.2.3 Geochemistry

The analysis of geochemical proxies for palaeoproductivity, redox conditions, and detritism does not show significant trends in the Arroyo Mingarrón section. The yellowish marl-limestone alternance (NJT 5a and NJT 5b zones) displays an increasing trend of the TOC from 0.1 to 0.3 wt%. The $\delta^{13}\text{C}$ ranges between 0.45 and 0.89‰, and $\delta^{18}\text{O}$ ranges between -2.73 and -3.23 ‰.

The lower part of the blue-greyish marls (NJT 6 Zone) shows a progressive increase of $\delta^{13}\text{C}$ except for the decrease from 1.47 to 0.80‰ (a slight negative excursion of -0.77‰) coincident with the lowest diversity values of calcareous nannoplankton (Fig. 4.15). This is also coincident with the highest values of the Mg/Al ratio (a fluvial detrital proxy according to Chester et al. 1977). The lowest values of CaCO_3 content (26 wt%) together with the highest values of TOC (0.32 wt%) are recorded in the upper part of the NJT 6 Zone, 10 m above the minimum values of the calcareous nannoplankton diversity.

The upper part of the blue-greyish marls, corresponding to the NJT 7a Zone, evidences an increasing carbonate content (Fig. 4.15). The highest values of $\delta^{13}\text{C}$ are recorded at the beginning of this zone (3.08‰) and subsequently decrease to the top (1.74‰). The $\delta^{18}\text{O}$ does not change and keeps values around -2‰ . The TOC values are very low (from 0.23 to 0.09 wt%). The Total Sulphur curve describes the same trends as the TOC. The lowest values from Arroyo Mingarrón section for Mg/Al ratio are recorded at the top of the NJT 7a.

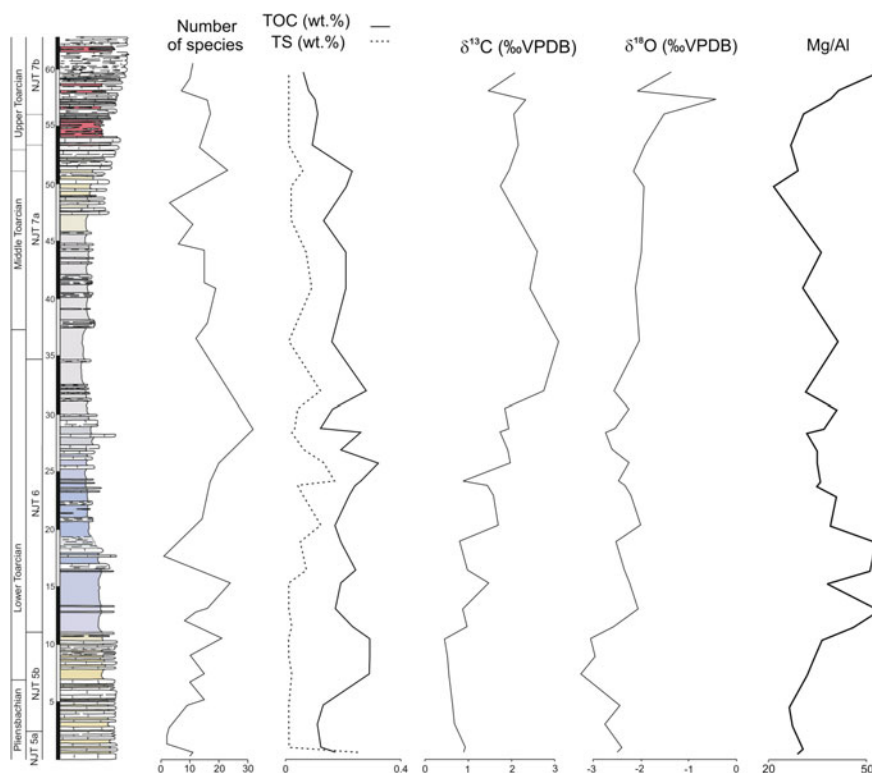


Fig. 4.15 Stratigraphic distribution of the diversity of calcareous nannoplankton (number of species), total organic carbon (TOC), total sulphur (TS), $\delta^{13}\text{C}$, $\delta^{18}\text{O}$ and the detrital proxy (Mg/Al ratio). The redox and palaeoproductivity proxies are not represented because there is not a stratigraphic trend

The reddish marly-limestones and pseudo-nodular limestones (NJT 7b Zone) experiment an abrupt increase in CaCO_3 and Mg/Al ratio. The organic matter content is extremely low (0.10–0.06 wt%). A positive excursion of the $\delta^{18}\text{O}$ occurs (reaching -0.42%).

Taking into account the geochemical data and trends, it is difficult to locate the position of the T-OAE due to the absence of a clear negative carbon isotopic excursion. Moreover, the redox proxies, TS and TOC do not correspond to oxygen depleted conditions. Only the minimum values of nannoplankton diversity in the lower part of the blue-greyish marls of the NJT 6 Zone with decreasing CaCO_3 , slight $\delta^{13}\text{C}$ fluctuations, and increasing Mg/Al ratio could indicate environmental changes during the early Toarcian.

4.2.4 Interpretation

The Toarcian Ammonitico Rosso context

The ammonitico rosso that characterises part of the Tethyan Jurassic has been interpreted as deposited at significant distance from a major continental landmass (e.g., Hallam 1967; Jenkyns 1971; Braga et al. 1981; Cecca et al. 1992). Deposition of the study sedimentary succession took place on the slopes of a sedimentary swell-trough system developed in the Subbetic during the Late Pliensbachian, with a maximum development during the Toarcian (e.g., Braga et al. 1981; Vera 1988; Reolid et al. 2015). The pelagic swells were common during the Jurassic in the Tethys Domain, being related to an extensional phase of the continental rifting and controlled by tectonic subsidence (e.g., Cecca et al. 1992; Santantonio 1994). The main evidence underlying this interpretation for ammonitico rosso facies from the Subbetic is the thickness variability of the Toarcian deposits between different sections (e.g., Iznalloz, Colomera, Arroyo Mingarrón, and La Cerradura) together with facies changes, in close space-time spans (e.g., Braga et al. 1981; Sandoval et al. 2012; Reolid et al. 2014b). The pelagic character of the swells results in isolation or a poor connection with the emerged areas and the shallow platform. Hence, the input of sediment coming from these areas, including the carbonate factory, is severely reduced. Moreover, due to the fact that the pelagic swells are topographic high at the sea bottom, sediment transport by bottom currents is also limited (Fig. 4.16). The sedimentation is restricted to the rain of calcareous nannoplankton and radiolarian carcasses, as well as the accumulation of cephalopod shells (mainly ammonites and secondarily nautiloids and belemnites). In the nodular limestones, however, the calcareous nannoplankton is relatively scarce compared with other sections of the Subbetic made up of marl-limestone rhythmites (Reolid et al. 2014b; Mattioli pers. commun.). This could be interpreted as sediment winnowing by currents or a diagenetic effect related to the genesis of nodules.

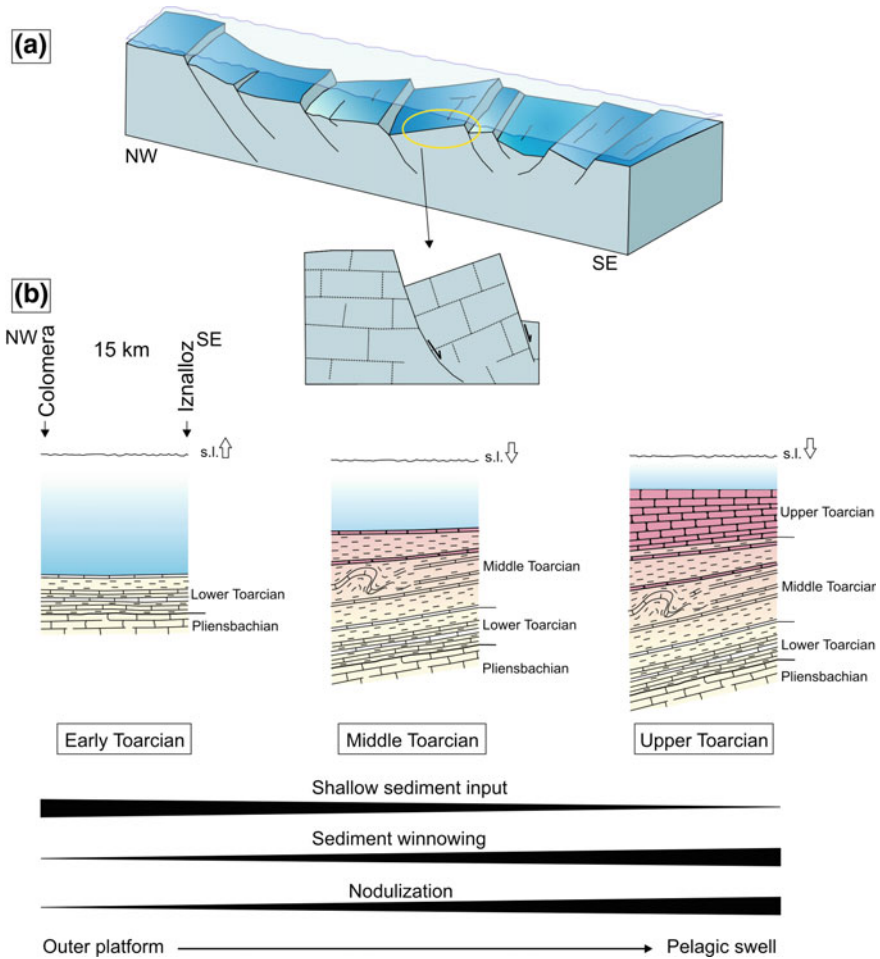


Fig. 4.16 Interpretative model for the Lower Toarcian of the Median Subbetic. **a** Transect of the Median Subbetic. **b** Evolution of the Colomera-Iznalloz transect during the Toarcian with the progressive fragmentation of the carbonate platform and tilting of blocks

Nanno-organisms may have been destroyed by recrystallisation as occurred with overgrown specimens of *Schizosphaerella*, with development of secondary fringes).

Clay minerals (illite, smectite, chlorite and kaolinite) are the main allochthonous component. The white laminated limestones occurring in the Iznalloz section, other allochthonous deposits, are not recorded in the Arroyo Mingarrón and Colomera sections.

The nodular appearance of the ammonitico rosso is mainly related to the combined action of burrowing and compaction. Dissolution appears to be important only at the top of the section (Aalensis Zone), where spheroidal nodules with sharp edges occur.

Previous researches on the nodular formation of ammonitico rosso facies proposed early marine dissolution of mainly aragonitic shells and subsequent reprecipitation as the cause of the lithification and then the formation of nodules. Factors controlling dissolution and cementation, and the early marine nodular lithification, include the submarine winnowing of the carbonate mud at the seafloor and the alteration of sediment properties by burrowing (e.g., Kennedy and Garrison 1975; Mullins et al. 1980).

The original sediment was probably a homogeneous mix of clay minerals, micrite, and bioclasts (calcite such as crinoids and aragonitic such as ammonoid shells). In a context of low sedimentation rate, e.g., pelagic swells, the dissolution of aragonite produces the Ca^{2+} and HCO_3^- saturation of pore-water in the sediment-water interface and the precipitation of Mg-rich polymorphs of calcite. Therefore, an early diagenetic microenvironmental differentiation (incipient nodulation) of the micritic matrix takes place in the marine porewater zone close to the sediment-sea-water interface. Yet as sedimentation advances, it produces the upward migration of the sediment-water interface, and the input of Ca^{2+} and HCO_3^- into the precipitation horizon (where nodules are growing) is reduced. Finally, a new precipitation horizon begins in the sediment-water interface when saturation is reached. Polished slab with different nodular horizons clearly shows this upward migration process (Fig. 4.9). There is evidence of carbonate-solution processes during the early diagenesis in the ammonitico rosso of the Arroyo Mingarrón and Iznalloz sections, with a selective solution of carbonate in some parts of the sediment and its precipitation in other parts, forming nodules (Reolid et al. 2015). A frequent effect of dissolution is the disappearance of radiolarids in the matrix. Different intensities of the solution-precipitation processes result in variable nodule edge grading from diffuse (Bifrons to Reynesi zones) to sharp (Aalensis Zone). At the top of the Iznalloz and Arroyo Mingarrón sections, in calcareous ammonitico rosso facies from the Aalensis Zone, the growth of the nodules proceeded to the extent of coalescence to produce a semicontinuous or continuous layer of interlocking nodules or a massive rock band. In an extreme case, the reddish matrix is comparatively clay-rich and has a fluidal appearance due to the arrangement of filaments.

Moreover, topographic sea-bottom highs from oceanic and epi-oceanic domains are often affected by increased current intensity because of the interaction of bottom currents with local topography. Enhanced current velocities provide a mechanism for seawater circulation in the uppermost sediment column, thereby providing Ca^{2+} and HCO_3^- for early cementation in the sediment-water interface (McLaughlin and Brett 2004), and triggering early marine lithification (e.g., Mullins et al. 1980; Comas et al. 1981; Reolid et al. 2010). An increased current velocity and hence a decreased sediment accumulation would be expected during sea-level lowstand conditions, such as after the Early Toarcian sea-level maximum (Haq et al. 1987; Hallam 1988, 2001; Jacquin and de Graciansky 1998).

The differentiation between carbonate-rich and clay-rich areas within the sediment, in association with nodulation, is also favoured by burrowing (Fürsich 1973, 1979). Organic (mucilaginous) substances on the walls of some trace fossils, as well as organic matter in the sediment infilling the gallery, could favour dissolution-reprecipitation processes in two opposite ways: (a) it could imply higher alkalinity and selective cementation (Fürsich 1973), or (b) the organic matter might produce acid porewater within the gallery infilling sediment, leading to selective dissolution of early diagenetic carbonate cements and the subsequent heterogeneous compaction of the sediment resulting in nodularity (Eller 1981). Given the abundance of burrows in the nodular limestones of the Iznalloz section, it is evident that the activity of burrowers enhanced sediment permeability and porewater circulation, and thus the dissolution-reprecipitation processes. The composition and abundance of trace fossils from the red nodular limestones (calcareous ammonitico rosso) and nodular marly limestones (marly ammonitico rosso) agree with the influence of bioturbation on nodular appearance, mainly in the Iznalloz section (Reolid et al. 2015).

Finally, syndimentary rework of sediment with different lithification degrees on the talus slope of epi-oceanic swells could contribute to nodulation, as described by Coudray and Michel (1981), Elmi (1981), and Elmi and Ameur (1984), among others. The presence of slumps and intraclasts would confirm this resedimentation. However, there is no evidence of biogenic encrustations or borings on nodules, so that intense exhumation processes affecting nodules may be excluded.

References

- Berner RA (1969) Goethite stability and the origin of red beds. *Geochim Cosmochim Acta* 33:267–273
- Bosellini A (1973) Modello geodinamico e paleotettonico delle Alpi Meridionali durante il Giurassico–Cretacico. Sue possibili applicazioni agli Appennini. In: Accordi B (ed) *Moderne vedute sulla Geologia dell’Appennino*. Accademia Nazionale Lincei, Quaderni 183:163–205
- Boulila S, Galbrum B, Huret E, Hinnov LA, Rouget I, Gardin S, Bartolini A (2014) Astronomical calibration of the Toarcian Stage: implications for sequence stratigraphy and duration of the early Toarcian OAE. *Earth Planet Sci Lett* 386:98–111
- Braga JC, Comas MC, Delgado F, García-Hernández M, Jiménez AP, Linares A, Rivas P, Vera JA (1981) The Liassic Rosso Ammonitico facies in the subbetic zone (Spain). Genetic consideration. In: Farinacci A, Elmi S (eds) *Rosso ammonitico symposium proceedings*. Tecnocienza, Rome, pp 61–76
- Caracuel JE, Monaco P, Olóriz F (1997) Eventos de depósito y colonización del substrato en facies ammonitico rosso (Subbético externo, Kimmeridgiense). *Geogaceta* 21:63–65
- Caracuel JE, Monaco P, Olóriz F (2000) Taphonomic tools to evaluate sedimentation rates and stratigraphic completeness in rosso ammonitico facies (epioceanic tethyan Jurassic). *Riv Ital Paleontol Stratigr* 106:353–368
- Cecca F, Fourcade E, Azéma J (1992) The disappearance of the “Ammonitico Rosso”. *Palaeogeogr Palaeoclimatol Palaeoecol* 99:55–70

- Chester R, Baxter GB, Behairy AKA, Connor K, Cross D, Elderfield H, Padgham RC (1977) Soil-sized eolian dusts from the lower troposphere of the eastern Mediterranean Sea. *Mar Geol* 24:201–217
- Comas MC, Olóriz F, Tavera JM (1981) The red nodular limestones (Ammonitico Rosso) and associated facies: a key for settling slopes or swell areas in the Subbetic Upper Jurassic submarine topography (southern Spain). In: Farinacci A, Elmi S (eds) Rosso ammonitico symposium proceedings. Tecnocienza, Rome, pp 113–136
- Coudray J, Michel D (1981) Analyse sédimentologique des “calcaires noduleux” qui encadrent les radiolarites du dinantien de la Montagne Noire (France) et apport des données expérimentales à la compréhension de leur genèse. In: Farinacci A, Elmi S (eds) Proceedings Rosso Ammonitico Symposium. Tecnoscienza, Rome, pp 149–167
- D’Argenio B (1974) Le Piattaforme Carbonatiche Periadriatiche. Una rassegna di problemi nel quadro geodinámico del’area mediterranea. *Mem Soc Geol Ital* 13:1–28
- Dera G, Pellenard P, Neige P, Deconinck JF, Puceat E, Dommergues JL (2009) Distribution of clay minerals in Early Jurassic Peritethyan seas: palaeoclimatic significance inferred from multiproxy comparisons. *Palaeogeogr Palaeoclimatol Palaeoecol* 271:39–51
- Dera G, Brigaud B, Monna F, Laffont R, Puceat E, Deconinck JF, Pellenard P, Joachimski MM, Durlot C (2011) Climatic ups and downs in a disturbed Jurassic world. *Geology* 39:215–218
- Dercourt J, Zonenshain LP, Ricou LE, Kazmin VG, Le Pichon X, Knipper AL, Grandjacquet C, Sborshchikov IM, Boulin J, Sorokhtin O, Geyssant J, Lepvrier C, Biju-Duval B, Sibuet JC, Savostin LA, Westphal M, Lauer JP (1985) Présentation de 9 cartes paléogéographiques à 1:20.000.000 s’étendent de l’Atlantique au Pamir pour la période du Lias à l’actuel. *Bull Soc Géol Fr* 8:635–652
- El Kadiri K (2002) “Tectono-eustatic sequences” of the Jurassic successions from the Dorsale Calcaire (Internal Rif, Morocco): evidence from an eustatic and tectonic scenario. *Geol Romana* 36:71–103
- Eller MG (1981) The red chalk of Eastern England: a Cretaceous analogue of rosso ammonitico. In: Farinacci A, Elmi S (eds) Rosso ammonitico symposium proceedings. Tecnocienza, Rome, pp 207–231
- Elmi S (1981) Sédimentation rythmique et organisation séquentielle dans les ammonitico-rosso et les facies associées du Jurassique de la Méditerranée Occidentale. Interpretation des grumeaux et des nodules. In: Farinacci A, Elmi S (eds) Rosso ammonitico symposium proceedings. Tecnocienza, Rome, pp 251–299
- Elmi S, Almeras Y (1984) Physiography, palaeotectonics and palaeoenvironments as controls of changes in ammonite and brachiopod communities (an example from the early and middle Jurassic of western Algeria). *Palaeogeogr Palaeoclimatol Palaeoecol* 47:347–360
- Elmi S, Ameur M (1984) Quelques environnements des facies noduleux mésogées. *Geol Romana* 23:13–22
- Ettaki M, Chellaï EH (2005) Le Toarcien inférieur du Haut Atlas de Todra-Dadès (Maroc): sédimentologie et lithostratigraphie. *C R Géosci* 337:814–823
- Ettaki M, Chellaï EH, Milhi A, Sadki D, Boudchiche L (2000) Le passage Lias moyen-Lias supérieur dans la région de Todra-Dadès: événements biosédimentaires et géodynamiques (Haut Atlas central, Maroc). *C R Acad Sci, Paris* 331:667–674
- Funk H, Oberhanski R, Pfiffner A, Schmid S, Wildi W (1987) The evolution of the northern margin of Tethys in eastern Switzerland. *Episodes* 10:102–106
- Fürsich FT (1973) *Thalassinoides* and the origin of nodular limestone in the Corallian Beds (Upper Jurassic) of southern England. *Neues Jb Geol Paläontol Abh* 3:136–156
- Fürsich FT (1979) Genesis, environments, and ecology of Jurassic hardgrounds. *Neues Jb Geol Paläontol Abh* 158:1–163
- Gómez JJ, Fernández-López SR (1994) Condensation processes in shallow platforms. *Sed Geol* 92:147–159
- Gong Y (2001) Trace fossils from the flysch sequences of the Silurian, Carboniferous and Triassic of the Tianshan and Kunlun-Qinling orogenic belts of northwestern China. *Acta Palaeontol Sin* 40:177–188

- Gradstein FM, Ogg JG, Smith AG (2004) A geologic time scale 2004. Cambridge University Press
- Hallam A (1967) Sedimentology and palaeogeographic significance of certain red limestones and associated beds in the Lias of the Alpine region. *Scott J Geol* 3:195–220
- Hallam A (1988) A reevaluation of Jurassic eustasy in the light of new data and the revised Exxon curve. *SEPM Special Publication* 42, pp 261–273
- Hallam A (2001) A review of the broad pattern of Jurassic sea-level changes and their possible causes in the light of current knowledge. *Palaeogeogr Palaeoclimatol Palaeoecol* 167:23–37
- Han Y, Pickerill RK (1994) *Phycodes templus* isp. nov. from the Lower Devonian of northwestern New Brunswick, eastern Canada. *Atlantic Geol* 30:37–46
- Haq BU, Hardenbol J, Vail PR (1987) Chronology of fluctuating sea level since the Triassic. *Science* 235:1156–1167
- Helm C (2005) Riffe und fazielle Entwicklung der florigemma-Bank (Korallenoolith, Oxfordium) im Süntel und östlichen Wesergebirge (NW-Deutschland). *Geol Beitr Hannover* 7:1–39
- Hermoso M, Pellenard P (2014) Continental weathering and climatic changes inferred from clay mineralogy and paired carbon isotopes across the early to middle Toarcian in the Paris Basin. *Palaeogeogr Palaeoclimatol Palaeoecol* 399:385–393
- Jacquín TH, De Graciansky PC (1998) Major transgressive/regressive cycles: the stratigraphic signature of European basin development. In: De Graciansky PC, Hardenbol J, Jacquín TH, Vail PR (eds) *Mesozoic and Cenozoic Sequence Stratigraphy of European Basins*. *SEPM Special Publication* 60, pp 15–29
- Jenkyns HC (1971) The genesis of condensed sequences in the Tethyan Jurassic. *Lethaia* 4:327–352
- Jiménez AP (1986) Estudio paleontológico de los ammonites del Toarciense inferior y medio de las Cordilleras Béticas (Dactylioceratidae e Hildoceratidae). Ph.D. Thesis, Universidad de Granada
- Kennedy WJ, Garrison RE (1975) Morphology and genesis of nodular chalks and hardgrounds in the Upper Cretaceous of southern England. *Sedimentology* 22:311–386
- Krencker FN, Bodin S, Suan G, Heimhofer U, Kabiri L, Immenhauser A (2015) Toarcian extreme warmth led to tropical cyclone intensification. *Earth Planet Sci Lett* 425:120–130
- Mángano MG, Carmona NB, Buatois LA, Muñiz Guinea F (2005) A new ichnospecies of *Arthropycus* from the Upper Cambrian-Lower Tremadocian of northwest Argentina: implications for the Arthropycid lineage and potential in ichnostratigraphy. *Ichnos* 12:179–190
- Marok A, Reolid M (2012) Lower Jurassic sediments from the Rhar Roubane Mountains (Western Algeria): Stratigraphic precisions and synsedimentary block-faulting. *J Afr Earth Sc* 76:50–65
- Mattioli E, Erba E (1999) Synthesis of calcareous nannofossil events in tethyan Lower and Middle Jurassic successions. *Riv Ital Paleontol Stratigr* 105:343–376
- Mattioli E, Pittet B, Bucefalo-Palliani R, Röhl HJ, Schmid-Röhl A, Moretini E (2004) Phytoplankton evidence for the timing and correlation of palaeoceanographical changes during the early Toarcian oceanic anoxic event (Early Jurassic). *J Geol Soc London* 161:685–693
- Mattioli E, Plançq J, Boussaha M, Duarte LV, Pittet B (2013) Calcareous nannofossil biostratigraphy: new data from the Lower Jurassic of the Lusitanian Basin. *Comunicações Geológicas* 100, Especial I:69–76
- McLaughlin PI, Brett CE (2004) Sequence stratigraphy and stratinomy of marine hardgrounds: examples from the Middle Paleozoic of Eastern Laurentia. *Geological Society of America, Abstracts with programs* 36, p 110
- Miller W III (2001) *Thalassinoides-Phycodes* compound burrow systems in Paleocene deep-water limestone, Southern Alps of Italy. *Palaeogeogr Palaeoclimatol Palaeoecol* 170:149–156
- Monaco P, Trecci T (2014) Ichnocoenosis in the macigno turbidite basin system, lower miocene, trasimero (Umbrian apennines, Italy). *Ital J Geosci* 133:116–130
- Monaco P, Caracuel JE, Giannetti A, Soria JM, Yébenes A (2007) *Thalassinoides* and *Ophiomorpha* as cross-facies trace fossils of crustaceans from shallow-to-deep-water environments: Mesozoic and Tertiary examples from Italy and Spain. In: 3rd Symposium on Mesozoic and Cenozoic Decapod Crustaceans, Museo di Storia Naturale di Milano, pp 79–82

- Mouterde R, Linares A (1960) Nuevo yacimiento fosilífero del Lias superior, cerca de Iznalloz (Provincia de Granada, Cordillera Bética). *Notas Comun IGME* 58:101–104
- Mullins HT, Neumann AC, Wilber RJ, Boardman MR (1980) Nodular carbonate sediment on Bahamian slopes: possible precursor to nodular limestones. *J Sediment Petrol* 50:117–131
- Nieto LM, Ruiz-Ortiz PA, Rey J, Benito MI (2008) Strontium-isotope stratigraphy as a constraint on the age of condensed levels: examples from the Jurassic of the Subbetic Zone (southern Spain). *Sedimentology* 55:1–29
- Nieto LM, Rodríguez-Tovar FJ, Molina JM, Reolid M, Ruiz-Ortiz PA (2014) Unconformity surfaces in pelagic carbonate environments: a case from the Middle Bathonian of the Betic Cordillera, SE Spain. *Ann Soc Geol Pol* 84:281–295
- Ogg J, Hinnov LA (2012) The Jurassic period. In: Gradstein F, Ogg J, Ogg G, Smith D (eds) *A geological time scale 2012*. Elsevier, pp 731–791
- Oliveira LCV, Perilli N, Duarte LV (2007) Calcareous nannofossil assemblages around the Pliensbachian/Toarcian boundary in the reference section of Peniche (Portugal). *Ciências Terra (UNL)* 16:45–50
- Olóriz F, Reolid M, Rodríguez-Tovar FJ (2012) Palaeogeography and relative sea-level history forcing eco-sedimentary contexts in Late Jurassic epicontinental shelves (Prebetic Zone, Betic Cordillera): an ecostratigraphic approach. *Earth Sci Rev* 111:154–178
- Palomo I (1987) Mineralogía y geoquímica de sedimentos pelágicos del Jurásico inferior de las Cordilleras Béticas (SE de España). Ph.D. Thesis, Universidad de Granada
- Parisi G, Ortega-Huertas M, Nocchi M, Palomo I, Monaco P, Ruiz F (1996) Stratigraphy and geochemical anomalies of the Early Toarcian oxygen-poor interval in the Umbria-Marche Apennines (Italy). *Geobios* 29:469–484
- Petrash DA, Lalonde SV, Gingras MK, Konhauser KO (2010) A surrogate approach to studying the chemical reactivity of burrow mucous lining in marine sediments. *Palaios* 26:594–600
- Reolid M (2014) Stable isotopes for foraminifera and ostracods for interpreting incidence of the Toarcian Oceanic Anoxic Event in Westernmost Tethys: role of water stagnation and productivity. *Palaeogeogr Palaeoclimatol Palaeoecol* 395:77–91
- Reolid M, Nagy J, Rodríguez-Tovar FJ, Olóriz F (2008) Foraminiferal assemblages as palaeoenvironmental bioindicators in Late Jurassic epicontinental platforms: relation with trophic conditions. *Acta Palaeontol Pol* 53:706–722
- Reolid M, Molina JM, Löser H, Navarro V, Ruiz-Ortiz PA (2009) Coral biostromes of the Middle Jurassic from the Subbetic (Betic Cordillera, southern Spain): facies, coral taxonomy, taphonomy and palaeoecology. *Facies* 55:575–593
- Reolid M, Nieto LM, Rey J (2010) Taphonomy of cephalopod assemblages from Middle Jurassic hardgrounds of pelagic swells (South-Iberian palaeomargin, Western Tethys). *Palaeogeogr Palaeoclimatol Palaeoecol* 292:257–271
- Reolid M, Sebane A, Rodríguez-Tovar FJ, Marok A (2012a) Foraminiferal morphogroups as a tool to approach the Toarcian Anoxic Event in the Western Saharan Atlas (Algeria). *Palaeogeogr Palaeoclimatol Palaeoecol* 323–325:87–99
- Reolid M, Rodríguez-Tovar FJ, Marok A, Sebane A (2012b) The Toarcian Oceanic Anoxic Event in the Western Saharan Atlas, Algeria (North African paleomargin): role of anoxia and productivity. *Geol Soc Am Bull* 124:1646–1664
- Reolid M, Chakiri S, Bejjaji Z (2013a) Adaptive strategies of the Toarcian benthic foraminiferal assemblages from the Middle Atlas (Morocco): palaeoecological implications. *J Afr Earth Sc* 84:1–12
- Reolid M, Nieto LM, Sánchez-Almazo IM (2013b) Caracterización geoquímica de facies pobremente oxigenadas en el Toarciense inferior (Jurásico inferior) del Subbético Externo. *Rev Soc Geol Esp* 26:69–84
- Reolid M, Marok A, Sebane A (2014a) Foraminiferal assemblages and geochemistry for interpreting the incidence of Early Toarcian environmental changes in North Gondwana palaeomargin (Traras Mountains, Algeria). *J Afr Earth Sc* 95:105–122

- Reolid M, Mattioli E, Nieto LM, Rodríguez-Tovar FJ (2014b) The Early Toarcian Oceanic Anoxic Event in the External Subbetic (Southiberian Palaeomargin, Westernmost Tethys): geochemistry, nanofossils and ichnology. *Palaeogeogr Palaeoclimatol Palaeoecol* 411:79–94
- Reolid M, Rivas P, Rodríguez-Tovar FJ (2015) Toarcian ammonitic rosso facies from the South Iberian paleomargin (Betic Cordillera, southern Spain): paleoenvironmental reconstruction. *Facies* 61:22. doi:10.1007/s10347-015-0447-3
- Rita P, Reolid M, Duarte LV (2016) Benthic foraminiferal assemblages record major environmental perturbations during the Late Pliensbachian—Early Toarcian interval in the Peniche GSSP, Portugal. *Palaeogeogr Palaeoclimatol Palaeoecol* 454:267–281
- Rivas P (1972) Estudio paleontológico-estratigráfico del Lías (Sector Central de las Cordilleras Béticas). Ph.D. Thesis, Universidad de Granada, Short Publication 29, p 77
- Rodríguez-Tovar FJ, Nieto LM (2013) Composite trace fossil assemblage in a distal carbonate setting from the Tethys (Middle Jurassic, Betic Cordillera, Southern Spain). *Ichnos* 20:43–53
- Rodríguez-Tovar FJ, Reolid M (2013) Environmental conditions during the Toarcian Oceanic Anoxic Event (T-OAE) in the westernmost Tethys: influence of the regional context on a global phenomenon. *Bull Geosci* 88:697–712
- Rodríguez-Tovar FJ, Uchman A (2010) Ichnofabric evidence for the lack of bottom anoxia during the lower Toarcian Oceanic Anoxic Event (T-OAE) in the Fuente de la Vidriera section, Betic Cordillera, Spain. *Palaios* 25:576–587
- Rozic B, Smuc A (2011) Gravity-flow deposits in the Toarcian Perbla formation (Slovenian basin, NW Slovenia). *Riv Ital Paleontol Stratigr* 117:283–294
- Ruebsam W, Münzberger P, Schwark L (2014) Chronology of the Early Toarcian environmental crisis in the Lorraine Sub-basin (NE Paris Basin). *Earth Planet Sci Lett* 404:273–282
- Sandoval J, Bill M, Aguado R, O’Dogherty L, Rivas P, Morard A, Guex J (2012) The Toarcian in the Subbetic basin (southern Spain): bio-events (ammonite and calcareous nanofossils) and carbon-isotope stratigraphy. *Palaeogeogr Palaeoclimatol Palaeoecol* 342–343:40–63
- Santantonio M (1993) Facies associations and evolution of pelagic carbonate platform/basin systems: examples from the Italian Jurassic. *Sedimentology* 40:1039–1067
- Santantonio M (1994) Pelagic carbonate platforms in the geologic record: their classification, and sedimentary and paleotectonic evolution. *AAPG Bull* 78:122–141
- Savrida CE (2012) Chalk and related deep-marine carbonates. In: Knaust D, Bromley RG (eds) Trace fossils as indicators of sedimentary environments. *Development in Sedimentology* 64, pp 777–806
- Soussi M, Ben Ismail MH (2000) Platform collapse and pelagic seamount facies: Jurassic development of central Tunisia. *Sed Geol* 133:93–113
- Soussi M, Enay R, Mangold C, Turki MM (2000) The Jurassic events and their sedimentary and stratigraphic records on the Southern Tethyan margin in Central Tunisia. *Mém Mus Natl d’Hist Nat, Paris* 182:57–92
- Uchman A, Tchoumatchenco P (2003) A mixed assemblage of deep-sea and shelf trace fossils from the Lower Cretaceous (Valanginian) Kamchia Formation in the Troyan Region, Central Fore-Balkan, Bulgaria. *Ann Soc Geol Pol* 73:27–34
- Vera JA (1988) Evolución de los sistemas de depósito en el Margen Ibérico de la Cordillera Bética. *Rev Soc Geol Esp* 1:373–391
- Vogel K, Bundschuh M, Glaub I, Hofmann K, Radtke G, Schmidt H (1995) Hard substrate ichnocoenoses and their relations to light intensity and marine bathymetry. *Neues Jb Geol Paläontol Abh* 195:49–61
- Winterer EL, Bosellini A (1981) Subsidence and sedimentation on Jurassic passive continental margin, Southern Alps, Italy. *AAPG Bull* 65:394–421
- Yelles-Chaouche AK, Ait-Ouali R, Bracène R, Derder MEM, Djellit H (2001) Chronologie de l’ouverture du bassin des Ksour (Atlas Saharien, Algérie) au début du Mésozoïque. *Bull Soc Géol Fr* 172:285–293

Chapter 5

General Conclusions

The south Iberian Palaeomargin during the Pliensbachian and Toarcian was a complex context as evidenced by the detailed analysis of the reference sections of the External and Median Subbetic. The fragmentation of the palaeomargin during the Late Pliensbachian and the configuration in different tilted blocks with variable subsidence determined differences in thickness and facies during the Toarcian as well as the presence of stratigraphic discontinuities, hardgrounds and omission surfaces.

In this context, the record of the T-OAE is not homogeneous in the palaeomargin and is very different to the typical black shales of the central and north Europe sections. As evidenced in the text, sections from Mediterranean and Submediterranean provinces are characterised by low values of TOC. In the case of the Subbetic sections, the higher TOC values are usually less than 1 wt% during the Early Toarcian biotic crisis and the negative CIE.

In the context of the Betic Cordillera, the External Subbetic records the more typical facies of the T-OAE with comparatively higher record of TOC, the presence of the negative CIE, as well as evidences of local oxygen depleted conditions as showed by the analyses of redox geochemical proxies, trace fossils and foraminiferal assemblages. Good examples are La Cerradura, Cueva del Agua and Fuente Vidriera sections. Changes in lithofacies are registered around the transition from Pliensbachian to Toarcian related to decreasing carbonate content and the development of dark marls (but not black shales *s.s.*). The T-OAE in the External Subbetic is identified by the increase of TOC, the negative CIE, the increase of redox sensitive elements as well as biotic evidences of oxygen depleted conditions. Trace fossil assemblages decrease in diversity during the Serpentinum Zone and locally they are absent associated to maximum values of TOC and the CIE. The foraminiferal assemblages in this area are characterised by decreasing abundance and diversity as well as proliferation of some opportunist forms just before the negative CIE. The more adverse conditions are commonly recorded by a thin benthic barren interval. The recovery is evidenced by the increasing values of diversity and abundance, initially with the colonisation by opportunists showing

decreasing in size (Lilliput Effect). In the case of ostracods, the biotic crisis determines the extinction of *Metacopina* and the recovery with a very different assemblage composition (see Cueva del Agua section). Changes in water column conditions are also evidenced by the composition and diversity of the calcareous nanofossils and in the Cueva del Agua section by the proliferation of radiolarians.

In the case of the Median Subbetic, the record of the T-OAE is more complicated due to the presence of omission surfaces and probably associated hiatuses. The thickness of the different sections is variable as well as the observed lithofacies and microfacies. The negative CIE is not recorded in the Iznalloz section where the Lower Toarcian is represented by reduced thicknesses of marls and marly limestones with intercalations of tempestite layers. In the case of the Arroyo Mingarrón section, more expanded succession, the negative CIE is not clearly recorded in spite of the prevailing marl and marly limestone alternance nature. The TOC values are also lower than in the External Subbetic and there is not a clear maximum in the Serpentinum Zone. Redox geochemical proxies are also without a clear stratigraphic trend. These unfavourable aspects determine that this area has been poorly studied and more works are necessary for the future, mainly focused in the foraminiferal and trace fossil assemblages. Actually, we can recognise a variable incidence of the T-OAE, lower in the Median than in the External Subbetic. However, data from the Median Subbetic allow understanding the evolution of the palaeomargin and the development of the lithofacies and microfacies during the Toarcian with the record of the ammonitico rosso facies. External and Median Subbetic determine a complex setting for understanding the evolution of this part of the Western Tethys. They are far from the typically reported T-OAE with well-developed black shales and negative CIE from the classical works in central and North Europe, being essential for understanding the complexity of the global T-OAE.